Network Rewiring and Spatial Targeting: Optimal Disease Mitigation in Multilayer Social Networks

Konig, Michael; Marray, Kieran; Takes, Frank; Candogan, Ozan

2025

Network Rewiring and Spatial Targeting: Optimal Disease Mitigation in Multilayer Social Networks

Ozan Candogan
Booth School of Business, University of Chicago, 5807 South Woodlawn Avenue, Chicago, Illinois 60637, United States.

Michael D. König
CEPR, KOF-ETH Zurich and Dep. of Spat. Econ., VU Amsterdam, De Boelelaan 1105, 1081 HV Amsterdam, The Netherlands.

Kieran Marray
Department of Spatial Economics, VU Amsterdam, De Boelelaan 1105, 1081 HV Amsterdam, The Netherlands.

Frank W. Takes
Leiden Institute of Advanced Computer Science, Leiden University, Einsteinweg 55, 2333 CC Leiden, The Netherlands.

Abstract
We study disease spread on a social network where individuals adjust contacts to avoid infection. Susceptible individuals rewire links from infectious individuals to other susceptibles, reducing infections and causing the disease to only become endemic at higher infection rates. We formulate the planner's problem of implementing targeted lockdowns to control endemic disease as a semidefinite program that is computationally tractable even with many groups. Rewiring complements policy by allowing more intergroup contact as the rewiring rate increases. We apply our model to compute optimal spatially-targeted lockdowns for the Netherlands during Covid-19 using a population-level contact network for 17.26 million individuals. Our findings indicate that, with rewiring, a targeted lockdown policy permits 12% more contacts compared to one without rewiring, underscoring the significance of accounting for network endogeneity in effective policy design. (JEL: I12, I15, I18, I19, C63, E23)

Keywords: epidemics, networks, structural estimation, spatially-targeted policy.

1. Introduction

There is ongoing debate about the effectiveness of different non-pharmaceutical interventions that target particular types of contact, such as work-based distancing and school closures (NPIs) in mitigating pandemic spread while minimizing societal costs (cf. Acemoglu et al.

Acknowledgments: We would like to thank Abishek Ananth, Pierpaolo Batigalli, David Frazier, Sanjeev Goyal, Fabian Greimel, Matt Jackson, Frank Pijpers, Edouard Schaal, Alex Teytelboym, Fernando Vega-Redondo, Yves Zenou, Lina Zhang, and participants at the 1st International Workshop on Population-Scale Social Network Analysis (October 2022) for helpful comments. We are grateful to Statistics Netherlands (CBS) for providing access to the social network data. The data has been aggregated to the municipality level and interactions have been weighted with information from survey data so that only anonymized information has been used.

E-mail: Ozan.Candogan@chicagobooth.edu (Candogan); m.d.konig@vu.nl (König); k.j.marray@vu.nl (Marray); f.w.takes@liacs.leidenuniv.nl (Takes)

2021; Birge et al. 2022). However, studies often ignore the changes in contact networks due to disease spread, which can significantly impact infection growth and immunity (Thurner et al. 2020; Britton et al. 2020; Gupta et al. 2020; Bootsma and Ferguson 2007). Contagion-risk averse individuals tend to limit interactions early in a pandemic (Acemoglu et al. 2024; Carnehl et al. 2023). Current epidemic models typically fail to account for these endogenous network responses, which can lead to biased and inefficient policy recommendations (cf. Bootsma and Ferguson 2007; Alvarez et al. 2021; Fajgelbaum et al. 2021).

We study how endogenous changes in contact networks affect optimal targeted mitigation policy by introducing a multi-group susceptible-infectious-recovered (SIR) model where individuals adjust contacts to avoid infection. Susceptible individuals rewire links away from infectious neighbours, changing the network's structure as the disease spreads. This model is represented by a set of ordinary differential equations (Kurz 1971; Taylor et al. 2012) that allows us to incorporate various groups and types of connections. Endogenous network dynamics typically flatten infections and reduce deaths compared to models without rewiring.[1] Through the model, rewiring, recovery, and infection rates are estimable from aggregate cases and deaths plus an initial contact network. This allows us to estimate how much people rewire.

The key analytic result of our theoretical model (Theorem 2) is a semidefinite programming problem, which allows us to assess the impact of rewiring on optimal mitigation policies. The constraint in the program ensures that the disease does not become endemic, and the formulation is adapted to efficiently handle a large number of groups and types of connections between them, making it possible to study large social contact network data.

We apply our model to the second Covid-19 wave in the Netherlands, constructing a population-level contact network for 17.26 million individuals using multi-layered social network data and contact surveys. The layers of the network contain different types of contact (neighbourhood, household, work, school and family), allowing us to target each type of connection differently. We find that susceptible individuals rewire 9% of links to infectious per day. Targeted policies that take into account both contact network structure and types of connection are far more efficient than uniform ones, allowing 75.24% of contacts to continue, compared to only 45.40% in the uniform case, resulting in a 65.73% increase in contacts. Rewiring increases the efficiency of targeted policies. Comparing a targeted policy with and without rewiring allows for an additional 12.26% of contacts. This highlights the importance of accounting for network endogeneity in policy design. The optimal targeting of different types of connection differs across different parts of the network. We observe the largest reductions in household contacts in municipalities within the Dutch "Bible Belt", a region characterized by a

1. See also Online Appendix E.1.

higher-than-average Christian population, larger household sizes, and tightly-knit communities (Ruijs et al. 2011). Further, analyzing the Pareto frontier describing the trade-off between cases and economic costs, we find that targeting and accounting for endogenous network response (through rewiring) yields the greatest improvements. This effect is particularly pronounced for higher values of the basic reproduction number, where heterogeneous network structures in each layer can be most effectively leveraged in the optimal policy to limit disease spread.

Our work extends recent studies that endogenize behavior in epidemic models (e.g. Alberto and Andrea 2020; Carnehl et al. 2023; Acemoglu et al. 2024) by explicitly considering the adaptation of contacts in response to the epidemic in an estimable way. It improves upon previous studies using a reduced form matching function to represent the contact network (such as Alvarez et al. 2021; Acemoglu et al. 2021) by explicitly modeling and estimating from data the endogenous rewiring of contacts.[2] It also relates to studies on lockdown effectiveness in spatially differentiated models (Fajgelbaum et al. 2021; Bisin and Moro 2022; Chandrasekhar et al. 2021), showing how network adaptivity affects the impact of targeted interventions. Moreover, our multi-layer network model is related to Chandrasekhar et al. (2024), who examine how different layers in a social network affect information diffusion, and Zenou and Zhou (2024), who design optimal interventions in linear-quadratic games on multi-layer networks. In contrast to the model presented here, these studies treat the network structure as exogenous and do not incorporate the endogenous formation of the network.

The paper is organized as follows. Section 2 introduces the theoretical model. Section 3 analyzes the stationary state. Section 4 discusses the planner's optimal lockdown policy. Section 5 describes the data, Section 6 discusses the estimation framework, and Section 7 provides an application to the Covid-19 pandemic in the Netherlands. Section 8 concludes. Additional relevant material can be found in the Online Appendix.

2. The Model

2.1. Epidemic and Network Dynamics

Consider $\mathcal{N} = \{1, \ldots, N\}$ agents connected in an unweighted, undirected network, $G(t)$, which evolves in continuous time $t \in [0, T]$. Assume that each agent belongs to one of a finite set of groups or types $\mathcal{K} = \{1, \ldots, K\}$ (e.g their district or city). Each agent in each group is in one of four compartments: susceptible, infectious, recovered, or deceased, and some infectious are

2. A notable exception is Fosco et al. (2010). However, these authors consider a different application related to the adoption of behavioral norms in endogenous social networks and do not empirically estimate their model.

hospitalized. Let $S_k(t)$ denote the number of susceptibles, $I_k(t)$ the number of infectious, $R_k(t)$ the number of recovered, $H_k(t)$ the number of hospitalized, and $D_k(t)$ the number of deceased, per capita, respectively, at time t in group k. We normalize the population size to one, such that, $\forall t \in [0,T]$ and $k \in \mathcal{K}$, $S_k(t) + I_k(t) + R_k(t) + D_k(t) = N_k$ and $\sum_{k\in\mathcal{K}}^{K} N_k = N = 1$.[3] Assume further that we observe multiple different types of connections between agents (e.g. family, school, household, work, etc.). Call these types "layers", indexing them by $l \in \mathcal{L}$. Let $m^l(A_k, B_j)(t)$ denote the number of links between the agents in group k in compartment A and group j in compartment B at time t in layer l divided by N (density of links per capita). To generate non-trivial steady states we introduce *vital dynamics* (see e.g. Brauer et al. 2008), corresponding to exogenous births and deaths of individuals and links. Individuals are born without any links at rate $\lambda > 0$, and die with all their links at rate $\mu > 0$. New links form between susceptibles in groups $k, j \in \mathcal{K}$ in layer $l$at rate $\kappa^l_{kj} > 0$, and die at rate $\nu^l > 0$.[4] Following, e.g., Acemoglu et al. (2021) we further assume that a planner implements lockdowns that allow a fraction $L^l_{k,j} \in [0,1]$ of pre-existing contacts between groups $k, j \in \mathcal{K}$ in layer $l \in \mathcal{L}$.

We can then describe the evolution of the fraction of individuals in each compartment by the following system of differential equations:

$$\frac{dS_k}{dt} = \lambda - \beta \sum_{l\in\mathcal{L}, j\in\mathcal{K}} m^l(S_k, I_j)(t) L^l_{kj} - \mu S_k(t) \tag{1}$$

$$\frac{dI_k}{dt} = \beta \sum_{l\in\mathcal{L}, j\in\mathcal{K}} m^l(S_k, I_j)(t) L^l_{kj} - \gamma I_k(t) - \mu I_k(t), \tag{2}$$

$$\frac{dR_k}{dt} = \delta_{rk} H_k(t) + \gamma(I_k(t) - H_k(t)) - \mu R_k(t), \tag{3}$$

$$H_k(t) = \iota_k I_k(t), \tag{4}$$

$$\frac{dD_k}{dt} = \delta_{dk} H_k(t). \tag{5}$$

Infectious individuals infect susceptible neighbours at rate β per link, reducing the number of susceptibles by the infection rate times the density of links between susceptible and infectious (Eq. (1)). The number of infectious increases by the corresponding amount (the

3. Abstracting from natural births and death rates that are small over the time period that we consider (Chowell et al. 2007).

4. The formation of links in each layer follows a so called *stochastic block model* (Holland et al. 1983). A stochastic block model considers a partition of the nodes into disjoint subsets k; and link probabilities $\kappa^l_{kk'} \geq 0$ between subsets, k and k', respectively, in layer l. The link is then sampled at random such that any two nodes i in group k and j in group k' are connected by a link with probability $\kappa^l_{kk'}$. Assuming a stochastic block model for the creation of links, the total density of new links formed between susceptibles will be $\kappa^l_{kk'} S_k(t) S_{k'}(t)$.

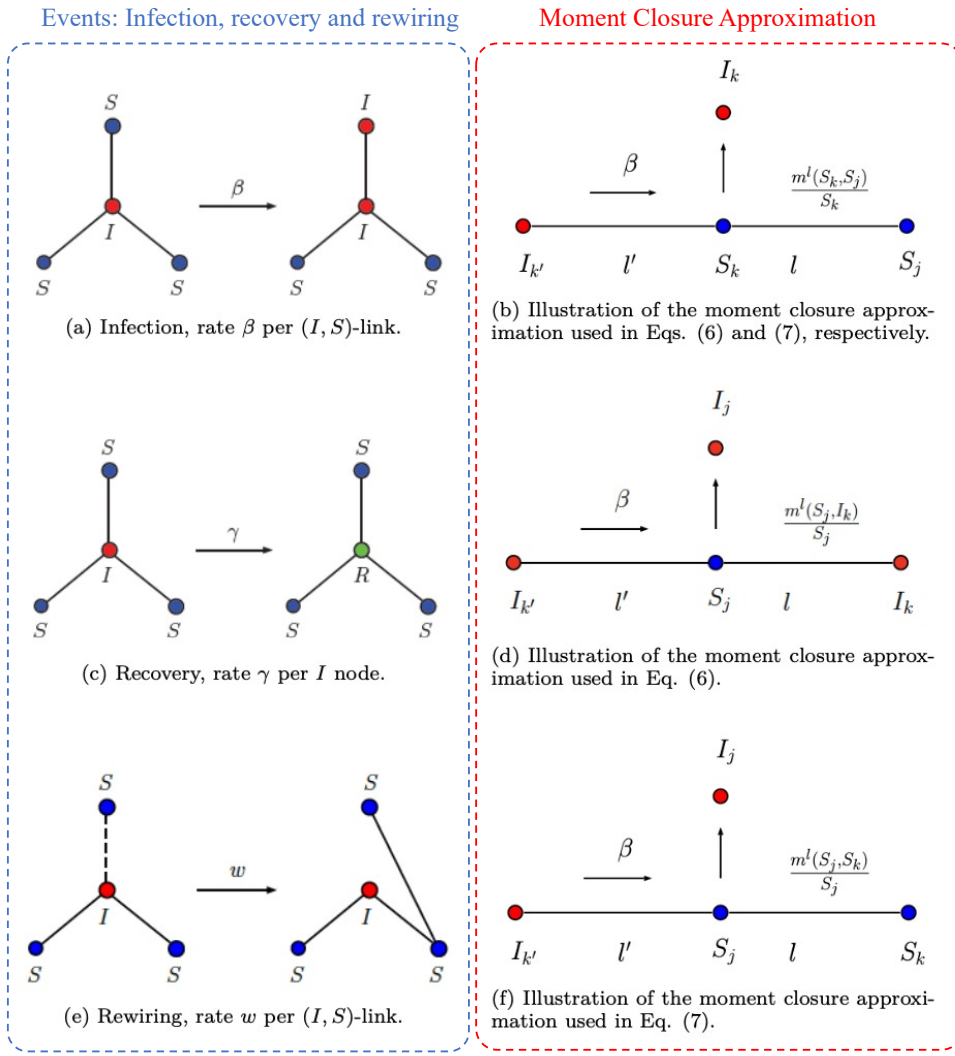

FIGURE 1. Panels (a), (c) and (e): Infection, recovery, and rewiring events. Panels (b), (d) and (f): Illustration of the moment closure approximation used in Eqs. (6) and (7), respectively. Blue denotes susceptible nodes (S), red denotes infectious nodes (I), and green denotes recovered nodes (R).

first part of Eq. (2)). A constant fraction ι of infectious agents are hospitalized (Eq. (4)). Infectious agents who are not hospitalized recover at rate γ (the second term in Eq. (3)). Hospitalized agents either recover at rate δ_r (the first term of Eq. (3)), or die at rate δ_d (Eq. (5)). Finally, $\delta_r + \delta_d = \gamma$ (the final term in Eq. (2)). The different events are illustrated in Panels (a) and (c) in Figure 1.

We further allow for an endogenous behavioral response of agents to the pandemic (cf. e.g. Acemoglu et al. 2024; Carnehl et al. 2023). In particular, we assume susceptible agents prefer to avoid getting infectious and thus remove links with infectious neighbours to reform – or *rewire* – them with other susceptibles at a rate $w > 0$.[5] An illustration can be found in Panel (e) in Figure 1. Rewiring and the spread of disease give link densities that evolve by the following differential equations:

$$\begin{aligned}\frac{dm^l(I_k,S_j)}{dt} &= \beta \sum_{l'\in\mathcal{L},k'\in\mathcal{K}} L^{l'}_{k'k} \underbrace{m^{l'}(I_{k'},S_k)(t)\frac{m^l(S_k,S_j)(t)}{S_k(t)}}_{\text{Panel (b) in Figure 1}} \\ &\quad - \beta \sum_{l'\in\mathcal{L},k'\in\mathcal{K}} L^{l'}_{k'j} \underbrace{m^{l'}(I_{k'},S_j)(t)\frac{m^l(S_j,I_k)(t)}{S_j(t)}}_{\text{Panel (d) in Figure 1}} \\ &\quad - (\gamma + w + \nu^l + 2\mu) m^l(I_k,S_j)(t), \end{aligned} \tag{6}$$

and

$$\begin{aligned}\frac{dm^l(S_k,S_j)}{dt} &= w\frac{S_j(t)}{\sum_{k'\in\mathcal{K}} S_{k'}(t)} \sum_{k'\in\mathcal{K}} m^l(I_{k'},S_k)(t) L^l_{k'k} \\ &\quad + w\frac{S_k(t)}{\sum_{k'\in\mathcal{K}} S_{k'}(t)} \sum_{k'\in\mathcal{K}} m^l(I_{k'},S_j)(t) L^l_{k'j} \\ &\quad - \beta \sum_{l'\in\mathcal{L},k'\in\mathcal{K}} L^{l'}_{k'k} \underbrace{m^{l'}(I_{k'},S_k)(t)\frac{m^l(S_k,S_j)(t)}{S_k(t)}}_{\text{Panel (b) in Figure 1}} \\ &\quad - \beta \sum_{l'\in\mathcal{L},k'\in\mathcal{K}} L^{l'}_{k'j} \underbrace{m^{l'}(I_{k'},S_j)(t)\frac{m^l(S_j,S_k)(t)}{S_j(t)}}_{\text{Panel (f) in Figure 1}} \\ &\quad + \kappa^l_{kj} S_k(t) S_j(t) L^l_{kj} - (\nu^l + 2\mu) m^l(S_k,S_j)(t). \end{aligned} \tag{7}$$

Infections generate new infectious susceptible links and remove old susceptible-susceptible links – the links between the newly infectious and their susceptible neighbours. The number of these

5. This is a reduced-form description of individual behavior with a preference for constant socialization. Including it as a parameter allows us to estimate it from data. A behavioral microfoundation for rewiring can be found in Online Appendix A. Our formulation is related to Atkeson (2020), Atkeson et al. (2021), Carnehl et al. (2023) and Acemoglu et al. (2024), where endogenous behavior in an epidemic is modeled as susceptible individuals choosing to reduce their exposure levels when randomly meeting an infectious individual.

is the number of $(I_{k'}, S_k, S_j)$-triples in each layer. We compute the number of these triples using a *moment-closure approximation* (Taylor et al. 2012)–that the number of $(I_{k'}, S_k, S_j)$-triples in the layer l is the product of the link density between infectious and susceptible $m^{l'}(I_{k'}, S_k)(t)$ and the expected density of susceptible-susceptible links for a susceptible $m^l(S_k, S_j)(t)/S_k(t)$ which yields $m^l(I, S)(t)m^l(S, S)(t)/S(t)$. (the first term in Eq. (6) and third in Eq. (7)).[6] The second term in Eq. (6), as well as the third and fourth terms in Eq. (7) can be derived in a similar way. Panels (b), (d) and (f) in Figure (1) provide an illustration. The moment-closure approximation allows one to obtain a system of ODEs that is closed at the level of single state variables (I and S) and pairwise interactions ($m(I, S)$ and $m(S, S)$). Rewiring increases the number of susceptible-susceptible links (the first two terms in Eq. (7)). More specifically, we assume that susceptible individuals rewire links to any other susceptible in the population uniformly at random.[7] Then the density of links in layer l between susceptibles in groups k' and k from susuceptibles in group k' increases by

$$w \times \frac{S_k(t)}{\sum_{k' \in \mathcal{K}} S_{k'}(t)} \sum_{k' \in \mathcal{K}} m^l(I_{k'}, S_k)(t) L^l_{k'k} \tag{8}$$

–the density of the links susceptibles in group k' rewire times the proportion of those links that go to susceptibles in group k. With uniform rewiring the proportion of links that go to susceptibles in group k is just the proportion of susceptibles in group k in the total population of susceptibles. Further, infections, recovery and rewiring reduce infectious-susceptible links (the third term in Eq. (6)). Finally, births and deaths of individuals and links give the last two terms in Eq, (6).[8,9]

---

6. See Theorem 1 in Taylor et al. (2012), as well as Fosco et al. (2010), Keeling and Eames (2005), Gross et al. (2006), Gleeson (2011) and Kuehn (2016) for further details and examples for the moment-closure approximation.

7. In Online Appendix E.6 we discuss the case where links are rewired to all non-infectious individuals. We show that the assumption that links are rewired to susceptible individuals only as we do in the current section does not strongly affect the epidemic dynamics, especially in the early stages of the epidemic (when there are only few infectious individuals), but it reduces the number of equations to analyze significantly.

8. A formal derivation of Eqs. (1) to (7) based on the results in Kurtz (1971) can be found in Theorem 3 in Online Appendix I. Moreover, extensive simulation results comparing our system of ODEs to the average from Monte-Carlo simulations of the jump process using the *next reaction method* (also known as Gibson-Bruck algorithm; cf. e.g. Anderson (2013) and Wilkinson (2018)) can be found in Online Appendix E.

9. Note that our model is equivalent to one in which at a rate $q > 0$ an infectious individual self-quarantines and all the links of this individual to susceptible individuals get rewired to other susceptible individuals at random. Then the ODEs in Eqs. (6) and (7) would be identical except for replacing the rewiring rate w with the self-quarantine rate q. The reason for this equivalence is that the mean field dynamics in these equations does not discriminate between synchronous and asynchronous rewiring of links. See also Online Appendix D for further

3. Asymptotic Behavior and Stability Analysis

The disease-free state in which there are no infectious individuals is a fixed point (equilibrium) of our system of ODEs. The following theorem identifies the disease-free equilibrium as a function of the birth and deaths rates, and provides a condition for its stability.

THEOREM 1. *Denote by*

$$F^{l,l'}_{j,k,u,v}(\mathbf{L}) = \frac{\beta m^l(S_k, S_j)}{S_k} L^{l'}_{uk}\delta_{vk},$$

and

$$V^{l,l'}_{j,k,u,v}(w) = (\gamma + w + \nu^l + 2\mu)\delta_{u,k}\delta_{v,j}\delta_{l,l'}, \tag{9}$$

for $l, l' \in \mathcal{L}$ and $j, k, u, v \in \mathcal{K}$, where δ_{ij} is the Kronecker delta with the property that $\delta_{ij} = 1$ if $i = j$ and zero otherwise. Then the disease-free equilibrium $[S_k, I_k, m^l(S_k, S_j), m^l(I_k, S_j)] = [\lambda/\mu, 0, \frac{\kappa^l_{kj}}{\nu^l+2\mu}\frac{\lambda^2}{\mu^2}, 0]$ is asymptotically stable[10] if and only if $\mathbf{F}(\mathbf{L}) \prec \mathbf{V}(w)$.

Note that the rewiring rate w enters linearly into our $\mathbf{V}$ matrix in Eq. (9) in the same way as the recovery rate γ. For interpretation, consider the case with one group, a single layer and no lockdowns. Then from Theorem 1 we have that the disease-free equilibrium is unstable if and only if[11]

$$\frac{\beta m(S, S)}{S} > \gamma + w + \nu + 2\mu. \tag{10}$$

Equilibrium stability is decreasing in the density of the contact network. As the average number of links per individual, $\frac{m(S,S)}{S}$, increases, the stability condition will only hold for a lower β fixing γ and w (and the remaining parameters q, ν and μ). The more individuals rewire, the higher infection rate needed for the disease to spread in the population. The rewiring rate w and recovery rate γ are additive in our stability condition. So, in the long run, rewiring has the same effect on the spread of disease as increasing the recovery rate.[12]

---

discussion. An alternative approach can be found in Alvarez et al. (2021) where testing and self-quarantine are treated as the solution to a planner's problem.

10. Let $||.||$ denote the L^2 norm in $\mathbb{R}^n$. The dynamical system $\frac{dx}{dt} = f(x)$, for $x \in \mathbb{R}^n$ is asymptotically stable around an equilibrium point x^* if and only if: (i) for any $\varepsilon > 0, \exists\delta > 0$ such that if $||x(t_0) - x^*|| < \delta$, $||x(t_0) - x(t)|| < \varepsilon$, $\forall t > t_0$; and (ii) $\exists\eta$ such that if $||x(t_0) - x^*|| < \eta$, $x(t) \to x^*$ as $t \to \infty$ (Dahleh et al. 2011).

11. One can show that (10) is equivalent to the basic reproduction number being larger than one. See also Footnote 15 and Online Appendix B for further details.

12. In Online Appendix B we derive an analytic characterization of the critical infection rate β^c (Proposition 2) and the critical rewiring rate w^c (Proposition 1) for which the disease-free equilibrium becomes unstable in

4. Optimal Lockdowns

We model a planner picking the level of lockdowns to ensure local stability of disease-free equilibrium at lowest cost. The goal is to prevent the spread of a newly introduced disease through the population at the lowest cost.

Suppose that we associate a convex quadratic cost function $C(\mathbf{L})$ with lockdown policy matrix $\mathbf{L} = [L^l_{kj}]$, $k, j \in \mathcal{K}$, $l \in \mathcal{L}$, where cost is decreasing in $\mathbf{L}$ (locking down more costs more). Then, using the result from Theorem 1 (and taking the closure of the feasible region) we can formulate the following optimization problem:

$$\begin{aligned} \min_{L^l_{kj} \in [0,1], \forall k,j,l} \quad & C(\mathbf{L}), \\ \text{s.t.} \quad & \mathbf{F}(\mathbf{L}) \preceq \mathbf{V}(w), \\ & k, j \in \mathcal{K}, l \in \mathcal{L}. \end{aligned} \tag{11}$$

Similar to e.g. Chowell et al. (2007) in the following we will assume that the time-scale of the epidemic is much faster than characteristic times for demographic processes (natural birth and death). The latter (comparatively small) effects can be neglected for the computation of the eigenvalues in Equation (9). This assumption effectively corresponds to a slight tightening of the constraints in the planner's problem (11). The solution to this problem remains near optimal (and is arbitrarily close to the true optimal solution for small natural birth/death rate, by Berge's maximum theorem (Berge 1963).

The following theorem then characterizes the solution to the planner's problem (11) in the case of heterogeneous, group-specific lockdowns for an arbitrary (and potentially large) number of groups.

THEOREM 2. *Consider a linear lockdown cost $C(\mathbf{L})$ with $C'(\mathbf{L}) > 0$, homogeneous birth and death rates across groups, and let $\hat{\mathbf{\Omega}}^l$ be a symmetric $K \times K$ matrix with elements $\beta m^l(S_j, S_k) L^l_{kj} / \sqrt{S_j S_k}$. Then, the planner's problem (11) is the semidefinite program (SDP) given by $\min C(\mathbf{L})$ subject to $\sum_{l \in \mathcal{L}} \hat{\mathbf{\Omega}}^l \preceq (\gamma + w)\mathbf{I}$.*

As the number of rows/columns in $\hat{\mathbf{\Omega}}^l$ is of the order $O(K)$, the problem remains tractable even when the number of groups, K, becomes large. The elements of the matrix $\hat{\mathbf{\Omega}}^l$ depend

closed form for up to three groups ($K = 2, 3$) (cf. Fosco et al. 2010). We find that the rates related to recovery (γ), rewiring (w), self-quarantine (q), link decay (ν) and node decay (μ) all increase the threshold β^c, while the birth rates of nodes (λ) and links (κ) decrease it. Similarly, the critical rewiring rate w^c is increasing with the infection rate β.

on the infection rate, the number of contacts between each group relative to the size of each group, and the amount of contact the planner allows between each group. The more contacts there are between groups, or the higher the infection rate, the more the planner should reduce contact between them. The more susceptible individuals rewire links away from infectious neighbours, the more slack the constraint becomes. Thus, the planner can allow more links between individuals.[13]

5. Data

We apply our model to study optimal policy during the second wave of Covid-19 in the Netherlands using a novel population-scale dataset that maps social contacts likely to transmit flu-like diseases. This multi-layered social network, constructed from registry data of Statistics Netherlands (van der Laan 2022) and reweighted using contact frequencies from flu-like infection surveys, captures the likelihood of Covid-19 transmission through various contact types, such as family, work, household, school, and neighbourhood interactions. The dataset covers 17.26 million individuals and represents 827 million potential contacts; the network structure is described in more detail in the work by Bokányi et al. (2023).

To model disease transmission, we reweigh the network using contact matrices from the POLYMOD survey (Mossong et al. 2008), aligning contact settings with social network layers (family, home, work, school, neighbourhood). This produced a weighted network reflecting average daily contact rates and transmission probabilities. To ensure privacy and practically feasible analysis, we aggregated these individual connections into a municipality-level contact network, enabling us to estimate transmission patterns across 380 municipalities. An illustration is provided in Figure 2, with further data collection details in the Online Appendix F.

6. Estimation

In Proposition 3 in Online Appendix G.3, we show that the parameters (β, γ, w) of our system of differential equations (1) to (7) are identified from data on susceptibles, infectious, and

13. In Online Appendix C we provide an analytic solution to (11) for the case of uniform lockdowns ($L^l_{kj} = L \in [0,1]$) and two groups. We show that the optimal lockdown intensity and the rewiring rate w are substitutes at a rate that is the inverse of the sum of the infection rate β times the average degree of susceptible type k nodes among the same type k nodes. The case of uniform lockdowns will be an important benchmark in the counterfactuals analyzed in Section 7.

FIGURE 2. Contacts per individual per day for flu-like infectious diseases between municipalities in the Netherlands. Darker weights indicate more contacts. Connections containing fewer than 12,000 individual links are omitted for ease of reading, and to preserve privacy of individuals in small municipalities.

infectious-susceptible links over time. So, we can estimate infection, recovery, and rewiring rates by minimizing the distance between model solutions and data on these.

There are two complications, however. First, directly using the differential equations with many groups (1) to (7) for estimating the model's parameters is infeasible as the number of equations grows of the order of $O(K)$ per layer. For example, modeling each municipality in the Netherlands as a group with one type of contact gives 289,940 differential equations. To resolve this, we use the fact that the system's aggregate dynamics can be represented using a simpler set of ODEs for one group,[14] reducing the computational burden.

Second, we do not directly observe the number of links between infectious and susceptibles over time, only the initial condition from our contact network. To address this, we show that we can use new cases as a proxy for the density of links between infectious and susceptible individuals, conditional on the case reporting rate. We give further details on construction of epidemic data in Online Appendix G.

14. See Lemma 1 in Online Appendix G.

TABLE 1. Estimates of infection, recovery, and rewiring rates, second wave of Covid-19.

		With rewiring (1)	Without rewiring (2)
Infection rate	(β)	0.0296^{***}	0.0207^{***}
		(0.00139)	(0.00156)
Recovery rate	(γ)	0.191^{***}	0.174^{***}
		(0.00277)	(0.00159)
Rewiring rate	(w)	0.0917^{***}	
		(0.0142)	
RMSE		0.116	0.123

Notes: Covariance matrix estimated using Newey-West estimator. Standard errors in parentheses. Significance levels: * $p < 0.10$, ** $p < 0.05$, *** $p < 0.01$.

We report estimates with and without rewiring in columns (1) and (2) of Table 1. First, consider the estimates with rewiring in column (1). These correspond to a basic reproduction number of $\mathcal{R}_0 = 1.40$.[15] Our estimated recovery rate is close to the standard rate of 0.2 used to calibrate models of Covid-19 (e.g. Acemoglu et al. 2021). The estimated rewiring rate of 0.0917 corresponds to susceptibles rewiring 9.17% of their links to infectious per day.

Next, consider the estimates from a model without rewiring in column (2) in Table 1 ignoring latent network dynamics. The estimates imply basic reproduction number of $\mathcal{R}_0 = 1.67$, higher than the one we find with rewiring. The lower estimated basic reproduction number $\mathcal{R}_0$ (and higher infection rate β) in the case of an endogenous network with rewiring compared to a network without rewiring are due to the mitigating effect of rewiring links away from infectious individuals on disease transmission (note that the rewiring rate w enters additively in our stability condition (10)). This indicates a general downward bias in epidemic models of infectious disease spread that do not consider network adaptivity (i.e. ignore rewiring). Adding rewiring improves the fit of the model. The root mean squared error (RMSE) of the fitted model from data series falls from 0.123 without rewiring to 0.116 with rewiring.

15. The basic reproduction number, $\mathcal{R}_0$, represents the average number of secondary infections produced by a single infectious individual in a completely susceptible population (Anderson and May 1991). See Online Appendix B for further details.

7. Optimal Targeted Lockdowns in the Netherlands

Using our estimated parameters, we evaluate different potential lockdown policies in response to the second wave of Covid-19 in the Netherlands. First, we allow the planner to target based on the different layers in the municipality-municipality contact network, to break down which types of links (layers) are most important, and compare to the optimal uniform lockdown. Next, we use these results to characterize how rewiring and different types of targeting affect the trade-offs a policymaker faces between finite disease spread (or in terms of disease-induced deaths) and social costs from mitigation policy.

7.1. Optimal Targeting Across Layers with Rewiring

To explore whether and how it is optimal to set lockdowns heterogeneously across municipalities and layers, we analyze the following optimal control problem:

$$\begin{aligned} \min_{L^l_{kj}\in[0,1],\forall k,j,l} \quad & C(\mathbf{L}) = -\sum_{l\in\mathcal{L}}\sum_{k,j\in\mathcal{K}} L^l_{kj} s_k, \\ \text{s.t.} \quad & \sum_{l\in\mathcal{L}} \hat{\mathbf{\Omega}}^l \preceq (\gamma + w)\mathbf{I}, \\ & k, j \in \mathcal{K}, l \in \mathcal{L}, \\ & |\mathcal{K}| = 380, |\mathcal{L}| = 5. \end{aligned} \tag{12}$$

where s_k is the share of the population in municipality k and G^l_{kj} is the total number of connections between municipality k and municipality j in layer l. In words, the cost of locking down connections depends on the number of individuals that are affected.

From the solution to (12) we find that targeted policies are significantly more efficient than uniform policies (Acemoglu et al. 2021). With both rewiring and network-based targeting, 75.24% of contacts are allowed to continue under the optimal lockdown policy, compared to only 45.40% without these mechanisms (i.e. uniform lockdowns without rewiring). This means that network-based targeting allows the planner to preserve an additional 29.84% of total contacts (or a 65.73% increase). Rewiring further enhances the efficiency of targeted policies. Optimal targeted policies without rewiring permit 67.02% of total contacts. Accounting for endogenous changes in the contact network in response to disease spread (with rewiring) enables the planner to allow 8.22% more contacts (or 12.26% more contact overall).

A geographical representation of the optimal lockdowns from solving (12) for each layer (household, work, school and family) is shown in the top left and bottom panels of Figure

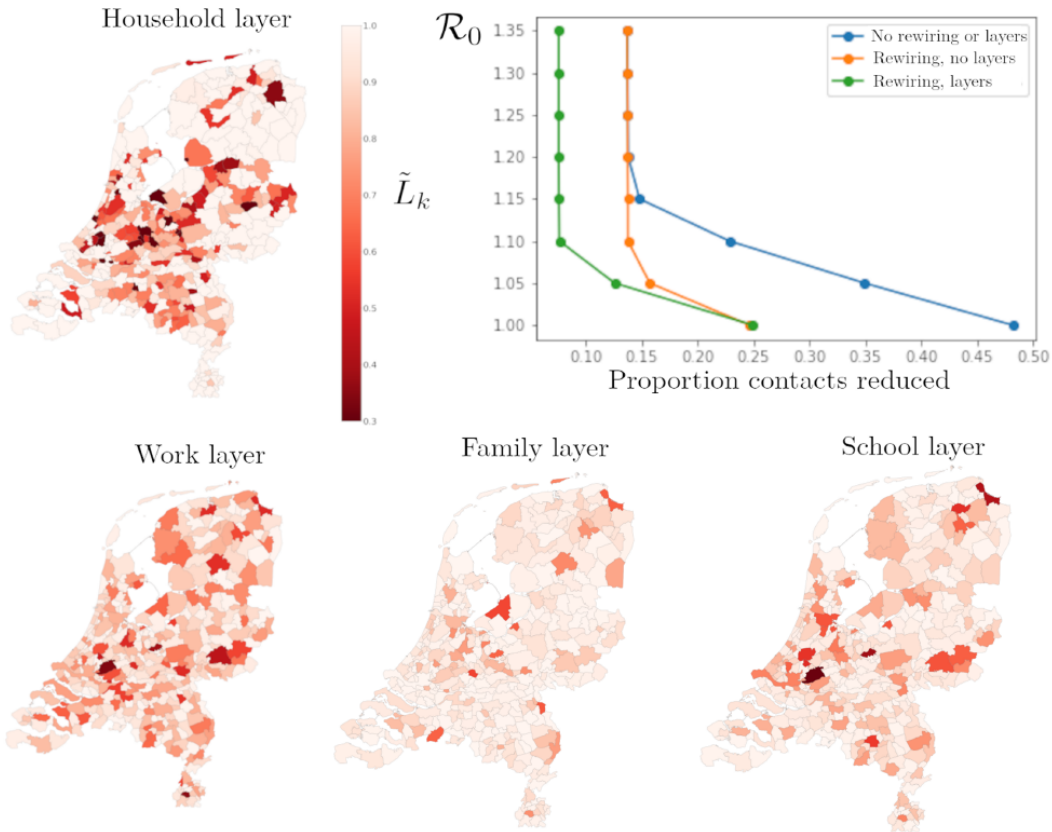

FIGURE 3. Optimal spatially targeted lockdowns from Covid-19 in the Netherlands using estimated parameters from the second wave of Covid-19. Lightest color denotes the most contacts allowed, and the darkest denotes the fewest contacts allowed. The color scale goes from 40% of contacts allowed (darkest) to 100% (lightest). The top right panel shows the Pareto frontier representing trade-offs between disease spread ($\mathcal{R}_0$) and lockdown intensities (proportion of contacts allowed) faced by policymakers. Points represent relaxations $\varepsilon \in \{0, 0.025, \ldots, 0.15\}$ corresponding to $\mathcal{R}_0 \in [1, 1.2]$. The results for three model specifications are shown: uniform lockdowns, rewiring without targeting and rewiring with targeting, where targeting includes both, municipalities and layers.

3.[16] We plot the share of original contacts allowed by municipality, which for municipality k is given by:

$$\widetilde{L}_k = \frac{\sum_{l \in \mathcal{L}} \sum_{j \in \mathcal{K}} G^l_{kj} L^l_{kj}}{\sum_{l \in \mathcal{L}} \sum_{j \in \mathcal{K}} G^l_{kj}}. \tag{13}$$

Optimal lockdowns vary significantly across municipalities within each layer. Instead of one

16. Neighbourhood contacts are omitted for readability.

targeted policy (e.g school closures) being optimal, we find that different types of targeted mitigation policies should be emphasised in different parts of the network depending on the relative position of each municipality in each layer. The planner imposes the largest reductions in household contacts in predominantly Christian municipalities within the so called "Bible Belt", where household sizes are larger, such as Urk, Harderwijk and Katwijk.[17] Despite accounting for population size, school contacts are still heavily reduced in larger municipalities with universities and primary/secondary schools, such as Amsterdam and Groningen. In contrast, neighbourhood contacts are largely left unchanged, likely because, based on our contact surveys, they contribute less to the spread of flu-like infectious diseases. We further find that the amount a municipality is targeted is highly correlated with the measure of flow-betweenness centrality in the municipality-municipality contact network in each layer (Brandes and Fleischer 2005). However, even though they are correlated, centrality measures do not fully explain the optimal targeted policy, as these static network statistics do not take network endogeneity into account.

7.2. Trade-Offs Between Deaths and Economic Damages

Next we study the trade-offs a planner faces between disease spread and costs of lockdowns given different types of targeting. In the previous section we have considered cases where a policymaker wants to preserve the stability of the disease free equilibrium. However, a policymaker may be unwilling to incur the damages required by lockdowns to keep the disease free equilibrium stable. They may be willing for the disease to circulate slowly, leading to some number of deaths, until the arrival of a vaccine to offset welfare damages from strict lockdowns (Acemoglu et al. 2021). To model this, we imagine a policymaker allowing for an $\varepsilon > 0$ relaxation of our stability constraint $\sum_{l \in \mathcal{L}} \hat{\mathbf{\Omega}}^l \preceq (\gamma + w + \varepsilon)\mathbf{I}$ in the planner's problem in (12). The size of ε determines how much greater than 1 the basic reproduction number, $\mathcal{R}_0$, can be (whereas the original problem (12) enforces $\mathcal{R}_0 \leq 1$). We then design lockdowns to minimize their total costs while managing disease spread, constrained by this relaxed upper bound on $\mathcal{R}_0$.[18]

The top right panel in Figure 3 plots these trade-offs when the planner implements different types of targeting with and without considering endogenous changes in the contact network.

17. A list of the most targeted municipalities (with and without rewiring) can be found in Online Appendix Figure H.2.

18. In additional specifications, we represent economic damages as a reduction in the share of total wages from a given group, weighted by the share who cannot work from home (Acemoglu et al. 2021). As wages covary very strongly with population size in the Netherlands, results are qualitatively similar.

Targeting not accounting for rewiring or types of contact leads to strictly worse trade offs that targeting accounting for rewiring when $\mathcal{R}_0$ is close to one. For higher values of the relaxation $\varepsilon > 0$ the relative importance of rewiring diminishes in the constraint $(\gamma + w + \varepsilon)\mathbf{I}$, and hence the two policies yield similar outcomes. Accounting for types of contact and rewiring yields a further improvement also for higher values of $\mathcal{R}_0$, where the heterogeneous network structures for each layer can be most effectively exploited in the optimal policy to limit the spread of the disease.[19]

8. Conclusions

We introduce a new SIR model for epidemic spread on a network that incorporates endogenous behavioral changes, where susceptible individuals rewire links away from infectious contacts. The planner's problem of minimizing the cost of preventing a disease becoming endemic can be formulated as a semidefinite program that is tractable as the number of groups and types of contact become large, allowing us to examine the impact of rewiring on optimal lockdowns. Rewiring flattens infection curves, creating a trade-off: the more individuals adjust their contacts, the less intense lockdowns need to be. Applying this model to Covid-19 in the Netherlands, we estimate optimal network targeted lockdowns using a population-scale social network and contact surveys. We find that rewiring reduces lockdowns in less connected municipalities linked to larger ones.

References

Acemoglu, Daron, Victor Chernozukhov, Ivan Werning, and Michael Whinston (2021). "Optimal targeted lockdowns in a multigroup SIR model." *American Economic Review: Insights*, 3, 487–502.

Acemoglu, Daron, Ali Makhdoumi, Azarakhsh Malekian, and Asuman Ozdaglar (2024). "Testing, voluntary social distancing, and the spread of an infection." *Operations Research*, 72(2), 533–548.

Ainslie, Kylie E C, Jantien A Backer, Pieter T de Boer, Albert Jan van Hoek, Don Klinkenberg, Hester Korthals Altes, Ka Yin Leung, Hester de Melker, Fuminari Miura, and Jacco Wallinga (2022). "A scenario modelling analysis to anticipate the impact of COVID-19 vaccination in adolescents and children on disease outcomes in the Netherlands, summer 2021." *Eurosurveillance*, 27(44).

Alberto, Bisin and Moro Andrea (2020). "Learning Epidemiology by Doing: The Empirical Implications of a Spatial SIR Model with Behavioral Responses." *NBER WP No. w27590*.

Alvarez, Fernando, David Argente, and Francesco Lippi (2021). "A simple planning problem for COVID-19 lock-down, testing, and tracing." *American Economic Review: Insights*, 3(3), 367–382.

19. In Online Appendix H.5 we show that our results are qualitatively robust when considering an age structure population as in Acemoglu et al. (2021). Comparing a targeted policy with and without rewiring when different age groups are taken into account allows for an additional 9.98% of contacts, which is similar to the benchmark specification.

Anderson, David (2013). *An introduction to stochastic processes with applications in the biosciences*. Lecture notes, Dept. of Mathematics, University of Wisconsin at Madison.

Anderson, Roy M and Robert M May (1991). *Infectious diseases of humans: Dynamics and control*. Oxford university press.

Anderson, Simon P, Andre De Palma, and Jacques-Francois Thisse (1992). *Discrete choice theory of product differentiation*. MIT press.

Atkeson, Andrew (2020). "A parsimonious behavioural SEIR model of the COVID epidemic in the United States and the United Kingdom." *Working paper*, 121, 1–11.

Atkeson, Andrew, Karen Kopecky, and Tao Zha (2021). "Behavior and the transmission of COVID-19." *American Economic Association Papers and Proceedings*, 111, 356–360.

Berge, Claude (1963). *Topological spaces*. Oliver & Boyd.

Billingsley, Patrick (2017). *Probability and measure*. John Wiley & Sons.

Birge, John R., Ozan Candogan, and Yiding Feng (2022). "Controlling Epidemic Spread: Reducing Economic Losses with Targeted Closures." *Management Science*, 68(5), 3175–3195.

Bisin, Alberto and Andrea Moro (2022). "Spatial-SIR with network structure and behavior: Lockdown rules and the Lucas critique." *Journal of Economic Behavior & Organization*, 198, 370–388.

Bokányi, Eszter, Eelke M Heemskerk, and Frank W Takes (2023). "The anatomy of a population-scale social network." *Scientific Reports*, 13(1), 9209.

Bootsma, Martin and Neil Ferguson (2007). "The effect of public health measures on the 1918 influenza pandemic in U.S. cities." *Proceedings of the National Academy of Sciences*, 104, 7588–7593.

Brandes, Ulrik and Daniel Fleischer (2005). "Centrality Measures Based on Current Flow." In *STACS 2005*, edited by Volker Diekert and Bruno Durand, pp. 533–544, Springer Berlin Heidelberg, Berlin, Heidelberg.

Brauer, Fred, Pauline van den Driessche, and Jianhong Wu (2008). *Mathematical Epidemiology*. Lecture notes in mathematics: Mathematical biosciences subseries, Springer, Heidelberg.

Braun, Martin (1993). "Differential equations and their applications: An introduction to applied mathematics."

Britton, Tom, Frank Ball, and Pieter Trapman (2020). "A mathematical model reveals the influence of population heterogeneity on herd immunity to SARS-CoV-2." *Science*, 369(6505), 846–849.

Carnehl, Christoph, Satoshi Fukuda, and Nenad Kos (2023). "Epidemics with behavior." *Journal of Economic Theory*, 207, 105590.

Chandrasekhar, Arun G., Vasu Chaudhary, Benjamin Golub, and Matthew O. Jackson (2024). "Multiplexing in Networks and Diffusion." *arXiv preprint arXiv:2412.11957*.

Chandrasekhar, Arun G, Paul Goldsmith-Pinkham, Matthew O Jackson, and Samuel Thau (2021). "Interacting regional policies in containing a disease." *Proceedings of the National Academy of Sciences*, 118(19), e2021520118.

Chowell, Gerardo, Hiroshi Nishiura, and Luis MA Bettencourt (2007). "Comparative estimation of the reproduction number for pandemic influenza from daily case notification data." *Journal of the Royal Society Interface*, 4(12), 155–166.

Dahleh, Mohammed, Munther A. Dahleh, and George Verghese (2011). *Lectures on dynamic systems and control*. Lecture notes, Department of Electrical Engineering and Computer Science, Massachuasetts Institute of Technology.

Den Haan, Wouter and Andrew Levin (1996). "Bootstrap critical values for tests based on generalised method-of-moments estimators." *Econometrica*, 64(4), 891–916.

Fajgelbaum, Pablo D., Amit Khandelwal, Wookun Kim, Cristiano Mantovani, and Edouard Schaal (2021). "Optimal lockdown in a commuting network." *American Economic Review: Insights*, 3(4), 503–522.

Ferguson, Neil, Daniel Laydon, Gemma Nedjati-Gilani, Natsuko Imai, Kylie Ainslie, Marc Baguelin, Sangeeta Bhatia, and et al. (2020). "Impact of non-pharmaceutical interventions (NPIs) to reduce COVID-19 mortality and healthcare demand." *Working paper*.

Fosco, Constanza, Fernando Vega-Redondo, and Matteo Marsili (2010). "Peer effects and peer avoidance: The diffusion of behavior in coevolving networks." *Journal of the European Economic Association*, 8(1), 169–202.

Gleeson, James (2011). "High-accuracy approximation of binary-state dynamics on networks." *Physical Review Letters*, 107, 068701.

Gross, Thilo, Carlos J. Dommar D'Lima, and Bernd Blasius (2006). "Epidemic Dynamics on an Adaptive Network." *Phys. Rev. Lett.*, 96, 208701.

Gupta, Sumedha, Kosali I Simon, and Coady Wing (2020). "Mandated and Voluntary Social Distancing During The COVID-19 Epidemic: A Review." *NBER working paper 28139*.

Hansen, L. and J. Scheinkman (1995). "Back to the future: generating moment implications for continuous-time Markov processes." *Econometrica*, 63(4), 767–804.

Hedde-von Westernhagen, Christine, Ayoub Bagheri, and Javier Garcia-Bernardo (2024). "Predicting COVID-19 infections using multi-layer centrality measures in population-scale networks." *Applied Network Science*, 9(1), 27.

Holland, Kathryn, P.W. Blackmond, and S. Leinhardt (1983). "Stochastic blockmodels: First steps." *Social networks*, 5(2), 109–137.

Keeling, Matt J and Ken T.D Eames (2005). "Networks and epidemic models." *Journal of The Royal Society Interface*, 2(4), 295–307.

Khalil, Hassan K (2002). *Nonlinear systems*. Prentice Hall.

Kuehn, Christian (2016). "Moment closure – a brief review." *Control of Self-organizing Nonlinear Systems*, pp. 253–271.

Kurtz, Thomas G (1971). "Limit theorems for sequences of jump Markov processes approximating ordinary differential processes." *Journal of Applied Probability*, 8(2), 344–356.

Kurz, Thomas (1971). "Limit theorems for sequences of jump Markov processes." *Journal of Applied Probability*.

Mossong, Joel, Niel Hens, Mark Jit, Philippe Beutels, Kari Auranen, Rafael Mikolajczyk, Marco Massari, Stefania Salmaso, Gianpaolo Scalia Tomba, Jacco Wallinga, Janneke Heijne, Malgorzata Sadkowska-Todys, Magdalena Rosinska, and W. John Edmunds (2008). "Social Contacts and Mixing Patterns Relevant to the Spread of Infectious Diseases." *PLOS Medicine*, 5, 1–1.

Newey, Whitney K. and Daniel McFadden (1994). "Large sample estimation and hypothesis testing." In *Handbook of econometrics*, vol. 4, edited by Robert Engle and Daniel McFadden, chap. 36, pp. 2212–2245.

Powell, Philip D (2011). "Calculating determinants of block matrices." *arXiv preprint arXiv:1112.4379*.

Ruijs, Wilhelmina LM, Jeannine LA Hautvast, Koos van der Velden, Sjoerd de Vos, Hans Knippenberg, and Marlies EJL Hulscher (2011). "Religious subgroups influencing vaccination coverage in the Dutch Bible belt: an ecological study." *BMC Public Health*, 11, 1–9.

Sandholm, William H (2010). *Population games and evolutionary dynamics*. MIT press.

Taylor, Michael, Péter L Simon, Darren M Green, Thomas House, and Istvan Z Kiss (2012). "From Markovian to pairwise epidemic models and the performance of moment closure approximations." *Journal of Mathematical Biology*, 64, 1021–1042.

Thurner, Stefan, Peter Klimek, and Rudolf Hanel (2020). "A network-based explanation of why most COVID-19 infection curves are linear." *Proceedings of the National Academy of Sciences*, 117(37), 22684–22689.

van der Laan, DJ (2022). *A person network of the Netherlands*. Statistics Netherlands Discussion Paper.

Wilkinson, Darren J (2018). *Stochastic modelling for systems biology*. Chapman and Hall/CRC.

Zenou, Yves and Junjie Zhou (2024). "Games on Multiplex Networks." *Available at SSRN 4772575*.

ONLINE APPENDIX

A. Behavioral Microfoundation of Rewiring

Following the notation in Carnehl et al. (2023) we let $\pi_S > 0$ denote the socialization utility of a susceptible individual, and the cost of getting infectious be given by $\eta > 0$. Let the utility of the susceptible individual maintaining the link to the infectious be given by

$$\pi_0 = \pi_S - \beta\eta + \varepsilon_0,$$

where $\beta > 0$ is the transmission rate and ε_0 is a random error term. Similarly, the utility of rewiring the link from the infectious individual to another susceptible is

$$\pi_1 = \pi_S - c + \varepsilon_1,$$

where $c > 0$ is a linking cost and ε_1 is a random error term. Assuming that the error terms are type 1 extreme value distributed with parameter ϑ, the probability that the utility of the susceptible individual from rewiring is higher than the utility from staying connected to the infectious individual is given by (Anderson et al. 1992):

$$\mathbb{P}(\pi_1 > \pi_0) = \frac{e^{\vartheta(\pi_s - c)}}{e^{\vartheta(\pi_s - c)} + e^{\vartheta(\pi_S - \beta\eta)}} = \frac{1}{1 + e^{\vartheta(c - \beta\eta)}}. \tag{A.1}$$

The rewiring rate w in the main text can be interpreted as the adjustment rate times Eq. (A.1).

B. Basic Reproduction Number and Epidemic Threshold

We can relate the asymptotic stability result of Theorem 1 to the basic reproduction number, $\mathcal{R}_0$, which represents the average number of secondary infections produced by a single infectious individual in a completely susceptible population (cf. Anderson and May 1991; Brauer et al. 2008). To simplify the discussion for the remainder of this section we consider a single layer.

Corollary 1. *Consider the case of a single group and no lockdowns. The basic reproduction number then is*

$$\mathcal{R}_0 = \frac{\beta m(S, S)}{S(\gamma + w + \nu + 2\mu)} \tag{B.1}$$

A comparison of Eq. (B.1) with Eq. (10) shows that the disease-free equilibrium is unstable if and only if the basic reproduction number $\mathcal{R}_0$ is larger than one. We can further see that the basic reproduction number is increasing in the average number of links per individual, $\frac{m(S,S)}{S}$, and that rewiring (w) and recovery (γ) affect the basic reproduction number in the same way.

While Theorem 1 characterizes the stability of the disease-free equilibrium in terms of eigenvalues for an arbitrary number of groups, the following proposition identifies the critical infection rate β for which the disease-free equilibrium becomes unstable in closed form for up to three groups.

PROPOSITION 1. *The critical value of the infection rate β for which the disease-free equilibrium becomes unstable is given by*

$$\beta^c = (2\mu(\nu+2\mu)(\gamma+w+\nu+2\mu)) \times \frac{1}{\lambda\left(\sum_{k=1}^{K}\kappa_{kk}L_{kk} + \sqrt{\left(\sum_{k=1}^{K}\kappa_{kk}L_{kk}\right)^2 + 4\sum_{k=1}^{K}\sum_{j=k+1}^{K}\left(\kappa_{kj}^2 L_{kj}^2 - \kappa_{kk}L_{kk}\kappa_{jj}L_{jj}\right)}\right)} \tag{B.2}$$

for $K = 2, 3$.

Eq. (B.2) shows that the rates related to recovery (γ), rewiring (w), link decay (ν) and node decay (μ) all increase the threshold β^c, while the birth rates of nodes (λ) and links (κ) decrease it. The latter implies that there more potential contacts there are, the less infectious a disease needs to be to spread through the population.

Similarly, we can identify the critical rewiring rate for which the disease-free equilibrium becomes unstable.

PROPOSITION 2. *The critical value of the rewiring rate w for which the disease-free equilibrium becomes unstable is given by*

$$w^c = \frac{\beta\lambda}{2\mu(\nu+2\mu)}\left(\sum_{k=1}^{K}\kappa_{kk}L_{kk} + \sqrt{\left(\sum_{k=1}^{K}\kappa_{kk}L_{kk}\right)^2 + 4\sum_{k=1}^{K}\sum_{j=k+1}^{K}\left(\kappa_{kj}^2 L_{kj}^2 - \kappa_{kk}L_{kk}\kappa_{jj}L_{jj}\right)}\right) - c, \tag{B.3}$$

where $c = \gamma + \nu + 2\mu$ and $K = 2, 3$.

Eq. (B.3) illustrates that the critical rewiring rate w^c is increasing with the infection rate β. Thus, the more infectious the disease, the higher the rewiring of links away from infectious individuals needs to be to prevent the disease from spreading.

C. Uniform Lockdowns

For simple cases, we can derive analytic properties of the resulting optimization problem stated in Eq. (11). For the purpose of illustration we consider in the following two groups ($|\mathcal{K}| = 2$), a uniform policy where $L^l_{kj} = L \in [0, 1]$, and a monotonic increasing cost function $C(\cdot)$ with $C'(\cdot) > 0$. The planner's problem can then be written as

$$\min_{L\in[0,1]} C(1-L)$$
$$\text{s.t. } \frac{\beta}{2}\left(\frac{m(S_1,S_1)}{S_1} + \frac{m(S_2,S_2)}{S_2} + \sqrt{\left(\frac{m(S_1,S_1)}{S_1} - \frac{m(S_2,S_2)}{S_2}\right)^2 + \frac{4m(S_1,S_2)^2}{S_1S_2}}\right) L \leq c,$$

where $c = \gamma + w + \nu + 2\mu$ and the inequality constraint comes from the requirement that the eigenvalues of the Jakobian of the dynamic system at the disease-free equilibrium are non-negative. The constraint is binding, and solving for L where the eigenvalue is zero yields

$$L^* = \frac{2(\gamma+w+\nu+2\mu)}{\beta}\left(\frac{m(S_1,S_1)}{S_1} + \frac{m(S_2,S_2)}{S_2} + \sqrt{\left(\frac{m(S_1,S_1)}{S_1} - \frac{m(S_2,S_2)}{S_2}\right)^2 + \frac{4m(S_1,S_2)^2}{S_1S_2}}\right)^{-1} \tag{C.1}$$

Further, inserting $[S_k, I_k,\ m(S_k,S_j),\ m(I_k,S_j)] = [\lambda/\mu, 0, \frac{\kappa_{kj}}{\nu+2\mu}\ \frac{\lambda^2}{\mu^2}, 0]$ and $m(S_k,S_j)\ /S_k = m(S_k,S_j)/S_j = \frac{\kappa_{kj}}{\nu+2\mu}\ \frac{\lambda}{\mu}$ in Equation (C.1) gives

$$L^* = \frac{2(\gamma+w+\nu+2\mu)(\nu+2\mu)\mu}{\beta\lambda}\left(\kappa_{11}+\kappa_{22}+\sqrt{(\kappa_{11}-\kappa_{22})^2+4\kappa_{12}^2}\right)^{-1} \tag{C.2}$$

In the special case of $m(S_1,S_2)^2 = m(S_1,S_1)m(S_2,S_2)$, as would occur if the initial population is "well-mixed" as in typical SIR models, the optimal lockdown is then given by

$$L^* = \frac{(\gamma+w+\nu+2\mu)(\nu+2\mu)\mu}{\beta\lambda(\kappa_{11}+\kappa_{22})}. \tag{C.3}$$

We next analyze the sensitivity of the optimal lockdown policy L^* with respect to the rewiring rate w. From Equation (C.3) we find that

$$\frac{\partial L^*}{\partial w} = \frac{1}{\frac{\beta\lambda\kappa_{11}}{(\nu+2\mu)\mu} + \frac{\beta\lambda\kappa_{22}}{(\nu+2\mu)\mu}}, \tag{C.4}$$

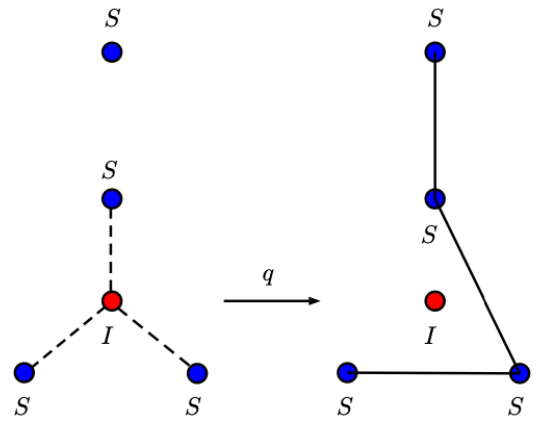

FIGURE D.1. Self-quarantine, at rate q per I node. Blue denotes susceptible nodes (S) and red denotes infectious nodes (I).

where $m(S_k, S_k)/S_k = \lambda\kappa_{kj}/\mu(\nu + 2\mu)$ is the average degree of susceptible type k nodes among the same type k nodes. Thus, the lockdown intensity L^* and the rewiring rate w are substitutes at a rate that is the inverse of the sum of the infection rate β times the average degree of susceptible type k nodes among the same type k nodes.

D. Self-Quarantine

We assume that at a rate $q > 0$ an infectious individual self-quarantines and all the links of this individual to susceptible individuals get rewired to other susceptible individuals at random. An illustration is shown in Figure D.1. In the case of self-quarantine of an infectious in group k, the average number of layer l links that get rewired is $m^l(I_{k'}, S_k)/I_k$. Summing over all infectious in group k gives a total of $m^l(I_{k'}, S_k)$ rewired layer l links per capita. Further, summing over all groups yields a total of $\sum_{k'\in\mathcal{K}} m^l(I_{k'}, S_k)(t)$ layer l links per capita. With uniform rewiring the proportion of links that go to susceptibles in group k is the proportion of susceptibles in group k in the total population of susceptibles. The increase in the density of links in layer l between susceptibles in groups k' and k from susceptibles in group k' by self-quarantines and rewiring is then given by

$$q \times \frac{S_k(t)}{\sum_{k'\in\mathcal{K}} S_{k'}(t)} \sum_{k'\in\mathcal{K}} m^l(I_{k'}, S_k)(t) L^l_{k'k}. \tag{D.1}$$

The dynamics for the fraction of links between susceptibles–susceptibles and susceptibles–infectious is then given by Eqs. (6) and (7) when replacing the rewiring rate w with the

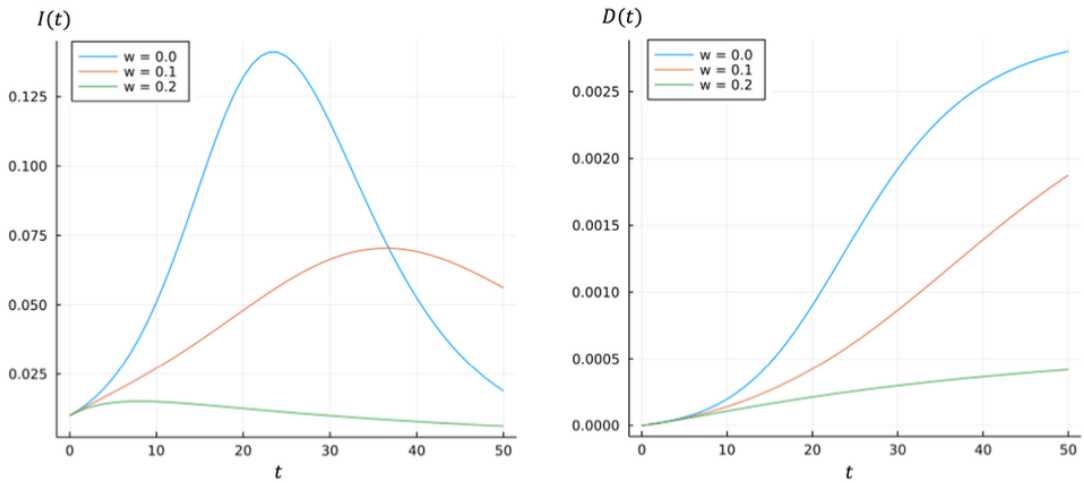

FIGURE E.1. Effect of rewiring on disease dynamics. The left panel shows paths of infections, $I(t)$. The right panel shows time paths of deaths, $D(t)$. Parameters are: $\beta = 0.038, \gamma = 0.2, w \in \{0, 0.1, 0.2\}, \delta^r = 0.19, \delta^d = 0.01, \iota = 0.076$, S(0) $= 0.99$, $I(0) = 0.01$, $R(0) = 0.0$ and average degree $\overline{d} = 10$.

self-quarantine rate q, while the dynamics for the fraction of susceptible, infectious, recovered, hospitalized and deaths over time is given by Eqs. (1), (2), (3), (4) and (5), respectively. The reason for this equivalence is that the mean field dynamics in these differential equations describing the network evolution represent population averages that do not discriminate between synchronous (in the case of self-quarantine) or asynchronous rewiring of links.

E. Additional Simulation Results

E.1. The Effect of Rewiring

Figure E.1 demonstrates the effect of rewiring on infections and deaths numerically from solving the ODEs in Equations (1) to (7). Parameters are calibrated as in typical SIR models of Covid-19 following Ferguson et al. (2020) and Acemoglu et al. (2021) – β is set to 0.038 (which corresponds to an effective reproduction number of $\mathcal{R}_0 = 1.9$) with an average recovery time of five days ($\gamma = 0.2$). Time is in days. The initial contact network is an Erdős-Rényi random network with a mean degree of 10.

Without rewiring, we see the usual SIR epidemic dynamics in Figure E.1. Infections initially take off sharply, reach a peak in around 25 days, and then decline quickly. As the rewiring rate increases, infections take off more slowly. Susceptibles adjust links to avoid the infectious. Thus, it takes longer for any given susceptible to become infectious. This spreads out the total

case load. Infections peak later than with no rewiring, and at a lower value. With a 10 percent rewiring rate, number of infectious peaks over 10 days later than with no rewiring, and at half the level than with no rewiring.

If the rewiring rate is high enough, rewiring can prevent the disease from spreading. Susceptibles separate their links with the infectious fast enough that the contact network separates into two components – a component containing infectious but no susceptible, and a component containing susceptible but no infectious. We see an example of this when the rewiring rate reaches 20 percent. Infections peak very quickly and then slowly fall to zero, long before the entire population becomes infectious. The number of deaths peaks at a small finite amount. Our example shows that rewiring flattens the curve of infections over time by reducing contacts between susceptible and infectious. Consequently, the higher the rewiring rate, the fewer deaths there will be from the epidemic before it dies out.[20]

E.2. Single-Group and Layer Epidemic and Network Dynamics

Figure E.2 shows a comparison from our system of ODEs in Equations (1) to (6) to the average from Monte-Carlo simulations of the jump process using the *next reaction method* also known as Gibson-Bruck algorithm (cf. e.g. Anderson (2013) and Wilkinson (2018)). We see that the averages across realisations of the jump process match our ODEs well, even for a relatively small network size.

E.3. Multi-Group Epidemic and Network Dynamics

Figure E.3 shows a comparison of mean-field ODEs for the epidemic dynamics in Eqs. (1), (2)„ (3), (4)„ (5), and the network dynamics in Eqs. (6) and (7) with mean jump-process dynamics. We see that the averages across realisations of the jump process match our ODEs well, even for a relatively small network.

E.4. Vital Dynamics: Births and deaths of individuals and links

In Figure E.4 we compare the dynamics of a numerical simulation of the stochastic block model initialized with an empty network to our ODEs in Eqs.(1), (6) and (7), respectively.

20. Note, however, that rewiring differs from severing links (e.g. due to self quarantine; cf. Section D) as it changes the structure of the network while preserving the network density. Around the parameter values where the disease-free equilibrium becomes unstable, this can lead to multiple waves of infection. Susceptibles rewire at a fast enough rate to slow the spread of disease, creating clusters of susceptibles connected by a few links to infectious. Once the disease reaches these clusters, infections increase again as the disease spreads between the densely connected susceptibles (cf. Gross et al. 2006).

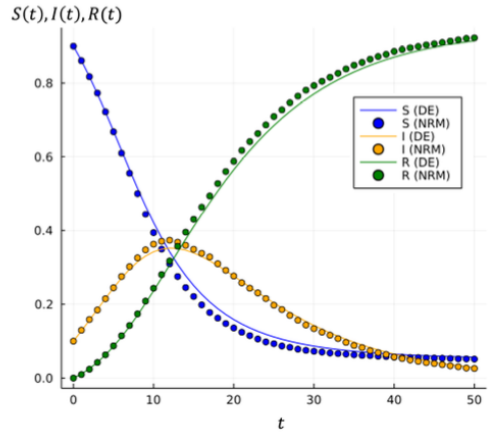

FIGURE E.2. Comparison of mean-field ODEs for the epidemic dynamics in Eqs. (1), (2), (3), (4), (5), and the network dynamics in Eqs. (6) and (7) with mean jump-process dynamics. DE denotes paths from system of ODEs. NRM denotes means from Monte-Carlo simulation of jump process using the next-reaction method. For the jump-process we generate 30 simulations with 240 nodes. The initial conditions are $S(0) = 0.9$, $I(0) = 0.1$, $R(0) = 0.0$, $m(S, S)(0) = 4.05$, and $m(I, S)(0) = 0.9$. The parameters used are $\beta = 0.06$, $\gamma = 0.1$ and $w = 0.1$.

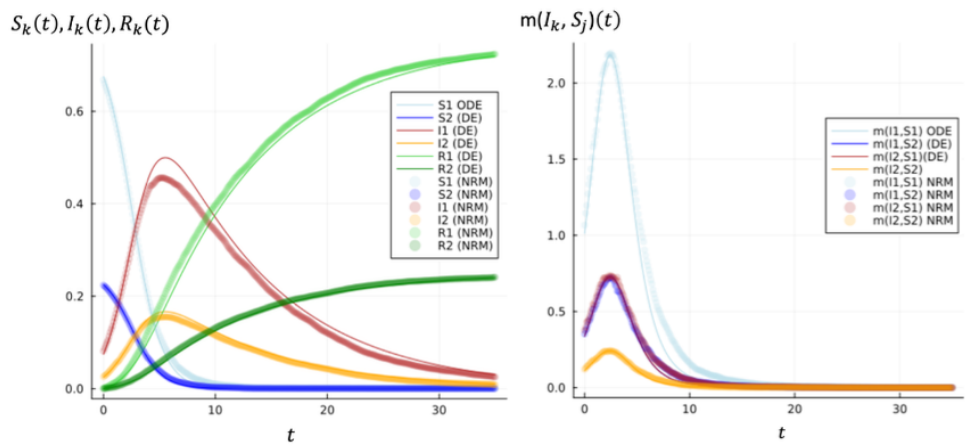

FIGURE E.3. Comparison of mean-field ODEs for the epidemic dynamics in Eqs. (1), (2), (3), (4), (5), in the left panel, and the network dynamics in Eqs. (6) and (7) in the right panel with mean jump-process dynamics for multiple groups. DE denotes paths from system of ODEs. NRM denotes means from Monte-Carlo simulation of jump process using the next-reaction method. For the jump-process we average across 15, respectively, 40 simulations with 400 nodes, 300 in group 1 and 100 in group 2, drawing a different network from the Erdős-Rényi distribution $G(400, 0.05)$ on each run. Initial conditions are $S_1(0) = 0.9 \times 0.75$, $S_2(0) = 0.9 \times 0.25$, $I_1(0) = 0.1 \times 0.75$, $I_2(0) = 0.1 \times 0.25$, $R_1(0) = 0.0$, $R_1(0) = 0.0$, $m(S_i, S_j)(0) = 20 \times S_i(0) \times S_j(0)$, and $m(I_i, S_j)(0) = 20 \times I_i(0) \times S_j(0)$. The parameters used are $\beta = 0.048$, $\gamma = 0.174$ and $w = 0.025$.

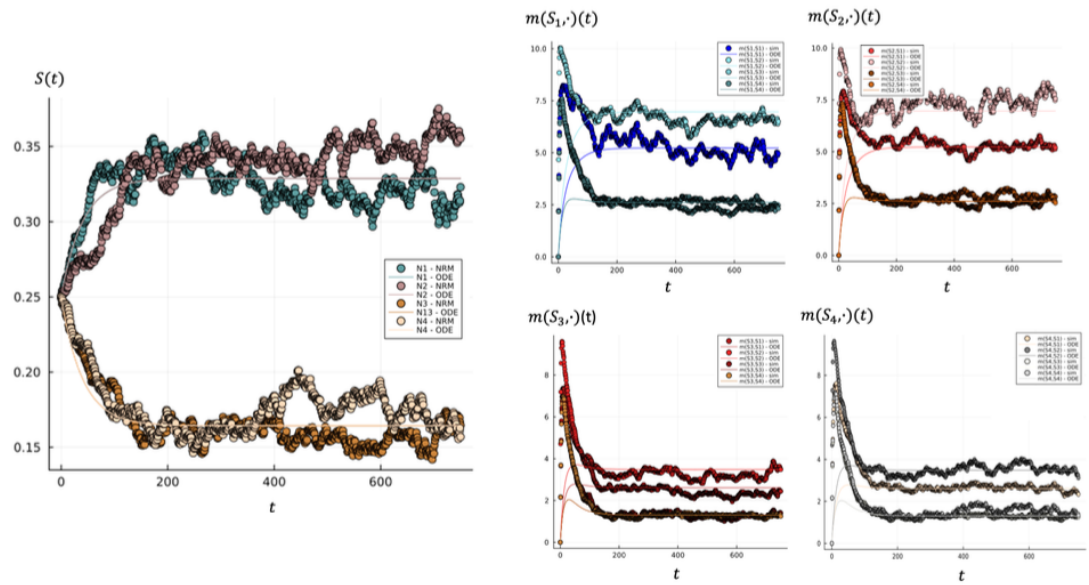

FIGURE E.4. Comparison of the total number of links from the ODEs in Eqs. (1), (6) and (7) with the mean jump-process dynamics for a stochastic block model with four types. DE denotes paths from system of ODEs. NRM denotes averages from Monte-Carlo simulations of the jump process using the next-reaction method.

We see that both converge to the same stationary state, illustrating that the ODEs represent the mean dynamics of the jump process with link creation according to the stochastic block model well.

E.5. Full Network Dynamics

In the background of the model defined by Eqs. (1), (2), (3), (4), (5), (7), (6), there is a larger set of link dynamics including changes in links between infectious and infectious, and changes in links between the recovered and all other compartments. In the model analyzed in the main text, we ignore the latter for tractability. Here, we show that this simplified system can sufficiently describe the full dynamic epidemic process. The full set of ODEs governing

the network dynamics (considering only one group and one layer for simplicity) are:

$$\begin{aligned}
\frac{dm(S,S)}{dt} &= wm(I,S)(t) - 2\beta\frac{m(I,S)(t)m(S,S)(t)}{S(t)},\\
\frac{dm(I,S)}{dt} &= \beta\frac{m(I,S)(t)}{S(t)}\left(2m(S,S)(t) - m(I,S)(t)\right) - (\gamma+w)m(I,S)(t),\\
\frac{dm(I,I)}{dt} &= \beta\frac{m(I,S)(t)m(I,S)(t)}{S(t)} - 2\gamma m(I,I)(t),\\
\frac{dm(I,R)}{dt} &= 2\gamma m(I,I)(t) + \beta\frac{m(I,S)(t)m(S,R)(t)}{S(t)} - \gamma m(I,R)(t)\\
\frac{dm(S,R)}{dt} &= \gamma m(I,S)(t) - \beta\frac{m(I,S)(t)m(S,R)(t)}{S(t)},\\
\frac{dm(R,R)}{dt} &= \gamma m(I,R)(t).
\end{aligned} \tag{E.1}$$

The first two lines in Equation (E.1) correspond to Equations (7) and (6), in the main text, respectively. The rest describe the changes in links between infectious and infectious, and recovered and others. We see that changes in links between susceptibles and susceptibles, and between susceptibles and infectious, do not depend on any of the other quantities. Thus, we can safely ignore all but the first two equations. A comparison of the simulations of the jump process to full network dynamics of the ODEs in (E.1) can be seen in Figure E.5. To validate these equations, we simulate our jump process as in the main text keeping track of all of the link densities, and compare the results to Eq. (E.1). We show the results in Figure E.5 illustrating that our differential equations match the jump process well.

E.6. Rewiring to All Non-Infectious

One could more generally assume that susceptible individuals rewire links to all non-infectious individuals, not just other susceptibles. Then, susceptible rewire links away from infectious neighbours to other susceptibles and recovered, not just other susceptibles as we have assumed in the main text. Here, we show that which we choose makes little difference until the fraction of recovered in the population is very high. In this case our model is defined by Eqs. (1), (2), (3), (4), (5) plus

$$\frac{dm(S,S)}{dt} = w\frac{S(t)}{S(t)+R(t)}m(I,S)(t) - 2\beta\frac{m(I,S)(t)m(S,S)(t)}{S(t)}, \tag{E.2}$$

$$\frac{dm(I,S)}{dt} = \beta\frac{m(I,S)(t)}{S(t)}\left(2m(S,S)(t) - m(I,S)(t)\right) - (\gamma+w+q)m(I,S)(t), \tag{E.3}$$

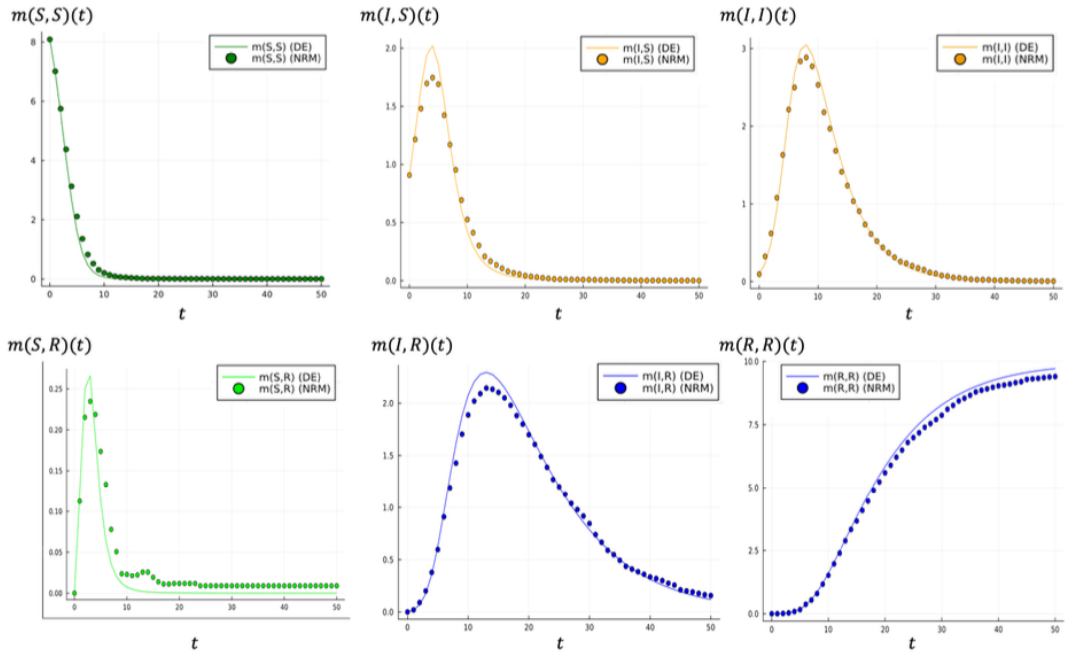

FIGURE E.5. Comparison of the simulations of the jump process to full network dynamics. For the jump-process we generate 20 simulations with 600 nodes. DE denotes paths from system of ODEs in (E.1). NRM denotes means from Monte-Carlo simulation of jump process using the next-reaction method. The initial conditions are $S(0) = 0.9$, $I(0) = 0.1$, $R(0) = 0.0$, $m(S,S)(0) = 4.05$, and $m(I,S)(0) = 0.9$. The parameters used are $\beta = 0.12$, $\gamma = 0.1$ and $w = 0.0$.

in liu of Eqs. (6) and (7). We see that when $R(t)$ is small, then $\frac{S(t)}{S(t)+R(t)} \approx \frac{S(t)}{S(t)} = 1$. Then the equations above define the same network dynamics as in (6) and (7) in the main text.

To show where this holds in practice, we simulate both the system defined by Eqs. (1), (2), (3), (4), (5), (7), (6) and defined by Eqs. (1), (2), (3), (4), (5), (E.2), (E.3) in Figure E.6. We see that the ODEs only begin to diverge when the proportion of the population who has had the disease is in the region of 30% to 40%, which is unrealistically high for diseases we might consider. Furthermore, the divergence in number of infectious is relatively small. Thus, we can ignore the potential for rewiring to recovered without serious error.

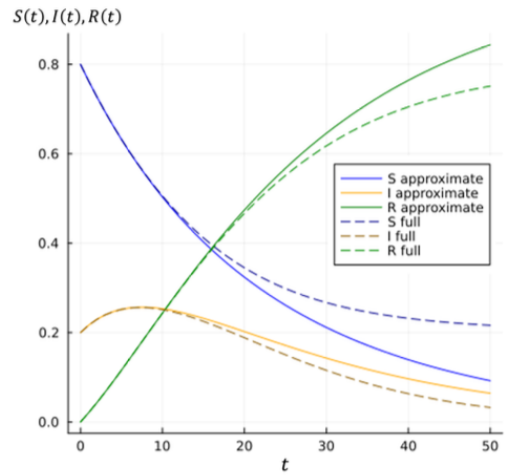

FIGURE E.6. Comparison of disease dynamics with rewiring uniform at random versus to susceptibles. Initial conditions are $S(0) = 0.8$, $I(0) = 0.2$, and $R(0) = 0.0$. Parameters are $\beta = 0.06$, $\gamma = 0.2$, $w = 0.1$, and $\theta = 0.0$.

F. Contact Network and Epidemiological Data

F.1. Social Network Data

We utilize a population-scale social network of the Netherlands created from Statistics Netherlands registry data. A detailed description of various network properties of these data can be found in van der Laan (2022) and Bokányi et al. (2023). Our network contains each of the 17.26 million individuals in the population register of the Netherlands as of 2018.[21] There are five layers, each encoding a different type of connection between two individuals: family connections, work connections, household connections, school connections, and neighbourhood connections.

Family connections represent all family members up to the second degree (cousins, grandparents, or closer). Work connections represent all colleagues at the same workplace. Household connections represent individuals who are registered at the same address. School connections represent individuals who attend the same school, university, or university of applied sciences, in the same program and the same year-group. Next-door neighbourhood connections connect individuals to the individuals in the 10 nearest households to each

21. We use data from 2018 as it is the closest available to the beginning of the Covid-19 pandemic at the time of analysis. It is worth noting that existing contact surveys used for epidemiological analysis are carried out in 2005.

individual. Data was pseudonymized before analysis, ensuring privacy of the individuals, and no personally identifiable information was used. All analysis involving this data took place within the secure server environment of Statistiscs Netherlands. Between the layers, the network captures the potential contacts of each individual in the Netherlands. There are 827 million links between all of the layers.

F.2. Constructing a Population-Level Contact Network

We reweight each layer based on results from the POLYMOD contact survey for flu-like infectious diseases (Mossong et al. 2008) – a set of nationally representative contact surveys for flu-like infectious diseases undertaken across a range of European countries in 2005-2006. These are the standard contact datasets used in mathematical modelling of Covid-19. Participants record daily contacts sufficient to spread a flu-like infectious disease in a contact diary on randomly assigned days.[22] Individuals record the age of the contact, and the setting in which it occurred. There are six possible settings: 'within the home', 'at work', 'at school', 'in transport', 'during leisure activities', and 'other'. Contact matrices are smoothed averages of reported contact numbers using tensor splines. The mean number of contacts per subject per day is 14.

We start by matching each type of contact in POLYMOD to a layer in our social network data. We assume that contacts within the home occur with members of the household, work contacts occur with work colleagues, and school contacts with individuals at the same school or university. We assume that leisure contacts occur with family members, and contacts during transport and other activities occur with individuals in the same neighbourhood.[23]

We then weight each link in each layer in our social network data the mean number connections per individual in that layer matches the average number of contacts in the respective setting per day in POLYMOD. The resulting weights encode the probability that a given link between individuals is sufficient to spread Covid-19 each day.

Our procedure gives us a weighted contact network. Each node is an individual in the population of the Netherlands. Each edge encodes the probability that those two individuals will have a contact sufficient to spread a flu-like infectious disease on a given day.

For tractability, we aggregate links by municipality to generate a municipality-municipality contact network. The Netherlands is split into 380 such municipalities. An example is the city

22. One individual has a contact with another if they either have skin-to-skin contact or a two-way conversation consisting of three or more words in the presence of each other.

23. As we then aggregate the network to the municipality level, in practice we only have to assume that these contacts occur with individuals within the same municipality.

of Amsterdam, which is its own municipality. So we have 380 different types of agents, and a 380×380 municipality-municipality contact network. The weight from municipality i to municipality j is the expected number of contacts sufficient to spread a flu-like infectious disease between individuals in municipality i and municipality j. Aggregation further ensures the privacy of individuals within our data, as it is impossible to recover individual links from the aggregated data.

F.3. Epidemiological data

We use data on daily cases and deaths from Covid-19 in the Netherlands from 6th of August 2020 to 19th of November 2020. The summer period of the Covid-19 pandemic is an ideal setting to estimate the model and analyse the effect of policy. At the beginning of the first wave of Covid-19, the government of the Netherlands adopted an 'intelligent lockdown' policy. The policy involved encouraging masking, social distancing measures, and closing venues such as schools. These measures became stricter through March and April. During June, the government relaxed many of the measures adopted. By July, they were mostly gone. Our start date of 6th of August corresponds to the reopening of schools and universities. By this time, terraces had been reopened, and restrictions on leisure activities were loosened. At this point, Covid-19 cases were negligible, and a tiny fraction of the population were infectious. Covid-19 cases then began to rise again. Stricter measures began to be reintroduced on October 14, when the government announced some closures to counter the rise in infections. Our end point of 19th of November corresponds to the banning of large gatherings and reintroduction of a work from home order. These measures were extended to a full lockdown from December 15th. A vaccination roll-out began on January 8th 2021. So, during this period, a disease is spreading in the population for a relatively long period with light mitigation and relatively small changes in policy.[24] Light mitigation allows us to get more accurate estimates of the infection rate. Large changes in policy would confound our estimates. The time period is short enough that we do not have to worry about large amounts of reinfections. Thus, a model without reinfection is still appropriate.

Data comes from the Institute for Public Health and the Environment (RIVM) of the Netherlands. To reduce the effect of noise and reporting patterns, we construct 7-day rolling averages of both series.

Reported cases depends on the individuals who get official Covid-19 tests, which is highly heterogeneous by age. To account for this, we map cases into eight discrete age-groups

24. See Ainslie et al. (2022) for full description of all of the changes in policy by the Dutch government over the pandemic.

corresponding Ainslie et al. (2022). We then use the case reporting rates for the Netherlands in Ainslie et al. (2022) to transform reported case counts to actual case counts.

The relation between reported deaths and actual infectious depends on both the infection fatality ratio and the rate that deaths from Covid-19 are correctly reported. To correct for this, we reweigh the series of aggregate deaths to match the average proportion of infectious in the population in the first two weeks where the series overlaps with the Covid-19 infection radar surveys. This is a web-based weekly survey designed to detect the proportion of individuals with Covid-19 in the populations. After recruitment, individuals report potential Covid-19 symptoms each week, and the results of any tests. These are the most reliable measure of the proportion of the population infectious in the Netherlands at any given time.

G. Identification and Estimation Algorithm

G.1. Aggregate Dynamics

Note that, for K groups, we have a system of $2K^2 + 3K$ non-linear differential equations. As the number of groups grows, the size of the system quickly becomes uncomfortably large to solve. For example, if we consider each Wijken (the spatial division below municipality) in the Netherlands as a single group, we have 3098 groups, giving a system of $19,204,502$ differential equations. In our main specification, where we consider each municipality in the Netherlands as a single group, we have 380 groups, giving a system of $289,940$ differential equations. Furthermore, the quantities in each disease compartment are shares in the population. Thus, as the number of groups becomes large, the proportion of the population within each compartment becomes very small. This leads to serious numerical error in solutions and gradients of the solution with respect to parameters if we try to take our system to data directly.

To solve this problem, we note that we also can describe the aggregate dynamics of our the system with our system of ordinary differential equations with one group and the same parameters. We formalize this result in the lemma below.

LEMMA 1. *For each system*

$$\{S_k(t), I_k(t), R_k(t), m(S_k, S_{k'})(t), m(I_k, S_{k'})(t)\}_{t=0,k,k' \in \mathcal{K}}^{T}$$

following Eqs. (1), (2), (3), (4), (5), (6) and (7) there is a unique equivalent representation

$$\{\sum_{k \in \mathcal{K}} S_k(t), \sum_{k \in \mathcal{K}} I_k(t), \sum_{k \in \mathcal{K}} R_k(t), \sum_{j,k \in \mathcal{K}} m(S_j, S_k)(t), \sum_{j,k \in \mathcal{K}} m(I_j, S_k)(t)\}_{t=0}^{T}$$

with mean-field dynamics that can be described by the single-group Eqs. (1), (2), (3), (6) and (7).

The size of the system with one group is independent of the number of groups. Therefore, we can solve this system regardless of the number of groups in our data.

G.2. Identification with Latent Network Dynamics

Our second problem is that we do not observe the number of links between infectious and susceptibles and the number of links between susceptibles over time. These network dynamics are latent. We only observe an initial condition, coming from our population-level contact network.

We solve this in two steps. First, we use the number of reported new deaths are a sufficient statistic for the number of infectious conditional on the infection-fatality ratio and death reporting rate. From Equation (5), we have that

$$\frac{dD_k}{dt} = \lambda_d \iota_k \delta_{dk} I_k(t)$$

where $\iota_k \delta_{dk}$ is the group-specific infection-fatality ratio. Then, we have that

$$\sum_{k \in \mathcal{K}} \frac{\Delta D_k(t)}{\lambda_d \iota_k \delta_{dk}} = \sum_{k \in \mathcal{K}} I_k(t).$$

New cases are a sufficient statistic for the density of links between infectious and susceptible conditional on the case reporting rate λ_c. We can write the total number of new cases

$$\begin{aligned} C(t) &= \lambda_c \sum_{k \in \mathcal{K}} \left(\frac{dI_k}{dt} + \gamma I_k(t)\right) \\ &= \lambda_c \left(\beta \sum_{k,j \in \mathcal{K}} m(I_k, S_j)(t) - \gamma I_k(t) + \gamma I_k(t)\right) \\ &= \lambda_c \beta \sum_{k,j \in \mathcal{K}} m(I_k, S_j)(t). \end{aligned}$$

Conditional on a value of λ_c, each β defines a one-to-one mapping between the number of cases and the number of infectious susceptible links in the population.

G.3. GMM Estimation

We apply a Generalized Method of Moments (GMM) approach to estimate the parameters of our Markov diffusion process (cf. Hansen and Scheinkman 1995). Define

$$\begin{bmatrix} X^N(\theta,1) \\ X^N(\theta,2) \\ \vdots \\ X^N(\theta,t) \\ \vdots \\ X^N(\theta,T) \end{bmatrix} = \begin{bmatrix} S^N(\theta,1) & I^N(\theta,1) & R^N(\theta,1) & m^N(S,S)(\theta,1) & m^N(I,S)(\theta,1) \\ S^N(\theta,2) & I^N(\theta,2) & R^N(\theta,2) & m^N(S,S)(\theta,2) & m^N(I,S)(\theta,2) \\ \vdots & \vdots & \vdots & \vdots & \vdots \\ S^N(\theta,t) & I^N(\theta,t) & R^N(\theta,t) & m^N(S,S)(\theta,t) & m^N(I,S)(\theta,t) \\ \vdots & \vdots & \vdots & \vdots & \vdots \\ S^N(\theta,T) & I^N(\theta,T) & R^N(\theta,T) & m^N(S,S)(\theta,T) & m^N(I,S)(\theta,T) \end{bmatrix}$$

as the $T \times 5$ matrix of a single realisation from our jump process with sample size N. Write this compactly as

$$X^N(\theta) = (S^N(\theta), I^N(\theta), R^N(\theta), m^N(S,S)(\theta), m^N(I,S)(\theta)). \tag{G.1}$$

Let

$$Y^N(\theta) = [S^N(\theta), I^N(\theta), m^N(I,S)(\theta)]$$

be the $T \times 3$ matrix of the first, second, and fifth series in X^N. Define

$$X(\theta) = [S(\theta), I(\theta), R(\theta), m(S,S)(\theta), m(I,S)(\theta)]$$

as the $T \times 5$ matrix of the solution to Eqs. (1), (2), (3), (7), (6) given an initial condition for the full state space

$$X(0) = [S(0), I(0), R(0), m(S,S)(0), m(I,S)(0)]$$

and a parameter θ. Let

$$Y(\theta) = [S(\theta), I(\theta), m(I,S)(\theta)].$$

Define the functions

$$\hat{Q}_N(\theta) = -||Y(\theta) - Y^N(\theta_0)||_{2,1}$$

and

$$Q_0(\theta) = -||Y(\theta) - Y(\theta_0)||_{2,1}$$

where $||.||_{2,1}$ denotes the $L_{2,1}$ matrix norm.[25] Writing the norm explicitly, we have

$$||Y(\theta) - Y^N(\theta_0)||_{2,1} = ||S(\theta) - S^N(\theta_0)||_2 + ||I(\theta) - I^N(\theta)||_2 + ||m(I,S)(\theta) - m^N(I,S)(\theta_0)||_2.$$

where $||.||_2$ denotes the Euclidean norm, i.e. $||x||_2 = \sqrt{x_1^2 + \ldots + x_n^2}$. Given the above, the GMM estimator of parameters is unbiased and consistent.

PROPOSITION 3. *Let* $\hat{Q}_N(\theta) = -||Y(\theta) - Y^N(\theta_0)||_{2,1}$ *with* $Y^N(\theta) = [S^N(\theta),\ I^N(\theta),\ m^N(I,S)(\theta)]$ *from the jump process with sample size* N *and* $Y(\theta) = [S(\theta), I(\theta), m(I,S)(\theta)]$ *from the solution to Eqs. (1), (2) and (6). Assume that the fraction of susceptibles in the population is bounded away from zero. Then*

$$\hat{\theta} = max_{\theta \in \Theta} \hat{Q}_N(\theta)$$

is a consistent estimator of θ_0.

To correct for autocorrelation in deviations from sample moments we follow Newey and McFadden (1994) and Den Haan and Levin (1996), and estimate the variance-covariance matrix of $\hat{\theta}$ as

$$V(\hat{\theta}) = (DD')^{-1} D \hat{\Sigma} D' (DD')^{-1},$$

where

$$D = \frac{\partial (Y(\theta) - Y^N(\theta_0))}{\partial \theta}|_{\theta = \hat{\theta}},$$

Further, we compute $\hat{\Sigma}$ non-parametrically using a Newey–West estimator with a bandwidth of 7 days. We pick a bandwidth of 7 days to correspond to the smoothing we apply to the data. We checked robustness by experimenting with bandwidths of up to 14 days. Rejection of tests at the given critical values are robust to all of these bandwidth selections.

H. Additional Counterfactual Results

In the following sections we discuss additional counterfactuals assuming w.l.o.g. a single layer. First, in Section H.1 we discuss the gains of a spatially targeted lockdown policy over a uniform policy. Next, in Section H.2 we evaluate how rewiring can increase the contacts allowed over a targeted policy without rewiring. Further, in Section H.3 we relate the optimal targeted

25. The $L_{2,1}$ norm is the sum of the Euclidean norms of the columns of the matrix $A = [a_{ij}]$: $\|A\|_{2,1} = \sum_{j=1}^{n} \left(\sum_{i=1}^{m} |a_{ij}|^2\right)^{1/2}$.

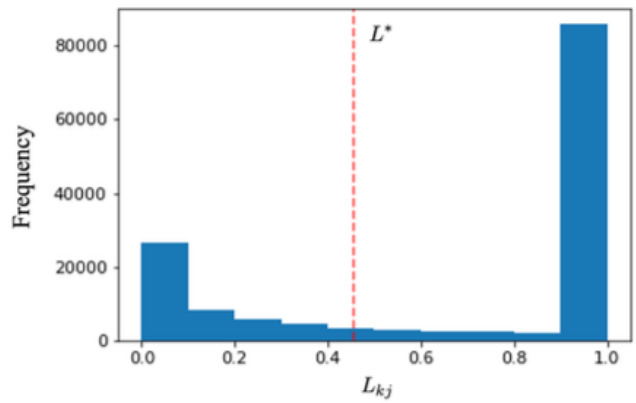

FIGURE H.1. Targeted lockdowns by municipality-municipality pair, L_{kj}, for Covid-19 in the Netherlands with estimated parameters (Table 1). The dashed line gives the optimal uniform lockdown level L^* (cf. Online Appendix C).

policy to various centrally measures considered in the epidemiological literature. In Section H.4 we consider a more fine grained spatial targeting policy (at the "Wijken" level). Finally, in Section H.5 we also distinguish between different age groups in the planners' optimal targeting problem.

H.1. Targeted vs. Uniform Lockdowns

Targeted policies are more efficient because the optimal reductions in contacts between pairs of municipalities are highly heterogeneous. Figure H.1 plots the distribution of the proportions of contacts the planner allows between all possible pairs of municipalities. We see that the planner allows all, or almost all, contact between most pairs of municipalities. But, the planner should reduce contact between a small, but sizeable, set of municipalities to almost zero. By contrast, the optimal uniform policy must reduce contacts between municipalities by the same amount (cf. Online Appendix C).

H.2. Targeted Lockdowns with and without Rewiring

Considering the spatial distribution of the shares of contacts allowed across the Netherlands reveals that optimal targeted lockdowns are highly heterogeneous across space. Figure H.2 plots the share of contacts allowed by the planner by municipality with and without rewiring. Connections coming into some municipalities are reduced much more than connections into

(A) Without rewiring

Table: Ten most targeted municipalities without rewiring.

Municipality (k)	Share contacts allowed ($\sum_{j \in \mathcal{K}} L_{kj}$)	Rank
Urk	0.3837	1
Midden-Groningen	0.4957	2
Ede	0.5142	3
Barneveld	0.5143	4
Rijssen-Holten	0.5192	5
Katwijk	0.5207	6
Utrecht	0.5232	7
Zwolle	0.5267	8
Groningen	0.5344	9
Amersfoort	0.5364	10

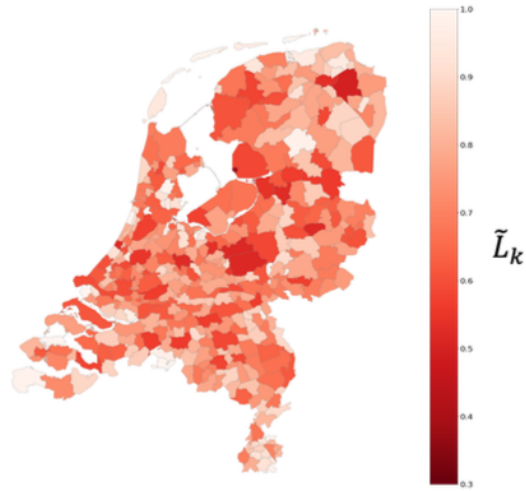

(B) With rewiring

Table: Ten most targeted municipalities with estimated rewiring

Municipality (k)	Share contacts allowed ($\sum_{j \in \mathcal{K}} L_{kj}$)	Rank
Urk	0.4315	1
Midden-Groningen	0.5649	2
Barneveld	0.5808	3
Rijssen-Holten	0.5884	4
Ede	0.5889	5
Katwijk	0.5908	6
Utrecht	0.5988	7
Zwolle	0.6034	8
Amersfoort	0.6127	9
Groningen	0.6134	10

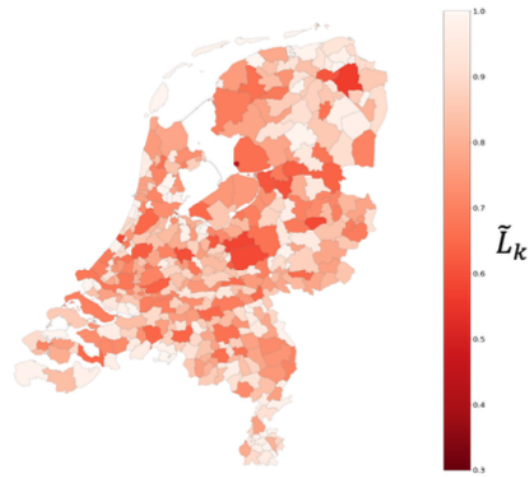

FIGURE H.2. Optimal spatially targeted lockdowns from Covid-19 in the Netherlands using estimated parameters from the second wave of Covid-19 (Table 1). The lightest color denotes the most contacts allowed, and the darkest denotes the fewest contacts allowed. Panel (A) shows the optimal targeted solution without rewiring and panel (B) with rewiring. Tables show the ten most targeted municipalities in each case.

others. This illustrates that optimal targeting based on the network structure leads to heterogeneous targeting across space, because contacts are highly heterogeneous across space.

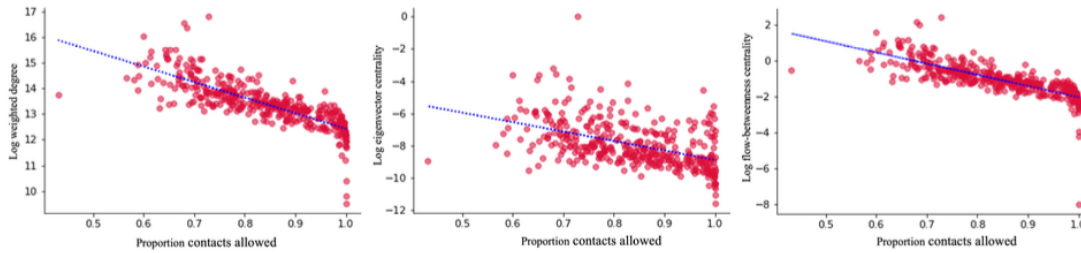

FIGURE H.3. Relationship between centrality measures and optimal lockdown levels. The left panel shows the proportion of original contacts the planner allows by municipality ($\sum_{j \in \mathcal{K}} L_{kj}$) against the natural logarithm of the degree centrality, the middle panel the log eigenvector centrality and the right panel the flow-betweenness centrality (Brandes and Fleischer 2005).

H.3. Targeted Lockdowns and Network Centrality

Optimal lockdowns reduce contacts into moderately sized cities (Groningen, Utrecht, Tilburg, Nijmegen), and small municipalities that are densely connected within the municipality (Urk, Katwijk, Midden-Groningen), the most. This accords with their positions in the network relative to others. Figure H.3 compares the proportion of contacts allowed in a given municipality to various common measures of network centrality in the municipality-municipality contact network. The amount a municipality is targeted is most closely related to its flow-betweenness centrality (Brandes and Fleischer 2005). No centrality measure, however, fully explains our targeting results, which is in line with earlier findings presented by Hedde-von Westernhagen et al. (2024).

The planner does not reduce contacts of individuals in large cities (Amsterdam, Rotterdam, the Hague) the most though the planner does reduce the contacts of individuals in these cities significantly. This is because their large populations make lockdowns between them and others especially costly.

Accounting for rewiring reduces the heterogeneity in contacts allowed between municipalities. This comes because the planner has to target the most targeted municipalities by less. The most targeted municipalities remain the same (though the rank-order is not entirely preserved).

H.4. Wijken-based Targeting

In this section we solve for the optimal spatially targeted mitigation measures at the finest level that we can. There are 3097 "Wijken", which are a subdivision of municipalities. We construct Wijken-Wijken optimal targeted lockdowns L_{ij} weighting the cost of lockdowns by

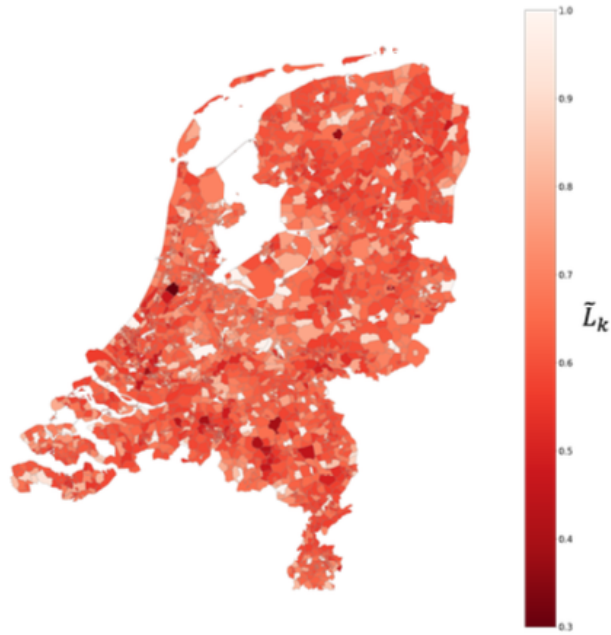

FIGURE H.4. Optimal spatially targeted lockdowns at Wijken level from Covid-19 in the Netherlands using estimated parameters from second wave of Covid-19 (Table 1). Lightest color denotes the most contacts allowed and darkest denotes the fewest contacts allowed.

the size of the population locked down. Our control problem is

$$\begin{aligned} \min_{L_{kj}\in[0,1],\forall k,j\in\mathcal{K}} \quad & -\sum_{k,j\in\mathcal{K}} L_{kj}s_k \\ s.t. \quad & \mathbf{\Omega} \preceq (\gamma+w)\mathbf{I}, \\ & k,j\in\mathcal{K}=\{1,\ldots,3097\}, \end{aligned}$$

where $\mathbf{\Omega}$ is computed with our Wijken-Wijken contact network (cf. Theorem 2), and $s_k \in [0,1]$ is the share of the population in Wijken k. The planner looks to reduce connections between municipalities such that the disease does not become endemic ($\mathcal{R}_0 < 1$) at minimum social cost. The cost of locking down connections between groups is assumed to be increasing linearly in the number of individuals that the planner is locking down. The finer the planner can spatially target, the greater the proportion of contacts they can allow. Total losses move from -322.5 when the planner can target by Gemeente (i.e. municipality) to -462.9 when they can also

target by Wijken in Gemeente that contain large cities (Amsterdam, Rotterdam, Utrecht, 's-Gravenhage), to −1931.75 when targeting by Wijken across the entire country.

H.5. Age-Structured Population

Acemoglu et al. (2021) look at the effect of heterogeneous costs and contacts by age on optimal lockdown policies. We incorporate heterogeneity in costs and contacts by age into our optimal policy problem. Results are qualitatively similar.

We start by constructing Gemeente-Gemeente level contact data partitioned by age. First, we group individuals in the Netherlands into three age categories within each Gemeente. Following Acemoglu et al. (2021), we partition individuals into: 'young' (0–49 years old), 'middle-aged' (50–64 years old), and 'old' (65+ years old). Next, we construct average contacts between age group from POLYMOD (Mossong et al. 2008). Within POLYMOD surveys, individuals record both their own age, the age of their contact, and the setting in which it occurred. There are six possible settings: 'within the home', 'at work', 'at school', 'in transport', 'during leisure activities', and 'other'. We reweight contacts between age-groups and Gemeente based on the average number of contacts between age categories by type of contact.

We construct municipality–age-group-municipality–age-group optimal targeted lockdowns L_{ij} assuming that the cost of locking down connections between groups is increasing linearly in the number of individuals locked down, weighted by differing costs per age category.

As in Acemoglu et al. (2021) we assume that

$$c_k = \begin{cases} 0.26 \text{ if age group } k \text{ is 'old'} \\ 1 \text{ otherwise.} \end{cases}$$

Our resulting control problem is

$$\begin{aligned} \min_{L_{kj}\in[0,1],\forall k,j\in\mathcal{K}} \quad & -\sum_{k,j\in\mathcal{K}} c_k L_{kj} s_k, \\ \text{s.t.} \quad & \boldsymbol{\Omega} \preceq (\gamma + w)\mathbf{I}, \\ & k, j \in \mathcal{K} = \{1, \ldots, 1140\}, \end{aligned}$$

where $\boldsymbol{\Theta}$ is computed with our municipality-age-group by municipality-age-group contact network (cf. Theorem 2), and $s_k \in [0, 1]$ is the share of the population in municipality-age-group pair k.

Figure H.5 shows the optimal policy frontier with and without rewiring. Including age groups leaves the results qualitatively unchanged. Proportions of the population locked down are of course different, because of the differing costs associated with locking down each age group.

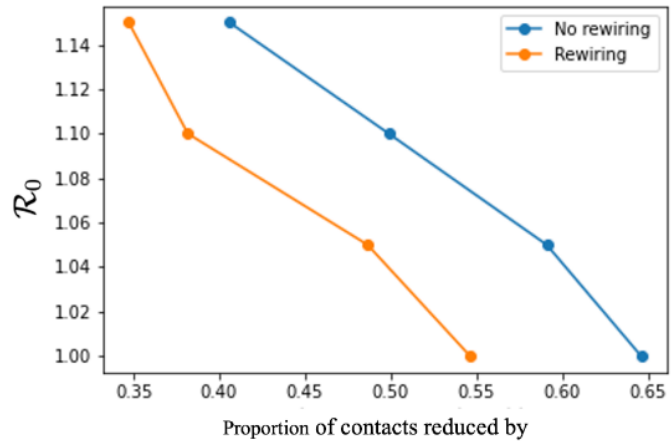

FIGURE H.5. Pareto frontier representing trade-offs between basic reproduction number ($\mathcal{R}_0$) and lockdown intensities (proportion of contacts reduced by) faced by policymakers with heterogeneity by age in contacts and costs of locking down as in Acemoglu et al. (2021). Points represent relaxations $\varepsilon \in \{0, 0.05, \ldots, 0.15\}$.

I. Proofs

We begin by formally stating and proving that the mean-field dynamics of the continuous time Markov process (with transitions corresponding to the events illustrated in Figure 1) can be represented using a system of ordinary differential equations. Before stating the result, we need the following lemma:

LEMMA 2. *Consider* $X(t) = (S(t), I(t), m(I,S)(t), m(S,S)(t))^\top$ *satisfying*

$$\frac{dX}{dt} = F(X), \tag{I.1}$$

with the function $F(X)$ *corresponding to the RHS of Eqs. (1), (2), (6) and (7). Assume that the fraction of susceptibles in the population is bounded away from zero. Then* $F(X)$ *is Lipschitz continuous with respect to* X*.*

Proof of Lemma 2. We have that $X(t) = (S(t), I(t), m(I,S)(t), m(S,S)(t))^\top$ and

$$F(X,t) = \begin{pmatrix} -\beta X_3(t) \\ -\gamma X_2(t) + \beta X_3(t) \\ -\gamma X_3(t) - w X_3(t) + \frac{\beta X_3(t)(2X_4(t) - X_3(t))}{X_1(t)} \\ w X_3(t) - \frac{2\beta X_3(t) X_4(t)}{X_1(t)} \end{pmatrix}$$

To show that $F(X)$ is Lipschitz continuous, we need to prove that there exists a constant $L \geq 0$ such that for any $X, Y \in \mathbb{R}^4$:

$$\|F(X) - F(Y)\|_1 \leq L\|X - Y\|_1.$$

We first calculate $F(X) - F(Y)$. Let $X = (X_1, X_2, X_3, X_4)^\top$ and $Y = (Y_1, Y_2, Y_3, Y_4)^\top$. The difference between $F(X)$ and $F(Y)$ is given by:

$$F(X) - F(Y) = \begin{pmatrix} -\beta(X_3 - Y_3) \\ -\gamma(X_2 - Y_2) + \beta(X_3 - Y_3) \\ -\gamma(X_3 - Y_3) - w(X_3 - Y_3) + \left(\frac{\beta X_3(2X_4 - X_3)}{X_1} - \frac{\beta Y_3(2Y_4 - Y_3)}{Y_1}\right) \\ w(X_3 - Y_3) - \left(\frac{2\beta X_3 X_4}{X_1} - \frac{2\beta Y_3 Y_4}{Y_1}\right) \end{pmatrix}. \tag{I.2}$$

For the first component we get $|-\beta(X_3 - Y_3)| = \beta\,|X_3 - Y_3|$. Clearly, this is Lipschitz with constant β. For the second component we can apply the triangle inequality:[26]

$$|-\gamma(X_2 - Y_2) + \beta(X_3 - Y_3)| \leq \gamma\,|X_2 - Y_2| + \beta\,|X_3 - Y_3|\,.$$

This is Lipschitz with constant $\gamma + \beta$. The third component is given by

$$\left|-(\gamma + w)(X_3 - Y_3) + \frac{\beta X_3(2X_4 - X_3)}{X_1} - \frac{\beta Y_3(2Y_4 - Y_3)}{Y_1}\right|.$$

The first term above can be bounded as follows:

$$|-(\gamma + w)(X_3 - Y_3)| \leq (\gamma + w)|X_3 - Y_3|.$$

For the fraction terms, note that

$$\begin{aligned} \left|\frac{\beta X_3(2X_4 - X_3)}{X_1} - \frac{\beta Y_3(2Y_4 - Y_3)}{Y_1}\right| &= \left|\frac{\beta X_3(2X_4 - X_3)}{X_1} - \frac{\beta Y_3(2Y_4 - Y_3)}{Y_1}\right| \\ &= \left|\frac{2\beta X_3 X_4}{X_1} - \frac{2\beta Y_3 Y_4}{Y_1} + \frac{\beta X_3^2}{X_1} - \frac{\beta Y_3^2}{Y_1}\right| \\ &\leq 2\beta\left|\frac{X_3 X_4}{X_1} - \frac{Y_3 Y_4}{Y_1}\right| + \beta\left|\frac{X_3^2}{X_1} - \frac{Y_3^2}{Y_1}\right| \end{aligned} \tag{I.3}$$

Note that by using the triangle inequality we can write:

$$\left|\frac{X_3 X_4}{X_1} - \frac{Y_3 Y_4}{Y_1}\right| \leq \left|\frac{X_3 X_4}{X_1} - \frac{X_3 Y_4}{Y_1}\right| + \left|\frac{X_3 Y_4}{Y_1} - \frac{Y_3 Y_4}{Y_1}\right|. \tag{I.4}$$

26. The triangle inequality states that for any vectors x and y in a normed vector space, the following holds: $\|x + y\| \leq \|x\| + \|y\|$.

The first term can be factored by X_3: $\left|\frac{X_3X_4}{X_1} - \frac{X_3Y_4}{Y_1}\right| = |X_3| \cdot \left|\frac{X_4}{X_1} - \frac{Y_4}{Y_1}\right| \leq d\left|\frac{X_4}{X_1} - \frac{Y_4}{Y_1}\right|$, where we have assumed that $|X_3|/|X_1| < d$ (i.e. an upper bound on the average degree) and $0 < |X_1| \leq 1$. Next we can write $\left|\frac{X_4}{X_1} - \frac{Y_4}{Y_1}\right| = \left|X_4 \cdot \frac{1}{X_1} - Y_4 \cdot \frac{1}{Y_1}\right|$. Using the distributive property, we expand this into two terms: $\left|X_4 \cdot \frac{1}{X_1} - Y_4 \cdot \frac{1}{Y_1}\right| = \left|X_4 \cdot \frac{1}{X_1} - X_4 \cdot \frac{1}{Y_1} + X_4 \cdot \frac{1}{Y_1} - Y_4 \cdot \frac{1}{Y_1}\right|$. Then, applying the triangle inequality, we get:

$$\left|\frac{X_4}{X_1} - \frac{Y_4}{Y_1}\right| \leq \left|X_4\left(\frac{1}{X_1} - \frac{1}{Y_1}\right)\right| + \left|\frac{1}{Y_1}(X_4 - Y_4)\right|. \tag{I.5}$$

To bound $\left|\frac{1}{X_1} - \frac{1}{Y_1}\right|$, we apply the mean value theorem to the function $f(x) = \frac{1}{x}$, which is differentiable for $x > 0$. By the mean value theorem,[27] for any two points X_1 and Y_1, there exists a point ξ between X_1 and Y_1 such that: $\frac{1}{X_1} - \frac{1}{Y_1} = f'(\xi) \cdot (X_1 - Y_1)$, where $f'(x) = -\frac{1}{x^2}$. Therefore, $\frac{1}{X_1} - \frac{1}{Y_1} = -\frac{1}{\xi^2} \cdot (X_1 - Y_1)$, where ξ is some value between X_1 and Y_1. Taking absolute values, we get: $\left|\frac{1}{X_1} - \frac{1}{Y_1}\right| = \frac{|Y_1 - X_1|}{\xi^2}$. Thus, the first term becomes: $\left|X_4\left(\frac{1}{X_1} - \frac{1}{Y_1}\right)\right| = |X_4| \cdot \frac{|Y_1 - X_1|}{\xi^2}$. If we assume that X_4 is bounded relative to X_1, specifically that $\frac{X_4}{X_1} \leq d$ for some constant d (i.e. an upper bound on the average degree), then we can write $|X_4| \leq d|X_1|$. This gives: $\left|X_4\left(\frac{1}{X_1} - \frac{1}{Y_1}\right)\right| \leq d|X_1| \cdot \frac{|Y_1 - X_1|}{\xi^2}$. If we assume Y_1 is bounded away from zero (say $Y_1 \geq c > 0$), then $\frac{1}{Y_1} \leq \frac{1}{c}$. This gives: $\left|\frac{1}{Y_1}(X_4 - Y_4)\right| \leq \frac{|X_4 - Y_4|}{c}$. Putting it all together in Eq. (I.5), we have: $\left|\frac{X_4}{X_1} - \frac{Y_4}{Y_1}\right| \leq d|X_1| \cdot \frac{|Y_1 - X_1|}{\xi^2} + \frac{|X_4 - Y_4|}{c} \leq \frac{d}{\xi^2}|Y_1 - X_1| + \frac{|X_4 - Y_4|}{c}$, where d is a constant bounding $\frac{X_4}{X_1}$, ξ is a point between X_1 and Y_1, and c is a lower bound for Y_1 to ensure Y_1 does not approach zero, and we have used the fact that $X_1 \leq 1$. Next, note that $\left|\frac{X_3Y_4}{Y_1} - \frac{Y_3Y_4}{Y_1}\right| = \frac{|Y_4|}{|Y_1|} \cdot |X_3 - Y_3|$. If we assume Y_1 is bounded away from zero (say $Y_1 \geq c > 0$), then $\frac{1}{Y_1} \leq \frac{1}{c}$, and we obtain the bound: $\left|\frac{X_3Y_4}{Y_1} - \frac{Y_3Y_4}{Y_1}\right| \leq \frac{|Y_4|}{c} \cdot |X_3 - Y_3| \leq \frac{d}{c} \cdot |X_3 - Y_3|$. This yields for Eq. (I.4) that

$$\begin{aligned}\left|\frac{X_3X_4}{X_1} - \frac{Y_3Y_4}{Y_1}\right| &\leq \left|\frac{X_3X_4}{X_1} - \frac{X_3Y_4}{Y_1}\right| + \left|\frac{X_3Y_4}{Y_1} - \frac{Y_3Y_4}{Y_1}\right| \\ &\leq \frac{d^2}{\xi^2}|Y_1 - X_1| + \frac{d}{c} \cdot |X_4 - Y_4| + \frac{d}{c} \cdot |X_3 - Y_3|. \end{aligned} \tag{I.6}$$

Next we bound the expression $\left|\frac{X_3^2}{X_1} - \frac{Y_3^2}{Y_1}\right|$. Rewrite the expression by separating the terms: $\left|\frac{X_3^2}{X_1} - \frac{Y_3^2}{Y_1}\right| = \left|X_3 \cdot \frac{X_3}{X_1} - Y_3 \cdot \frac{Y_3}{Y_1}\right|$. Now, using the distributive property, we can expand this as: $\left|X_3 \cdot \frac{X_3}{X_1} - Y_3 \cdot \frac{Y_3}{Y_1}\right| = \left|X_3 \cdot \frac{X_3}{X_1} - X_3 \cdot \frac{Y_3}{Y_1} + X_3 \cdot \frac{Y_3}{Y_1} - Y_3 \cdot \frac{Y_3}{Y_1}\right|$. Using the triangle inequality, we

27. The mean value theorem states that if a function $f(x)$ is continuous on the closed interval $[a, b]$, and differentiable on the open interval (a, b), then there exists a point c in (a, b) such that: $f'(c) = \frac{f(b) - f(a)}{b - a}$.

can separate this into two parts:

$$\left|\frac{X_3^2}{X_1}-\frac{Y_3^2}{Y_1}\right| \leq \left|X_3\left(\frac{X_3}{X_1}-\frac{Y_3}{Y_1}\right)\right| + \left|\frac{Y_3}{Y_1}\left(X_3-Y_3\right)\right|. \tag{I.7}$$

This allows us to handle each term individually. We can write $\left|\frac{X_3}{X_1}-\frac{Y_3}{Y_1}\right| = \left|X_3\cdot\frac{1}{X_1}-Y_3\cdot\frac{1}{Y_1}\right|$. Using the distributive property, we expand this into two terms: $\left|X_3\cdot\frac{1}{X_1}-Y_3\cdot\frac{1}{Y_1}\right| = \left|X_3\cdot\frac{1}{X_1}-X_3\cdot\frac{1}{Y_1}+X_3\cdot\frac{1}{Y_1}-Y_3\cdot\frac{1}{Y_1}\right|$. Then, applying the triangle inequality, we get:

$$\left|\frac{X_3}{X_1}-\frac{Y_3}{Y_1}\right| \leq \left|X_3\left(\frac{1}{X_1}-\frac{1}{Y_1}\right)\right| + \left|\frac{1}{Y_1}\left(X_3-Y_3\right)\right|. \tag{I.8}$$

To bound $\left|\frac{1}{X_1}-\frac{1}{Y_1}\right|$, we apply the mean value theorem (similar to above) where ξ is some value between X_1 and Y_1: $\left|\frac{1}{X_1}-\frac{1}{Y_1}\right| = \frac{|Y_1-X_1|}{\xi^2}$. Thus, the first term becomes: $\left|X_3\left(\frac{1}{X_1}-\frac{1}{Y_1}\right)\right| = |X_3|\cdot\frac{|Y_1-X_1|}{\xi^2}$. If we assume that X_3 is bounded relative to X_1, specifically that $\frac{X_3}{X_1}\leq d$ for some constant d, then we can write $|X_3|\leq d|X_1|$. This gives: $\left|X_3\left(\frac{1}{X_1}-\frac{1}{Y_1}\right)\right| \leq d|X_1|\cdot\frac{|Y_1-X_1|}{\xi^2}$. If we assume Y_1 is bounded away from zero (say $Y_1\geq c>0$), then $\frac{1}{Y_1}\leq\frac{1}{c}$. This gives: $\left|\frac{1}{Y_1}(X_3-Y_3)\right| \leq \frac{|X_3-Y_3|}{c}$. Putting it all together in Eq. (I.8), we have: $\left|\frac{X_3}{X_1}-\frac{Y_3}{Y_1}\right| \leq d|X_1|\cdot\frac{|Y_1-X_1|}{\xi^2}+\frac{|X_3-Y_3|}{c} \leq \frac{d}{\xi^2}|Y_1-X_1|+\frac{|X_3-Y_3|}{c}$, where d is a constant bounding $\frac{X_3}{X_1}$, ξ is a point between X_1 and Y_1, and c is a lower bound for Y_1 to ensure Y_1 does not approach zero, and we have used the fact that $0<|X_1|\leq 1$.

For the term $\left|\frac{Y_3}{Y_1}\left(X_3-Y_3\right)\right|$ in Eq. (I.7), if we assume that Y_1 is bounded away from zero (say $Y_1\geq c>0$), then $\frac{1}{Y_1}\leq\frac{1}{c}$. This gives: $\left|\frac{Y_3}{Y_1}\left(X_3-Y_3\right)\right| \leq \frac{|Y_3|}{c}\cdot|X_3-Y_3|$. If $|Y_3|$ is bounded by a multiple of $|Y_1|$ (i.e., $\frac{Y_3}{Y_1}\leq d$), then we get: $\left|\frac{Y_3}{Y_1}\left(X_3-Y_3\right)\right| \leq \frac{d|Y_1|}{c}\cdot|X_3-Y_3|$. Putting everything together in Eq. (I.7), we have:

$$\left|\frac{X_3^2}{X_1}-\frac{Y_3^2}{Y_1}\right| \leq \frac{d^2}{\xi^2}|Y_1-X_1|+\frac{d}{c}\cdot|X_3-Y_3|+\frac{d}{c}\cdot|X_3-Y_3|, \tag{I.9}$$

where d is a constant bounding the ratios $\frac{X_3}{X_1}$ and $\frac{Y_3}{Y_1}$, ξ is a point between X_1 and Y_1, c is a lower bound for Y_1 to prevent division by zero, and we have used the fact that $|X_1|\leq 1$ and $|Y_1|\leq 1$. Combining Eqs. (I.6) and (I.9) allows us to write Eq. (I.3) as follows

$$\begin{aligned}\left|\frac{\beta X_3(2X_4-X_3)}{X_1}-\frac{\beta Y_3(2Y_4-Y_3)}{Y_1}\right| \leq\ & 2\beta\left(\frac{d^2}{\xi^2}|Y_1-X_1|+\frac{d}{c}\cdot|X_4-Y_4|+\frac{d}{c}\cdot|X_3-Y_3|\right)\\ &+\beta\left(\frac{d^2}{\xi^2}|Y_1-X_1|+\frac{2d}{c}\cdot|X_3-Y_3|\right)\end{aligned}$$

Hence, there exists a constant $C_3 > 0$ such that:

$$\left| \frac{\beta X_3(2X_4 - X_3)}{X_1} - \frac{\beta Y_3(2Y_4 - Y_3)}{Y_1} \right| \leq C_3 \|X - Y\|.$$

Thus, the third component is Lipschitz with constant C_3. The fourth component is

$$\left| w(X_3 - Y_3) - \left(\frac{2\beta X_3 X_4}{X_1} - \frac{2\beta Y_3 Y_4}{Y_1} \right) \right|.$$

Using a similar bound for the terms involving fractions as in the previous derivation, we can bound the fourth component in Eq. (I.2) by a Lipschitz constant C_4.

Thus each component is Lipschitz continuous, with constants β, $\gamma + \beta$, C_3, and C_4. Let L be the maximum of these constants: $L = \max(\beta, \gamma + \beta, C_3, C_4)$. Thus, for all $X, Y \in \mathbb{R}^4$,

$$\|F(X) - F(Y)\|_1 \leq L \|X - Y\|_1.$$

This shows that the function $F(X)$ is Lipschitz continuous in X. □

After having established Lipschitz continuity, we can state the following theorem that states that the empirical population frequencies of the stochastic process can be approximated with the solution to a system of ODEs (so called mean field dynamics).[28]

THEOREM 3. *W.l.o.g. we consider the case of a single layer and one group. Assume that the fraction of susceptibles in the population is bounded away from zero. Then, in the large population limit,* $\lim_{N\to\infty} \mathbb{P}\left(\sup_{0\leq t\leq T} \left\| \frac{1}{N} X^N(t) - x(t) \right\| > \delta\right) = 0$ *for any* $T > 0$ *and* $\delta > 0$ *where* $X^N(t) = [S^N(t), I^N(t), m^N(S,I)(t), m^N(S,S)(t)]$ *are the respective frequencies for the number of infectious, susceptibles, links between infectious and infectious, and links between susceptibles and susceptibles per capita in a population of size* N*, and* $x(t)$ *solves the ordinary differential Eqs. (1), (2), (6) and (7).*

Proof of Theorem 3. We want to show the convergence of a sequence $\{X_t^N\}_{N\in\mathbb{N}}$, $X_t^N = [S^N(t),\ I^N(t),\ m^N(S,I)(t),\ m^N(S,S)(t)]$, $0 \leq t \leq T < \infty$, of Markov processes indexed by N with decreasing step sizes Δt. We suppose that the process indexed by N takes values in the state space $\mathcal{X}^N = \{x : Nx \in \mathbb{N}^4\}$ and λ^N denotes the jump rate vector of this process. The expected number of events that happen during the brief time interval $[t, t + \Delta t]$ is of order $\lambda^N \Delta t$. We next introduce the random variable ζ_x^N, whose distribution describes the stochastic

28. See also Kurz (1971).

increments of $(X^N(t))_{0\leq t\leq T}$ from the state x to state $x+z$ given by

$$\mathbb{P}\left(\zeta_x^N = z\right) = \mathbb{P}\left(X^N\left(t+\Delta t\right) = x+z \middle| X^N(t) = x\right).$$

The increments ζ_x^N describe the change due to infection, recovery or rewiring of $X^N(t)$. Further, we introduce the functions $F^N(x)$, $A^N(x)$ and $A_\delta^N(x)$ defined by $F^N(x) \equiv \lambda^N \mathbb{E}[\zeta_x^N]$, $A^N(x) \equiv \lambda^N \mathbb{E}[|\zeta_x^N|]$, and $A_\delta^N(x) \equiv \lambda^N \mathbb{E}[\left|\zeta_x^N \mathbb{1}_{\{|\zeta_x^N|>\delta\}}\right|]$. Consider some sequence $(\delta^N)_{N=N_0}^\infty$ with $\lim_{N\to\infty}\delta^N = 0$. In the following we want to show that the following three conditions hold: (i) $\lim_{N\to\infty}\sup_{x\in\mathcal{X}^N}\left|F^N(x)-F(x)\right| = 0$, (ii) $\sup_N \sup_{x\in\mathcal{X}^N} A^N(x) < \infty$, and (iii) $\lim_{N\to\infty}\sup_{x\in\mathcal{X}^N} A_{\delta^N}^N(x) = 0$.

To show this, we compute the expected increment per time unit $F^N(x)$ of the process $X^N(t)$. Defining the random variable ζ_x^N and jump rate $\lambda^N = N$ as above for x_1 (corresponding to S) we have that

$$\begin{aligned} F^N(x_1) &= \lambda^N \mathbb{E}[\zeta_{x_1}^N] \\ &= -N\frac{1}{N}\beta m(S,I) \\ &= -\beta m(S,I) \\ &= F(x_1), \end{aligned}$$

which is independent of N. Moreover, for x_2 (corresponding to I) we get that

$$\begin{aligned} F^N(x_2) &= \lambda^N \mathbb{E}[\zeta_{x_2}^N] \\ &= N\frac{1}{N}\beta m(S,I) - N\frac{1}{N}\gamma I \\ &= \beta m(S,I) - \gamma I \\ &= F(x_2), \end{aligned}$$

which is also independent of N. Similarly, for x_3 (corresponding to $m(I,S)$) we get

$$\begin{aligned} F^N(x_3) &= \lambda^N \mathbb{E}[\zeta_{x_3}^N] \\ &= N\frac{1}{N}\beta\frac{m(I,S)}{S}(2m(S,S)-m(I,S)) - N\frac{1}{N}(\gamma+w)m(I,S) \\ &= \beta\frac{m(I,S)}{S}(2m(S,S)-m(I,S)) - (\gamma+w)m(I,S) \\ &= F(x_3), \end{aligned}$$

independent of N, and for x_4 (corresponding to $m(S,S)$) we get

$$\begin{aligned} F^N(x_4) &= \lambda^N \mathbb{E}[\zeta_{x_4}^N] \\ &= N\frac{1}{N} w m(I,S) - N\frac{1}{N} 2\beta \frac{m(I,S)m(S,S)}{S} \\ &= w m(I,S) - 2\beta \frac{m(I,S)m(S,S)}{S} \\ &= F(x_4), \end{aligned}$$

which is also independent of N. Hence, $F^N(x) = F(x)$, independent of N. This implies that condition (i) is satisfied. Further, we have that $|\zeta_x^N| \leq c/N$ for some constant $c < \infty$, and hence, $(X^N(t))_{0\leq t\leq T}$ has jumps of at most $\sqrt{c}/N$. Thus, for $\delta^N = \sqrt{c}/N$ it follows that $A_{\delta^N}^N(x) = N\mathbb{E}\left[\left|\zeta_x^N I_{\{|\zeta_x^N| > \sqrt{c}/N\}}\right|\right] = 0$, and condition (iii) holds. Finally, we find that $A^N(x) = N\mathbb{E}[|\zeta_x^N|] \leq N\frac{\sqrt{c}}{N} = \sqrt{c} < \infty$, and also condition (ii) is satisfied.

Next, observe that due to Lemma 2, $F(x)$ is a Lipschitz continuous vector field in x with bounded derivatives. Together with conditions (i), (ii) and (iii), we then can apply Kurtz's Theorem (cf. Sandholm 2010, Chap.10.2), which states that for any solution $\{X(t)\}_{0\leq t\leq T}$ of the mean-field dynamics

$$\frac{dx}{dt} = F(x) \tag{I.10}$$

starting from x_0 we have that $\lim_{N\to\infty} \mathbb{P}\left(\sup_{t\in[0,T]} \left|X^N(t) - x(t)\right| \geq \varepsilon\right) = 0$, for any $T < \infty$ and $\varepsilon > 0$. □

Theorem 3 can be generalized to the ODEs (1) to (7) for different types/groups and layers.

Proof of Theorem 1. In the stationary state, $\frac{dS_k}{dt} = 0$. Further, in the disease free stationary state/equilibrium, $m(I_k, S_j) = 0$. It then follows from Equation (1) that

$$S_k = \frac{\lambda}{\mu}. \tag{I.11}$$

Moreover, in the disease-free equilibrium from Equation (7) it follows that

$$0 = \kappa_{kj}^l S_k S_j - (\nu^l + 2\mu) m^l(S_k, S_j),$$

so that

$$m^l(S_k, S_j) = \frac{\kappa_{kj}^l}{\nu^l + 2\mu} S_k S_j.$$

With Equation (I.11) this gives

$$m^l(S_k, S_j) = \frac{\kappa^l_{kj}}{\nu^l + 2\mu} \frac{\lambda^2}{\mu^2}. \tag{I.12}$$

We can write our system given by Eqs. (1), (2), (3), (4), (5), (6) and (7), respectively, as a dynamical system $\dot{y} = f(y)$, where y is the minimal state space sufficient for computing the steady state $y = [S_k, I_k, m^l(S_k, S_j), m^l(I_k, S_j)]_{k,j \in \mathcal{K}, l \in \mathcal{L}}$.[29] Then, the disease-free steady state is $[S_k, I_k, m^l(S_k, S_j), m^l(I_k, S_j)] = [\lambda/\mu, 0, \frac{\kappa^l_{kj}}{\nu^l + 2\mu} \frac{\lambda^2}{\mu^2}, 0]$.

Checking if the disease free equilibrium is asymptotically stable is equivalent to evaluating the Jakobian matrix $\mathbf{J}$ at the equilibrium and verifying that the real parts of the eigenvalues of $\mathbf{J}$ are negative (Khalil 2002). We index the rows/columns of the $(2|\mathcal{L}|n^2 + 2n) \times (2|\mathcal{L}|n^2 + 2n)$ dimensional Jakobian matrix $\mathbf{J}$ by $(m^l(I_k, S_j),\ I_k,\ S_k,\ m^l(S_k, S_j))$ with $l \in \mathcal{L}$ and $j, k \in \mathcal{K}$, Therefore, by inspecting our system of differential equations in Eqs. (1), (2), (3), (4), (5), (6) and (7), we see that at the disease-free equilibrium:

$$\frac{\partial \dot{m}^l(I_k, S_j)}{\partial I_{k'}} = 0, \frac{\partial \dot{m}^l(I_k, S_j)}{\partial S_{k'}} = 0, \frac{\partial \dot{m}^l(I_k, S_j)}{\partial m^{l'}(S_{j'}, S_{k'})} = 0,$$

$$\frac{\partial \dot{I}_k}{\partial S_{k'}} = 0, \frac{\partial \dot{I}_k}{\partial m^l(S_j, S_{k'})} = 0,$$

$$\frac{\partial \dot{S}_k}{\partial m^l(S_j, S_{k'})} = 0.$$

This implies that in the disease-free equilibrium the Jakobian has the following lower triangular block structure:

29. Cf. e.g. Chap. 6 in Brauer et al. (2008).

$$
\mathbf{J} = \begin{pmatrix}
 & \boxed{\begin{matrix} \hat{\mathbf{J}}^{1,1}_{n^2\times n^2} & \cdots & \hat{\mathbf{J}}^{1,|\mathcal{L}|}_{n^2\times n^2} \\ \vdots & \ddots & \vdots \\ \hat{\mathbf{J}}^{|\mathcal{L}|,1}_{n^2\times n^2} & \cdots & \hat{\mathbf{J}}^{|\mathcal{L}|,|\mathcal{L}|}_{n^2\times n^2} \end{matrix}}_{|\mathcal{L}|n^2\times|\mathcal{L}|n^2} & & 0 & & 0 & & 0 & \\
\begin{bmatrix} \beta L^1_{11} & 0 & 0 \\ 0 & \vdots & 0 \\ 0 & 0 & \beta L^1_{nn} \end{bmatrix}_{n\times n^2} & \cdots & \begin{bmatrix} \beta L^{|\mathcal{L}|}_{11} & 0 & 0 \\ 0 & \vdots & 0 \\ 0 & 0 & \beta L^{|\mathcal{L}|}_{nn} \end{bmatrix}_{n\times n^2} & \boxed{\begin{matrix} -\gamma-\mu & 0 & 0 \\ 0 & \vdots & 0 \\ 0 & 0 & -\gamma-\mu \end{matrix}}_{n\times n} & 0 & & 0 & \\
\begin{bmatrix} -\beta L^1_{11} & 0 & 0 \\ 0 & \vdots & 0 \\ 0 & 0 & -\beta L^1_{nn} \end{bmatrix}_{n\times n^2} & \cdots & \begin{bmatrix} -\beta L^{|\mathcal{L}|}_{11} & 0 & 0 \\ 0 & \vdots & 0 \\ 0 & 0 & -\beta L^{|\mathcal{L}|}_{nn} \end{bmatrix}_{n\times n^2} & 0 & \boxed{\begin{matrix} -\mu & 0 & 0 \\ 0 & \vdots & 0 \\ 0 & 0 & -\mu \end{matrix}}_{n\times n} & & 0 & \\
 & & & & & \boxed{\begin{matrix} -\nu^1-2\mu & 0 & 0 \\ 0 & \vdots & 0 \\ 0 & 0 & -\nu^1-2\mu \end{matrix}}_{n^2\times n^2} & \cdots & 0 & \\
Y & & 0 & Z & \vdots & \ddots & \vdots & \\
 & & & & 0 & \cdots & \boxed{\begin{matrix} -\nu^{|\mathcal{L}|}-2\mu & 0 & 0 \\ 0 & \vdots & 0 \\ 0 & 0 & -\nu^{|\mathcal{L}|}-2\mu \end{matrix}}_{n^2\times n^2} &
\end{pmatrix}
$$

where Y, Z are not explicitly specified. The top-left block matrix $\hat{\mathbf{J}} = [\hat{J}^{l,l'}_{j,k,u,v}]$ has dimension $(|\mathcal{L}|n^2) \times (|\mathcal{L}|n^2)$ with elements given by

$$\hat{J}^{l,l'}_{j,k,u,v} = \frac{\partial \dot{m}^l(I_k, S_j)}{\partial m^{l'}(I_u, S_v)},$$

for $l, l' \in \mathcal{L}$ and $j, k, u, v \in \{1, \ldots, n\}$. At the disease free equilibrium (which has $I_k = 0$ and $m^l(I_k, S_j) = 0$) we can write

$$\hat{J}^{l,l'}_{j,k,u,v} = \left.\frac{\partial \dot{m}^l(I_k,S_j)}{\partial m^{l'}(I_u,S_v)}\right|_{I_k = m^l(I_k,S_j)=0} = \frac{\beta m^l(S_k,S_j)}{S_k} L^{l'}_{uk}\delta_{vk} - (\gamma + w + \nu^l + 2\mu)\delta_{u,k}\delta_{v,j}\delta_{l,l'}, \tag{I.13}$$

where $\delta_{i,j}$ is the Kronecker delta with the property that $\delta_{ij} = 1$ if $i = j$ and zero otherwise. Apart from $\hat{\mathbf{J}}$ all of the on-diagonal blocks in the Jacobian $\mathbf{J}$ have only negative entries. Because of the lower triangular block structure of the Jacobian, and the fact that all the entries of the other on-diagonal blocks are less than or equal to zero, all eigenvalues are negative if and only if all eigenvalues of $\hat{\mathbf{J}}$ are negative.

In the following we denote by

$$F^{l,l'}_{j,k,u,v}(\mathbf{L}) = \frac{\beta m^l(S_k, S_j)}{S_k} L^{l'}_{uk}\delta_{vk},$$

where we have inserted Eqs. (I.11) and (I.12), respectively, and

$$V^{l,l'}_{j,k,u,v}(w) = (\gamma + w + q + \nu^l + 2\mu)\delta_{u,k}\delta_{v,j}\delta_{l,l'},$$

so that we can separate $\hat{\mathbf{J}}$ into its positive and negative parts

$$\hat{\mathbf{J}} = \mathbf{F}(\mathbf{L}) - \mathbf{V}(w). \tag{I.14}$$

Note that the matrix $\mathbf{F}(\mathbf{L})$ exhibits a linear dependence on lockdown levels $\mathbf{L}$ while the matrix $\mathbf{V}(w)$ is a diagonal matrix that depends on the rewiring rate w.

The disease-free equilibrium is asymptotically stable if all eigenvalues of $\mathbf{J}$ are negative. Due to the lower triangular block structure of $\mathbf{J}$, all eigenvalues of $\mathbf{J}$ are negative if and only if all eigenvalues of $\hat{\mathbf{J}}$ are negative. All eigenvalues of $\hat{\mathbf{J}}$ are negative if and only if $\hat{\mathbf{J}} = \mathbf{F}(\mathbf{L}) - \mathbf{V}(w)$ is negative definite. This can be written as $\mathbf{F}(\mathbf{L}) \prec \mathbf{V}(w)$. □

Proof of Corollary 1. Following the notation in Chapter 6 in Brauer et al. (2008) we partition our state space into "infectious compartments"

$$x = \begin{pmatrix} I \\ m(I,S) \end{pmatrix}$$

and "non-infectious compartments"

$$y = \begin{pmatrix} S \\ R \\ m(S,S) \end{pmatrix}.$$

Further, write

$$\begin{aligned} \frac{dx}{dt} &= \mathcal{F}(x,y) - \mathcal{V}(x,y), \\ \frac{dy}{dt} &= g(x,y). \end{aligned} \tag{I.15}$$

where

$$\begin{aligned} \mathcal{F} &= \begin{pmatrix} \beta m(I,S) \\ 2\beta \frac{m(S,S)}{S} m(I,S) \end{pmatrix}, \\ \mathcal{V} &= \begin{pmatrix} (\gamma+\mu)I \\ 2\beta \frac{m(I,S)^2}{S} + (\gamma + w + \nu + 2\mu) m(I,S) \end{pmatrix}. \end{aligned}$$

Next, we linearize our model about the disease-free equilibrium where $x = 0$. To ensure that this equilibrium exists, we need to verify the following assumptions for our model. (i) $\mathcal{F}(0,y) = 0, \mathcal{V}(0,y) = 0$ for all $y > 0$. All terms in the first row of the matrices are either multiplicative on I or $m(I,S)$, so must be zero when $I = 0, m(I,S) = 0$. All terms in the second row of the matrices are multiplicative on $m(I,S)$, so must be zero when $m(I,S) = 0$.(ii) $\mathcal{F}(x,y) > 0$ for $x, y > 0$. This follows from $\beta > 0$. (iii) Each $\mathcal{V}_i(x,y) \leq 0$ for $x = 0, y > 0$. This follows from the reasoning for the first assumption being satisfied. (iv) $\sum_{i=1}^{3} \mathcal{V}_i(x,y) > 0$ for $x, y > 0$. This follows from all parameters being defined as greater than zero. (v) There is a unique disease-free equilibrium $(0, y_\infty)$ that is asymptotically stable. Our system approaches this equilibrium from any $(0,y)$ as $t \to \infty$. Under these conditions, we can linearize our system around the disease-free equilibrium using

$$\frac{dx}{dt} = (F - V)x,$$

where $F_{ij} = \frac{\partial \mathcal{F}_i(0,y_0)}{\partial x_j}, V_{ij} = \frac{\partial \mathcal{V}_i(0,y_0)}{\partial x_j}$. Applying this to our system (I.15), we have

$$\begin{aligned} F &= \begin{pmatrix} 0 & \beta \\ 0 & \frac{m(S,S)(0)}{S(0)} \end{pmatrix}, \\ V &= \begin{pmatrix} (\gamma+\mu) & 0 \\ 0 & 2\beta \frac{m(I,S)(0)}{S(0)} + \gamma + w + \nu + 2\mu \end{pmatrix}. \end{aligned}$$

The expected time each infectious remains infectious, and each infectious-susceptible link remains an infectious-susceptible link is given by

$$\int_0^\infty \varphi(t, x_0)dt$$

where φ is the solution to our system of ODEs when $F = 0$. As $t \to \infty$, rearranging gives

$$\int_0^\infty \varphi(t, x_0)dt = \int_0^\infty e^{-Vt}x_0 dt \to V^{-1}x_0.$$

Therefore, the expected number of secondary infections and infectious susceptible links is the amount of new ones generated by each infectious for the time it remains in the compartment

$$FV^{-1}x_0$$

Computing this, we have that

$$FV^{-1} = \begin{pmatrix} \frac{\beta}{\gamma+\mu} & \beta\frac{1}{\frac{m(I,S)(0)}{S(0)}+(\gamma+w+\nu+2\mu)} \\ 0 & \beta\frac{m(S,S)(0)}{S(0)}\frac{1}{\frac{m(I,S)(0)}{S(0)}+(\gamma+w+\nu+2\mu)} \end{pmatrix}.$$

Using that $m(I, S)(0) = 0$ gives

$$FV^{-1} = \begin{pmatrix} \frac{\beta}{\gamma+\mu} & \beta\frac{1}{\gamma+w+\nu+2\mu} \\ 0 & \beta\frac{m(S,S)(0)}{S(0)}\frac{1}{\gamma+w+\nu+2\mu} \end{pmatrix}.$$

The (i, j)-entry of FV^{-1} is the expected number of secondary infections in compartment i produced by individuals initially in compartment j, assuming that the environment seen by the individual remains homogeneous for the duration of its infection. The basic reproduction number $\mathcal{R}_0$ is the expected number of secondary infections for each infectious individual in the disease-free steady state, which is given by the entry in the second row and second column of FV^{-1}. Thus we find that

$$\mathcal{R}_0 = \frac{\beta m(S, S)(0)}{S(0)(\gamma + w + \nu + 2\mu)}.$$

□

Proof of Theorem 2. Consider first the case of two groups ($|\mathcal{K}| = 2$) and two layers ($|\mathcal{L}| = 2$). Then we can write the positive part of the matrix $\hat{\mathbf{J}} = \mathbf{F}(\mathbf{L}) - \mathbf{V}(w)$ in Eq. (I.14) as

$$\mathbf{F}(\mathbf{L}) = \begin{pmatrix} \mathbf{F}^{1,1}(\mathbf{L}) & \mathbf{F}^{1,2}(\mathbf{L}) \\ \mathbf{F}^{2,1}(\mathbf{L}) & \mathbf{F}^{2,2}(\mathbf{L}) \end{pmatrix}$$

with the blocks

$$\mathbf{F}^{l,l'}(\mathbf{L}) = \begin{pmatrix} \frac{\beta m^l(S_1,S_1)L_{11}^{l'}}{S_1} & 0 & \frac{\beta m^l(S_1,S_1)L_{21}^{l'}}{S_1} & 0 \\ \frac{\beta m^l(S_1,S_2)L_{11}^{l'}}{S_1} & 0 & \frac{\beta m^l(S_1,S_2)L_{21}^{l'}}{S_1} & 0 \\ 0 & \frac{\beta m^l(S_1,S_2)L_{12}^{l'}}{S_2} & 0 & \frac{\beta m^l(S_1,S_2)L_{22}^{l'}}{S_2} \\ 0 & \frac{\beta m^l(S_2,S_2)L_{12}^{l'}}{S_2} & 0 & \frac{\beta m^l(S_2,S_2)L_{22}^{l'}}{S_2} \end{pmatrix},$$

for $l, l' \in \mathcal{L} = \{1, 2\}$. Moreover, the negative part denoted by $\mathbf{V}(w)$ is proportional to the identity matrix $\mathbf{I}$, i.e., $\mathbf{V}(w) = (\gamma + w)\mathbf{I}$. Thus, our objective is to find lockdowns that ensure that the eigenvalues of $\mathbf{F}(\mathbf{L})$ are less than $\gamma + w$.
Next, define

$$\mathbf{O} = \begin{pmatrix} 1 & 0 & 1 & 0 \\ 1 & 0 & 1 & 0 \\ 0 & 1 & 0 & 1 \\ 0 & 1 & 0 & 1 \end{pmatrix},$$

and

$$\hat{\mathbf{L}}^l = \begin{pmatrix} L_{11}^l & 0 & 0 & 0 \\ 0 & L_{12}^l & 0 & 0 \\ 0 & 0 & L_{21}^l & 0 \\ 0 & 0 & 0 & L_{22}^l \end{pmatrix}$$

and

$$\hat{\boldsymbol{\beta}}^l = \begin{pmatrix} \frac{\beta m^l(S_1,S_1)}{S_1} & 0 & 0 & 0 \\ 0 & \frac{\beta m^l(S_1,S_2)}{S_1} & 0 & 0 \\ 0 & 0 & \frac{\beta m^l(S_2,S_1)}{S_2} & 0 \\ 0 & 0 & 0 & \frac{\beta m^l(S_2,S_2)}{S_2} \end{pmatrix}$$

Then, we can write

$$\begin{aligned} \mathbf{F}^{l,l'}(\mathbf{L}) &= \hat{\boldsymbol{\beta}}^l \mathbf{O} \hat{\mathbf{L}}^{l'} \\ &= \begin{pmatrix} \frac{\beta m^l(S_1,S_1)L_{11}^{l'}}{S_1} & 0 & \frac{\beta m^l(S_1,S_1)L_{21}^{l'}}{S_1} & 0 \\ \frac{\beta m^l(S_1,S_2)L_{11}^{l'}}{S_1} & 0 & \frac{\beta m^l(S_1,S_2)L_{21}^{l'}}{S_1} & 0 \\ 0 & \frac{\beta m^l(S_1,S_2)L_{12}^{l'}}{S_2} & 0 & \frac{\beta m^l(S_1,S_2)L_{22}^{l'}}{S_2} \\ 0 & \frac{\beta m^l(S_2,S_2)L_{12}^{l'}}{S_2} & 0 & \frac{\beta m^l(S_2,S_2)L_{22}^{l'}}{S_2} \end{pmatrix}. \end{aligned}$$

Next, define

$$\hat{\boldsymbol{\beta}} = \begin{pmatrix} \hat{\boldsymbol{\beta}}^1 & 0 \\ 0 & \hat{\boldsymbol{\beta}}^2 \end{pmatrix},$$

and

$$\hat{\mathbf{L}} = \begin{pmatrix} \hat{\mathbf{L}}^1 & 0 \\ 0 & \hat{\mathbf{L}}^2 \end{pmatrix},$$

and

$$\mathbf{M} = \begin{pmatrix} \mathbf{O} & \mathbf{O} \\ \mathbf{O} & \mathbf{O} \end{pmatrix}.$$

Then, we can write that

$$\begin{aligned} \mathbf{F}(\mathbf{L}) &= \hat{\boldsymbol{\beta}}\mathbf{M}\hat{\mathbf{L}} \\ &= \begin{pmatrix} \boldsymbol{\beta}^1 & 0 \\ 0 & \boldsymbol{\beta}^2 \end{pmatrix} \begin{pmatrix} \mathbf{O} & \mathbf{O} \\ \mathbf{O} & \mathbf{O} \end{pmatrix} \begin{pmatrix} \hat{\mathbf{L}}^1 & 0 \\ 0 & \hat{\mathbf{L}}^2 \end{pmatrix} \\ &= \begin{pmatrix} \boldsymbol{\beta}^1 & 0 \\ 0 & \boldsymbol{\beta}^2 \end{pmatrix} \begin{pmatrix} \mathbf{O}\hat{\mathbf{L}}^1 & \mathbf{O}\hat{\mathbf{L}}^2 \\ \mathbf{O}\hat{\mathbf{L}}^1 & \mathbf{O}\hat{\mathbf{L}}^2 \end{pmatrix} \\ &= \begin{pmatrix} \boldsymbol{\beta}^1\mathbf{O}\hat{\mathbf{L}}^1 & \boldsymbol{\beta}^1\mathbf{O}\hat{\mathbf{L}}^2 \\ \boldsymbol{\beta}^2\mathbf{O}\hat{\mathbf{L}}^1 & \boldsymbol{\beta}^2\mathbf{O}\hat{\mathbf{L}}^2 \end{pmatrix} \end{aligned}$$

We can apply the similarity transformation

$$\hat{\boldsymbol{\beta}}^{-1}\mathbf{F}\hat{\boldsymbol{\beta}} = \hat{\boldsymbol{\beta}}^{-1}\hat{\boldsymbol{\beta}}\mathbf{M}\hat{\mathbf{L}}\hat{\boldsymbol{\beta}} = \mathbf{M}\hat{\mathbf{L}}\hat{\boldsymbol{\beta}}$$

where

$$\hat{\boldsymbol{\beta}}^{-1} = \begin{pmatrix} \frac{S_1}{\beta m^1(S_1,S_1)} & 0 & 0 & 0 & 0 & 0 & 0 & 0 \\ 0 & \frac{S_1}{\beta m^1(S_1,S_2)} & 0 & 0 & 0 & 0 & 0 & 0 \\ 0 & 0 & \frac{S_2}{\beta m^1(S_2,S_1)} & 0 & 0 & 0 & 0 & 0 \\ 0 & 0 & 0 & \frac{S_2}{\beta m^1(S_2,S_2)} & 0 & 0 & 0 & 0 \\ 0 & 0 & 0 & 0 & \frac{S_1}{\beta m^2(S_1,S_1)} & 0 & 0 & 0 \\ 0 & 0 & 0 & 0 & 0 & \frac{S_1}{\beta m^2(S_1,S_2)} & 0 & 0 \\ 0 & 0 & 0 & 0 & 0 & 0 & \frac{S_2}{\beta m^2(S_2,S_1)} & 0 \\ 0 & 0 & 0 & 0 & 0 & 0 & 0 & \frac{S_2}{\beta m^2(S_2,S_2)} \end{pmatrix}$$

which preserves the eigenvalues (that is, the eigenvalues of $\mathbf{F}(\mathbf{L})$ are identical to the eigenvalues of $\hat{\boldsymbol{\beta}}^{-1}\mathbf{F}(\mathbf{L})\hat{\boldsymbol{\beta}} = \mathbf{M}\hat{\mathbf{L}}\hat{\boldsymbol{\beta}}$). Further, note that

$$\hat{\mathbf{L}}\hat{\boldsymbol{\beta}} = \text{diag}(\boldsymbol{\omega}) = \begin{pmatrix} \omega_1 & 0 & 0 & 0 & 0 & 0 & 0 & 0 \\ 0 & \omega_2 & 0 & 0 & 0 & 0 & 0 & 0 \\ 0 & 0 & \omega_3 & 0 & 0 & 0 & 0 & 0 \\ 0 & 0 & 0 & \omega_4 & 0 & 0 & 0 & 0 \\ 0 & 0 & 0 & 0 & \omega_5 & 0 & 0 & 0 \\ 0 & 0 & 0 & 0 & 0 & \omega_6 & 0 & 0 \\ 0 & 0 & 0 & 0 & 0 & 0 & \omega_7 & 0 \\ 0 & 0 & 0 & 0 & 0 & 0 & 0 & \omega_8 \end{pmatrix}$$

where we have denoted by

$$\boldsymbol{\omega} = \begin{pmatrix} \omega_1 \\ \omega_2 \\ \omega_3 \\ \omega_4 \\ \omega_5 \\ \omega_6 \\ \omega_7 \\ \omega_8 \end{pmatrix} = \begin{pmatrix} L^1_{11}\frac{\beta m^1(S_1,S_1)}{S_1} \\ L^1_{12}\frac{\beta m^1(S_1,S_2)}{S_1} \\ L^1_{21}\frac{\beta m^1(S_2,S_1)}{S_2} \\ L^1_{22}\frac{\beta m^1(S_2,S_2)}{S_2} \\ L^2_{11}\frac{\beta m^2(S_1,S_1)}{S_1} \\ L^2_{12}\frac{\beta m^2(S_1,S_2)}{S_1} \\ L^2_{21}\frac{\beta m^2(S_2,S_1)}{S_2} \\ L^2_{22}\frac{\beta m^2(S_2,S_2)}{S_2} \end{pmatrix}$$

Thus, our objective is to find lockdowns ($\mathbf{L}$) that ensure that the eigenvalues of $\mathbf{M}\text{diag}(\boldsymbol{\omega})$ are less than $\gamma + w$.

Writing out the eigenvalue problem $\mathbf{M}\text{diag}(\omega)\mathbf{v} = \varphi\mathbf{v}$ for any eigenvector $\mathbf{v}$ and corresponding eigenvalue φ gives

$$\mathbf{M}\text{diag}(\boldsymbol{\omega})\mathbf{v} = \begin{pmatrix} \omega_1 v_1 + \omega_3 v_3 + \omega_5 v_5 + \omega_7 v_7 \\ \omega_1 v_1 + \omega_3 v_3 + \omega_5 v_5 + \omega_7 v_7 \\ \omega_2 v_2 + \omega_4 v_4 + \omega_6 v_6 + \omega_8 v_8 \\ \omega_2 v_2 + \omega_4 v_4 + \omega_6 v_6 + \omega_8 v_8 \\ \omega_1 v_1 + \omega_3 v_3 + \omega_5 v_5 + \omega_7 v_7 \\ \omega_1 v_1 + \omega_3 v_3 + \omega_5 v_5 + \omega_7 v_7 \\ \omega_2 v_2 + \omega_4 v_4 + \omega_6 v_6 + \omega_8 v_8 \\ \omega_2 v_2 + \omega_4 v_4 + \omega_6 v_6 + \omega_8 v_8 \end{pmatrix} = \varphi \begin{pmatrix} v_1 \\ v_2 \\ v_3 \\ v_4 \\ v_5 \\ v_6 \\ v_7 \\ v_8 \end{pmatrix}.$$

This system of equations implies that $v_1 = v_2 = v_5 = v_6 = x$, $v_3 = v_4 = v_7 = v_8 = y$ and we can write $\mathbf{v} = [x, x, y, y, x, x, y, y]^\top$. Hence, we have that

$$\begin{aligned} (\omega_1 + \omega_5)x + (\omega_3 + \omega_7)y &= \varphi x, \\ (\omega_2 + \omega_6)x + (\omega_4 + \omega_8)y &= \varphi y. \end{aligned} \tag{I.16}$$

By reorganizing the entries ω_1, ω_2, ω_3 and ω_4 into a full matrix $\mathbf{\Omega}^1$ given by

$$\mathbf{\Omega}^1 = \begin{pmatrix} \omega_1 & \omega_3 \\ \omega_2 & \omega_4 \end{pmatrix} = \begin{pmatrix} \frac{\beta m^1(S_1,S_1)L^1_{11}}{S_1} & \frac{\beta m^1(S_2,S_1)L^1_{21}}{S_2} \\ \frac{\beta m^1(S_1,S_2)L^1_{12}}{S_1} & \frac{\beta m^1(S_2,S_2)L^1_{22}}{S_2} \end{pmatrix}$$

and similarly

$$\mathbf{\Omega}^2 = \begin{pmatrix} \omega_5 & \omega_7 \\ \omega_6 & \omega_8 \end{pmatrix} = \begin{pmatrix} \frac{\beta m^2(S_1,S_1)L^2_{11}}{S_1} & \frac{\beta m^2(S_2,S_1)L^2_{21}}{S_2} \\ \frac{\beta m^2(S_1,S_2)L^2_{12}}{S_1} & \frac{\beta m^2(S_2,S_2)L^2_{22}}{S_2} \end{pmatrix}$$

we can write the above system of Equations (I.16) as

$$(\mathbf{\Omega}^1 + \mathbf{\Omega}^2)\begin{pmatrix} x \\ y \end{pmatrix} = \begin{pmatrix} \omega_1 + \omega_5 & \omega_3 + \omega_7 \\ \omega_2 + \omega_6 & \omega_4 + \omega_8 \end{pmatrix}\begin{pmatrix} x \\ y \end{pmatrix} = \begin{pmatrix} (\omega_1 + \omega_5)x + (\omega_3 + \omega_7)y \\ (\omega_2 + \omega_6)x + (\omega_4 + \omega_8)y \end{pmatrix},$$

and this implies that the nonzero eigenvalues of $\mathbf{\Omega} = \mathbf{\Omega}^1 + \mathbf{\Omega}^2$ and those of $\mathbf{M}\mathrm{diag}(\boldsymbol{\omega})$ coincide. Thus, our constraint (namely, that the eigenvalues of $\mathbf{M}\mathrm{diag}(\boldsymbol{\omega})$ are less than $\gamma + w$) is equivalent to ensuring that the eigenvalues of $\mathbf{\Omega}^1 + \mathbf{\Omega}^2$ are smaller than $\gamma + w$.

Note that the (i, j)th entry of $\mathbf{\Omega}^l$ is given by $\frac{\beta L^l_{ij} m^l(S_i,S_j)}{S_i}$. Consider the similarity transform $\hat{\mathbf{\Omega}}^l = \mathrm{diag}(\mathbf{S})^{-1/2}\mathbf{\Omega}^l\mathrm{diag}(\mathbf{S})^{1/2}$, and note that it preserves the eigenvalues of $\mathbf{\Omega}^l$. Moreover, the (i, j)th entry of this matrix is now given by $\frac{\beta L^l_{ij} m^l(S_i,S_j)}{\sqrt{S_i S_j}}$, and the matrix is symmetric if and only if $m^l(S_i, S_j)$ is symmetric. In particular, for $l = 1$ we get

$$\begin{aligned} \hat{\mathbf{\Omega}}^1 &= \mathrm{diag}(\mathbf{S})^{-1/2}\mathbf{\Omega}^1\mathrm{diag}(\mathbf{S})^{1/2} \\ &= \begin{pmatrix} \frac{1}{\sqrt{S_1}} & 0 \\ 0 & \frac{1}{\sqrt{S_2}} \end{pmatrix}\begin{pmatrix} \omega_1 & \omega_3 \\ \omega_2 & \omega_4 \end{pmatrix}\begin{pmatrix} \sqrt{S_1} & 0 \\ 0 & \sqrt{S_2} \end{pmatrix} \\ &= \begin{pmatrix} \omega_1\sqrt{S_1} & \omega_3\sqrt{S_2} \\ \omega_2\sqrt{S_1} & \omega_4\sqrt{S_2} \end{pmatrix} \\ &= \begin{pmatrix} \omega_1 & \frac{\omega_3\sqrt{S_2}}{\sqrt{S_1}} \\ \frac{\omega_2\sqrt{S_1}}{\sqrt{S_2}} & \omega_4 \end{pmatrix} \\ &= \begin{pmatrix} \frac{\beta m^1(S_1,S_1)L^1_{11}}{S_1} & \frac{\beta m^1(S_2,S_1)L^1_{21}}{\sqrt{S_1 S_2}} \\ \frac{\beta m^1(S_1,S_2)L^1_{12}}{\sqrt{S_1 S_2}} & \frac{\beta m^1(S_2,S_2)L^1_{22}}{S_2} \end{pmatrix} \end{aligned}$$

Similarly, for $l = 2$ we get

$$\begin{aligned}
\boldsymbol{\Omega}^2 &= \mathrm{diag}(\mathbf{S})^{-1/2}\boldsymbol{\Omega}^2\mathrm{diag}(\mathbf{S})^{1/2} \\
&= \begin{pmatrix} \frac{1}{\sqrt{S_1}} & 0 \\ 0 & \frac{1}{\sqrt{S_2}} \end{pmatrix} \begin{pmatrix} \omega_5 & \omega_7 \\ \omega_6 & \omega_8 \end{pmatrix} \begin{pmatrix} \sqrt{S_1} & 0 \\ 0 & \sqrt{S_2} \end{pmatrix} \\
&= \begin{pmatrix} \omega_5\sqrt{S_1} & \omega_7\sqrt{S_2} \\ \omega_6\sqrt{S_1} & \omega_8\sqrt{S_2} \end{pmatrix} \\
&= \begin{pmatrix} \omega_5 & \frac{\omega_7\sqrt{S_2}}{\sqrt{S_1}} \\ \frac{\omega_6\sqrt{S_1}}{\sqrt{S_2}} & \omega_8 \end{pmatrix} \\
&= \begin{pmatrix} \frac{\beta m^2(S_1,S_1)L_{11}^2}{S_1} & \frac{\beta m^2(S_2,S_1)L_{21}^1}{\sqrt{S_1S_2}} \\ \frac{\beta m^2(S_1,S_2)L_{12}^2}{\sqrt{S_1S_2}} & \frac{\beta m^2(S_2,S_2)L_{22}^2}{S_2} \end{pmatrix}
\end{aligned}$$

Next we show that the steps above generalize to an arbitrary number of groups and layers. Consider the matrix $\hat{\mathbf{J}}$ and denote the positive part as $\mathbf{F}(\mathbf{L})$. From the definition of $\hat{\mathbf{J}}$ above, we can write this $(|\mathcal{L}| \times |\mathcal{K}|^2) \times (|\mathcal{L}| \times |\mathcal{K}|^2)$ matrix in the block form

$$\mathbf{F}(\mathbf{L}) = \begin{pmatrix} \mathbf{F}^{1,1}(\mathbf{L}) & \mathbf{F}^{1,2}(\mathbf{L}) & \cdots & \mathbf{F}^{1,|\mathcal{L}|}(\mathbf{L}) \\ \mathbf{F}^{2,1}(\mathbf{L}) & \cdots & \cdots & \cdots \\ \vdots & \vdots & \vdots & \vdots \\ \mathbf{F}^{|\mathcal{L}|,1}(\mathbf{L}) & \cdots & \cdots & \mathbf{F}^{|\mathcal{L}|,|\mathcal{L}|}(\mathbf{L}) \end{pmatrix},$$

where each block $\mathbf{F}^{l,l'}(\mathbf{L})$ is the $|\mathcal{K}|^2 \times |\mathcal{K}|^2$ matrix

$$\mathbf{F}^{l,l'}(\mathbf{L}) = \begin{pmatrix} \begin{bmatrix} \frac{\beta L_{11}^{l'} m^l(S_1,S_1)}{S_1} & 0 & 0 & \cdots \\ \frac{\beta L_{11}^{l'} m^l(S_1,S_2)}{S_1} & 0 & 0 & \cdots \\ \frac{\beta L_{11}^{l'} m^l(S_1,S_3)}{S_1} & 0 & 0 & \cdots \\ \vdots & \vdots & \vdots & \ddots \end{bmatrix}_{|\mathcal{K}|\times|\mathcal{K}|} & \begin{bmatrix} \frac{\beta L_{12}^{l'} m^l(S_1,S_1)}{S_1} & 0 & 0 & \cdots \\ \frac{\beta L_{12}^{l'} m^l(S_1,S_2)}{S_1} & 0 & 0 & \cdots \\ \frac{\beta L_{12}^{l'} m^l(S_1,S_3)}{S_1} & 0 & 0 & \cdots \\ \vdots & \vdots & \vdots & \ddots \end{bmatrix}_{|\mathcal{K}|\times|\mathcal{K}|} & \begin{bmatrix} \frac{\beta L_{13}^{l'} m^l(S_1,S_1)}{S_1} & 0 & 0 & \cdots \\ \frac{\beta L_{13}^{l'} m^l(S_1,S_2)}{S_1} & 0 & 0 & \cdots \\ \frac{\beta L_{13}^{l'} m^l(S_1,S_3)}{S_1} & 0 & 0 & \cdots \\ \vdots & \vdots & \vdots & \ddots \end{bmatrix}_{|\mathcal{K}|\times|\mathcal{K}|} & \\ \begin{bmatrix} 0 & \frac{\beta L_{12}^{l'} m^l(S_2,S_1)}{S_2} & 0 & \cdots \\ 0 & \frac{\beta L_{12}^{l'} m^l(S_2,S_2)}{S_2} & 0 & \cdots \\ 0 & \frac{\beta L_{12}^{l'} m^l(S_2,S_3)}{S_2} & 0 & \cdots \\ \vdots & \vdots & \vdots & \ddots \end{bmatrix}_{|\mathcal{K}|\times|\mathcal{K}|} & \begin{bmatrix} 0 & \frac{\beta L_{22}^{l'} m^l(S_2,S_1)}{S_2} & 0 & \cdots \\ 0 & \frac{\beta L_{22}^{l'} m^l(S_2,S_2)}{S_2} & 0 & \cdots \\ 0 & \frac{\beta L_{22}^{l'} m^l(S_2,S_3)}{S_2} & 0 & \cdots \\ \vdots & \vdots & \vdots & \ddots \end{bmatrix}_{|\mathcal{K}|\times|\mathcal{K}|} & \begin{bmatrix} 0 & \frac{\beta L_{23}^{l'} m^l(S_2,S_1)}{S_2} & 0 & \cdots \\ 0 & \frac{\beta L_{23}^{l'} m^l(S_2,S_2)}{S_2} & 0 & \cdots \\ 0 & \frac{\beta L_{23}^{l'} m^l(S_2,S_3)}{S_2} & 0 & \cdots \\ \vdots & \vdots & \vdots & \ddots \end{bmatrix}_{|\mathcal{K}|\times|\mathcal{K}|} & \cdots \\ \begin{bmatrix} 0 & 0 & \frac{\beta L_{13}^{l'} m^l(S_3,S_1)}{S_3} & \cdots \\ 0 & 0 & \frac{\beta L_{13}^{l'} m^l(S_3,S_2)}{S_3} & \cdots \\ 0 & 0 & \frac{\beta L_{13}^{l'} m^l(S_3,S_3)}{S_3} & \cdots \\ \vdots & \vdots & \vdots & \ddots \end{bmatrix}_{|\mathcal{K}|\times|\mathcal{K}|} & \begin{bmatrix} 0 & 0 & \frac{\beta L_{23}^{l'} m^l(S_3,S_1)}{S_3} & \cdots \\ 0 & 0 & \frac{\beta L_{23}^{l'} m^l(S_3,S_2)}{S_3} & \cdots \\ 0 & 0 & \frac{\beta L_{23}^{l'} m^l(S_3,S_3)}{S_3} & \cdots \\ \vdots & \vdots & \vdots & \ddots \end{bmatrix}_{|\mathcal{K}|\times|\mathcal{K}|} & \begin{bmatrix} 0 & 0 & \frac{\beta L_{33}^{l'} m^l(S_3,S_1)}{S_3} & \cdots \\ 0 & 0 & \frac{\beta L_{33}^{l'} m^l(S_3,S_2)}{S_3} & \cdots \\ 0 & 0 & \frac{\beta L_{33}^{l'} m^l(S_3,S_3)}{S_3} & \cdots \\ \vdots & \vdots & \vdots & \ddots \end{bmatrix}_{|\mathcal{K}|\times|\mathcal{K}|} & \\ & \vdots & & \ddots \end{pmatrix}_{|\mathcal{K}|^2\times|\mathcal{K}|^2}$$

The negative part can be written as $\mathbf{V}(w) = (\gamma + w)\mathbf{I}$. Our objective is to find lockdowns ($\mathbf{L}$) that ensure that the eigenvalues of $\mathbf{F}(\mathbf{L})$ are less than $\gamma + w$. Define the $|\mathcal{K}|^2 \times |\mathcal{K}|^2$ matrix

$$\mathbf{O} = \begin{pmatrix} \begin{bmatrix} 1 & 0 & 0 & \cdots \\ 1 & 0 & 0 & \cdots \\ 1 & 0 & 0 & \cdots \\ \vdots & \vdots & \vdots & \ddots \end{bmatrix}_{|\mathcal{K}|\times|\mathcal{K}|} & \begin{bmatrix} 1 & 0 & 0 & \cdots \\ 1 & 0 & 0 & \cdots \\ 1 & 0 & 0 & \cdots \\ \vdots & \vdots & \vdots & \ddots \end{bmatrix}_{|\mathcal{K}|\times|\mathcal{K}|} & \begin{bmatrix} 1 & 0 & 0 & \cdots \\ 1 & 0 & 0 & \cdots \\ 1 & 0 & 0 & \cdots \\ \vdots & \vdots & \vdots & \ddots \end{bmatrix}_{|\mathcal{K}|\times|\mathcal{K}|} & \\ \begin{bmatrix} 0 & 1 & 0 & \cdots \\ 0 & 1 & 0 & \cdots \\ 0 & 1 & 0 & \cdots \\ \vdots & \vdots & \vdots & \ddots \end{bmatrix}_{|\mathcal{K}|\times|\mathcal{K}|} & \begin{bmatrix} 0 & 1 & 0 & \cdots \\ 0 & 1 & 0 & \cdots \\ 0 & 1 & 0 & \cdots \\ \vdots & \vdots & \vdots & \ddots \end{bmatrix}_{|\mathcal{K}|\times|\mathcal{K}|} & \begin{bmatrix} 0 & 1 & 0 & \cdots \\ 0 & 1 & 0 & \cdots \\ 0 & 1 & 0 & \cdots \\ \vdots & \vdots & \vdots & \ddots \end{bmatrix}_{|\mathcal{K}|\times|\mathcal{K}|} & \cdots \\ \begin{bmatrix} 0 & 0 & 1 & \cdots \\ 0 & 0 & 1 & \cdots \\ 0 & 0 & 1 & \cdots \\ \vdots & \vdots & \vdots & \ddots \end{bmatrix}_{|\mathcal{K}|\times|\mathcal{K}|} & \begin{bmatrix} 0 & 0 & 1 & \cdots \\ 0 & 0 & 1 & \cdots \\ 0 & 0 & 1 & \cdots \\ \vdots & \vdots & \vdots & \ddots \end{bmatrix}_{|\mathcal{K}|\times|\mathcal{K}|} & \begin{bmatrix} 0 & 0 & 1 & \cdots \\ 0 & 0 & 1 & \cdots \\ 0 & 0 & 1 & \cdots \\ \vdots & \vdots & \vdots & \ddots \end{bmatrix}_{|\mathcal{K}|\times|\mathcal{K}|} & \\ & \vdots & & \ddots \end{pmatrix}_{|\mathcal{K}|^2\times|\mathcal{K}|^2}$$

which can be written as

$$\mathbf{O} = \begin{pmatrix} \mathbf{O}^1 & \mathbf{O}^1 & \dots & \mathbf{O}^1 \\ \mathbf{O}^2 & \mathbf{O}^2 & \dots & \mathbf{O}^2 \\ \vdots & \vdots & \vdots & \vdots \\ \mathbf{O}^{|\mathcal{K}|} & \mathbf{O}^{|\mathcal{K}|} & \dots & \mathbf{O}^{|\mathcal{K}|} \end{pmatrix},$$

where $\mathbf{O}^j$ is a $|\mathcal{K}| \times |\mathcal{K}|$ matrix with

$$\mathbf{O}^j_{:,k} = \begin{cases} (1, 1, \dots, 1)^\top & \text{if and only if } k = j \\ (0, 0, \dots, 0)^\top & \text{otherwise.} \end{cases}$$

Further, define

$$\begin{aligned} \hat{\boldsymbol{\beta}}^l &= \operatorname{diag}\Big(\frac{\beta m^l(S_1, S_1)}{S_1}, \frac{\beta m^l(S_1, S_2)}{S_1}, \dots, \frac{\beta m^l(S_{|\mathcal{K}|}, S_{|\mathcal{K}|})}{S_{|\mathcal{K}|}}\Big), \\ \hat{\mathbf{L}}^{l'} &= \operatorname{diag}(L^{l'}_{11}, L^{l'}_{12}, \dots, L^{l'}_{|\mathcal{K}|,|\mathcal{K}|}). \end{aligned}$$

Then we can write

$$\mathbf{F}^{l,l'}(\mathbf{L}) = \hat{\boldsymbol{\beta}}^l \mathbf{O} \hat{\mathbf{L}}^{l'}$$

for arbitrary $|\mathcal{K}|$. Similarly, define $\hat{\boldsymbol{\beta}} = \operatorname{diag}(\hat{\boldsymbol{\beta}}^1, \hat{\boldsymbol{\beta}}^2, \ldots, \hat{\boldsymbol{\beta}}^{|\mathcal{L}|})$, $\hat{\mathbf{L}} = \operatorname{diag}(\hat{\mathbf{L}}^1, \hat{\mathbf{L}}^2, \ldots, \hat{\mathbf{L}}^{|\mathcal{L}|})$, and let

$$\mathbf{M} = \begin{pmatrix} \mathbf{O} & \mathbf{O} & \ldots & \mathbf{O} \\ \mathbf{O} & \mathbf{O} & \ldots & \mathbf{O} \\ \vdots & \vdots & \ddots & \vdots \\ \mathbf{O} & \mathbf{O} & \ldots & \mathbf{O} \end{pmatrix}_{(|\mathcal{K}|^2|\mathcal{L}|)\times(|\mathcal{K}|^2|\mathcal{L}|)}$$

Then

$$\begin{aligned} \mathbf{F}(\mathbf{L}) &= \hat{\boldsymbol{\beta}}\mathbf{M}\hat{\mathbf{L}} \\ &= \begin{pmatrix} \hat{\boldsymbol{\beta}}^1 & 0 & \ldots & 0 \\ 0 & \hat{\boldsymbol{\beta}}^2 & \ldots & 0 \\ \vdots & \vdots & \ddots & \vdots \\ 0 & 0 & \ldots & \hat{\boldsymbol{\beta}}^{|\mathcal{L}|} \end{pmatrix} \begin{pmatrix} \mathbf{O} & \mathbf{O} & \ldots & \mathbf{O} \\ \mathbf{O} & \mathbf{O} & \ldots & \mathbf{O} \\ \vdots & \vdots & \ddots & \vdots \\ \mathbf{O} & \mathbf{O} & \ldots & \mathbf{O} \end{pmatrix} \begin{pmatrix} \hat{\mathbf{L}}^1 & 0 & \ldots & 0 \\ 0 & \hat{\mathbf{L}}^2 & \ldots & 0 \\ \vdots & \vdots & \ddots & \vdots \\ 0 & 0 & \ldots & \hat{\mathbf{L}}^{|\mathcal{L}|} \end{pmatrix} \\ &= \begin{pmatrix} \hat{\beta}^1\mathbf{O}\hat{\mathbf{L}}^1 & \hat{\beta}^1\mathbf{O}\hat{\mathbf{L}}^2 & \ldots & \hat{\beta}^1\mathbf{O}\hat{\mathbf{L}}^{|\mathcal{K}|} \\ \hat{\beta}^2\mathbf{O}\hat{\mathbf{L}}^1 & \hat{\beta}^2\mathbf{O}\hat{\mathbf{L}}^2 & \ldots & \hat{\beta}^2\mathbf{O}\hat{\mathbf{L}}^{|\mathcal{K}|} \\ \vdots & \vdots & \ddots & \vdots \\ \beta^{|\mathcal{L}|}\mathbf{O}\hat{\mathbf{L}}^1 & \hat{\beta}^{|\mathcal{L}|}\mathbf{O}\hat{\mathbf{L}}^2 & \ldots & \beta^{|\mathcal{L}|}\mathbf{O}\hat{\mathbf{L}}^{|\mathcal{K}|} \end{pmatrix}. \end{aligned}$$

Next, we apply the similarity transform

$$\hat{\boldsymbol{\beta}}^{-1}\mathbf{F}(\mathbf{L})\hat{\boldsymbol{\beta}} = \hat{\boldsymbol{\beta}}^{-1}\hat{\boldsymbol{\beta}}\mathbf{M}\hat{\mathbf{L}}\hat{\boldsymbol{\beta}} = \mathbf{M}\hat{\mathbf{L}}\hat{\boldsymbol{\beta}},$$

which preserves the eigenvalues. Note further that for any two vectors $\mathbf{a} = (a_1, \ldots, a_n)$ and $\mathbf{b} = (b_1, \ldots, b_n)$, we have that $\operatorname{diag}(a_1, \ldots, a_n)\operatorname{diag}(b_1, \ldots, b_n) = \operatorname{diag}(a_1b_1, \ldots, a_nb_n)$. Applying this result we have that

$$\hat{\mathbf{L}}\hat{\boldsymbol{\beta}} = \operatorname{diag}(\boldsymbol{\omega}),$$

where we have denoted by

$$\boldsymbol{\omega} = \Big(L^1_{11}\frac{\beta m^1(S_1, S_1)}{S_1}, L^1_{12}\frac{\beta m^1(S_1, S_2)}{S_1}, \ldots, L^2_{11}\frac{\beta m^2(S_1, S_1)}{S_1}, \ldots, L^{|\mathcal{L}|}_{|\mathcal{K}|,|\mathcal{K}|}\frac{\beta m^L(S_{|\mathcal{K}|}, S_{|\mathcal{K}|})}{S_{|\mathcal{K}|}}\Big)^\top.$$

Thus, our objective is to show that the eigenvalues of $\mathbf{M}\operatorname{diag}(\boldsymbol{\omega})$ are less than $\gamma + w$.

The eigenvalue problem is $\mathbf{M}\operatorname{diag}(\boldsymbol{\omega})\mathbf{v} = \varphi\mathbf{v}$ for any eigenvector $\mathbf{v}$ and corresponding eigenvalue φ. Inspecting the matrix $\mathbf{M}$, we see that every $|\mathcal{K}|^2 \cdot |\mathcal{L}|$ horizontal block $\mathbf{O}^j, \mathbf{O}^j, \ldots, \mathbf{O}^j$ selects the same elements of $\mathbf{M}\operatorname{diag}(\boldsymbol{\omega})$. Therefore the eigenvalue problem results in a system of equations in $|\mathcal{K}|$ unknowns with $|\mathcal{K}|^2 \cdot |\mathcal{L}|$ coefficients given by the

unique entries of $\boldsymbol{\omega}$. Stacking these into matrices by layer $l \in \mathcal{L}$ as in the two-times-two case, we can write our eigenvalue problem as

$$(\boldsymbol{\Omega}^1 + \boldsymbol{\Omega}^2 + \ldots) \begin{pmatrix} v_1 \\ v_2 \\ \vdots \\ v_{|\mathcal{K}|} \end{pmatrix} = \varphi \begin{pmatrix} v_1 \\ v_2 \\ \vdots \\ v_{|\mathcal{K}|} \end{pmatrix},$$

which implies that the eigenvalues of $\sum_{l \in \mathcal{L}} \boldsymbol{\Omega}^l$ are the same as $\mathbf{M}\,\mathrm{diag}(\boldsymbol{\omega})$. Finally, we can apply the similarity transform

$$\begin{aligned} \mathrm{diag}(\mathbf{S})^{-\frac{1}{2}} \left(\boldsymbol{\Omega}^1 + \boldsymbol{\Omega}^2 + \ldots\right) \mathrm{diag}(\mathbf{S})^{\frac{1}{2}} &= \mathrm{diag}(\mathbf{S})^{-\frac{1}{2}} \boldsymbol{\Omega}^1 \mathrm{diag}(\mathbf{S})^{\frac{1}{2}} + \mathrm{diag}(\mathbf{S})^{-\frac{1}{2}} \boldsymbol{\Omega}^2 \mathrm{diag}(\mathbf{S})^{\frac{1}{2}} + \ldots \\ &= \sum_{l \in \mathcal{L}} \hat{\boldsymbol{\Omega}}^l \end{aligned}$$

which preserves the eigenvalues. This gives the result for arbitrary number of groups, $|\mathcal{K}|$, and layers, $|\mathcal{L}|$. □

We next state a lemma due to Powell (2011) that will be useful for the subsequent proof.

LEMMA 3. *Consider a matrix* $\mathbf{A}$ *with the following block structure*

$$\mathbf{A} = \begin{pmatrix} \mathbf{A}_{11} & \ldots & \mathbf{A}_{1K} \\ \vdots & \ddots & \vdots \\ \mathbf{A}_{K1} & \ldots & \mathbf{A}_{KK} \end{pmatrix},$$

The determinant of the block matrix $\mathbf{A}$ *can then be computed as*

$$\det(\mathbf{A}) = \prod_{k=1}^{K} \det(\boldsymbol{\alpha}_{kk}^{(K-k)}) \tag{I.17}$$

where

$$\begin{aligned} \boldsymbol{\alpha}_{ij}^{(0)} &= \mathbf{A}_{ij}, \\ \boldsymbol{\alpha}_{ij}^{(1)} &= \boldsymbol{\alpha}_{ij}^{(0)} - \boldsymbol{\alpha}_{iK}^{(0)} (\boldsymbol{\alpha}_{KK}^{(0)})^{-1} \boldsymbol{\alpha}_{Kj}^{(0)}, \\ &\vdots \\ \boldsymbol{\alpha}_{ij}^{(k+1)} &= \boldsymbol{\alpha}_{ij}^{(k)} - \boldsymbol{\alpha}_{i,K-k}^{(k)} (\boldsymbol{\alpha}_{K-k,K-k}^{(k)})^{-1} \boldsymbol{\alpha}_{K-k,j}^{(k)}, \end{aligned}$$

given that the inverse $(\boldsymbol{\alpha}_{K-k,K-k}^{(k)})^{-1}$ *exists for all* $k = 1, \ldots, K$.

For the case of $K = 2$ from Equation (I.17) we get that

$$\det(\mathbf{A}) = \det(\boldsymbol{\alpha}_{11}^{(1)}) \det(\boldsymbol{\alpha}_{22}^{(0)})$$

with

$$\boldsymbol{\alpha}_{ij}^{(0)} = \mathbf{A}_{ij}, \quad \boldsymbol{\alpha}_{ij}^{(1)} = \mathbf{A}_{ij} - \mathbf{A}_{i2}\mathbf{A}_{22}^{-1}\mathbf{A}_{2j},$$

and inserting yields

$$\det(\mathbf{A}) = \det(\mathbf{A}_{22}) \det(\mathbf{A}_{11} - \mathbf{A}_{12}\mathbf{A}_{22}^{-1}\mathbf{A}_{21}). \tag{I.18}$$

Next, for the case of $K = 3$ from Equation (I.17) we get

$$\det(\mathbf{A}) = \det(\boldsymbol{\alpha}_{11}^{(2)}) \det(\boldsymbol{\alpha}_{22}^{(1)}) \det(\boldsymbol{\alpha}_{33}^{(0)}),$$

where

$$\boldsymbol{\alpha}_{ij}^{(0)} = \mathbf{A}_{ij},$$

and

$$\boldsymbol{\alpha}_{ij}^{(1)} = \boldsymbol{\alpha}_{ij}^{(0)} - \boldsymbol{\alpha}_{i3}^{(0)}(\boldsymbol{\alpha}_{33}^{(0)})^{-1}\boldsymbol{\alpha}_{3j}^{(0)} = \mathbf{A}_{ij} - \mathbf{A}_{i3}\mathbf{A}_{33}^{-1}\mathbf{A}_{3j},$$

and

$$\begin{aligned}\boldsymbol{\alpha}_{ij}^{(2)} &= \boldsymbol{\alpha}_{ij}^{(1)} - \boldsymbol{\alpha}_{i2}^{(1)}(\boldsymbol{\alpha}_{22}^{(1)})^{-1}\boldsymbol{\alpha}_{2j}^{(1)} \\ &= \left(\mathbf{A}_{ij} - \mathbf{A}_{i3}\mathbf{A}_{33}^{-1}\mathbf{A}_{3j}\right) - \left(\mathbf{A}_{i2} - \mathbf{A}_{i3}\mathbf{A}_{33}^{-1}\mathbf{A}_{32}\right)\left(\mathbf{A}_{22} - \mathbf{A}_{23}\mathbf{A}_{33}^{-1}\mathbf{A}_{32}\right)^{-1}\left(\mathbf{A}_{2j} - \mathbf{A}_{23}\mathbf{A}_{33}^{-1}\mathbf{A}_{3j}\right).\end{aligned}$$

Inserting into the determinant gives

$$\begin{aligned}&\det(\mathbf{A}) = \det(\mathbf{A}_{33}) \\ &\times \det(\mathbf{A}_{22} - \mathbf{A}_{23}\mathbf{A}_{33}^{-1}\mathbf{A}_{32}) \\ &\times \det\left(\mathbf{A}_{11} - \mathbf{A}_{13}\mathbf{A}_{33}^{-1}\mathbf{A}_{31} - (\mathbf{A}_{12} - \mathbf{A}_{13}\mathbf{A}_{33}^{-1}\mathbf{A}_{32})(\mathbf{A}_{22} - \mathbf{A}_{23}\mathbf{A}_{33}^{-1}\mathbf{A}_{32})^{-1}(\mathbf{A}_{21} - \mathbf{A}_{23}\mathbf{A}_{33}^{-1}\mathbf{A}_{31})\right)\end{aligned} \tag{I.19}$$

With Lemma 3 we are now equipped to provide the proof for Propositions 1 and 2 in the following.

Proof of Propositions 1 and 2. In the following we provide an analytic characterization of the eigenvalues of $\hat{\mathbf{J}}$ in the case of two and three groups, respectively, for a single layer. First, we consider the case of two groups at the disease free equilibrium (which has $I_k = 0$ and

$m(I_k, S_j) = 0$). Then the matrix $\hat{\mathbf{J}}$ from Eq. (I.13) becomes

$$\hat{\mathbf{J}} = \begin{pmatrix} \frac{\beta m(S_1,S_1)L_{11}}{S_1} - c & 0 & \frac{\beta m(S_1,S_1)L_{21}}{S_1} & 0 \\ \frac{\beta m(S_1,S_2)L_{11}}{S_1} & -c & \frac{\beta m(S_1,S_2)L_{21}}{S_1} & 0 \\ 0 & \frac{\beta m(S_2,S_1)L_{12}}{S_2} & -c & \frac{\beta m(S_2,S_1)L_{22}}{S_2} \\ 0 & \frac{\beta m(S_2,S_2)L_{12}}{S_2} & 0 & \frac{\beta m(S_2,S_2)L_{22}}{S_2} - c \end{pmatrix},$$

with $c = \gamma + w + \nu + 2\mu$. The eigenvalues φ of the Jakobian $\hat{\mathbf{J}}$ can be obtained from the solution to the characteristic equation

$$0 = \left|\hat{\mathbf{J}} - \varphi \mathbf{I}_4\right| = \begin{vmatrix} \frac{\beta m(S_1,S_1)L_{11}}{S_1} - c - \varphi & 0 & \frac{\beta m(S_1,S_1)L_{21}}{S_1} & 0 \\ \frac{\beta m(S_1,S_2)L_{11}}{S_1} & -c - \varphi & \frac{\beta m(S_1,S_2)L_{21}}{S_1} & 0 \\ 0 & \frac{\beta m(S_2,S_1)L_{12}}{S_2} & -c - \varphi & \frac{\beta m(S_2,S_1)L_{22}}{S_2} \\ 0 & \frac{\beta m(S_2,S_2)L_{12}}{S_2} & 0 & \frac{\beta m(S_2,S_2)L_{22}}{S_2} - c - \varphi \end{vmatrix} \tag{I.20}$$

A solution to the characteristic equation (I.20) can be obtained by recognizing the block structure of the matrix $\mathbf{A} = \hat{\mathbf{J}} - \varphi \mathbf{I}_4$ where

$$\mathbf{A} = \begin{pmatrix} \mathbf{A}_{11} & \mathbf{A}_{12} \\ \mathbf{A}_{21} & \mathbf{A}_{22} \end{pmatrix}, \tag{I.21}$$

with

$$\mathbf{A}_{11} = \begin{pmatrix} -c - \varphi + \frac{\beta L_{11} m(S_1,S_1)}{S_1} & 0 \\ \frac{\beta L_{11} m(S_1,S_2)}{S_1} & -c - \varphi \end{pmatrix}$$

$$\mathbf{A}_{12} = \begin{pmatrix} \frac{\beta L_{21} m(S_1,S_1)}{S_1} & 0 \\ \frac{\beta L_{21} m(S_1,S_2)}{S_1} & 0 \end{pmatrix}$$

$$\mathbf{A}_{21} = \begin{pmatrix} 0 & \frac{\beta L_{12} m(S_1,S_2)}{S_2} \\ 0 & \frac{\beta L_{12} m(S_2,S_2)}{S_2} \end{pmatrix}$$

$$\mathbf{A}_{22} = \begin{pmatrix} -c - \varphi & \frac{\beta L_{22} m(S_1,S_2)}{S_2} \\ 0 & -c - \varphi + \frac{\beta L_{22} m(S_2,S_2)}{S_2} \end{pmatrix}$$

The block structure of $\mathbf{A}$ in Eq. (I.21) allows us to apply Equation (I.18) and write the characteristic equation as follows

$$0 = \det(\mathbf{A}) = \det(\mathbf{A}_{11}) \times \det\left(\mathbf{A}_{22} - \mathbf{A}_{21}\mathbf{A}_{11}^{-1}\mathbf{A}_{12}\right) \tag{I.22}$$

if the inverse $\mathbf{A}_{11}^{-1}$ exists, where

$$\mathbf{A}_{11}^{-1} = \begin{pmatrix} \frac{S_1}{\beta L_{11} m(S_1,S_1) - (c+\varphi)S_1} & 0 \\ -\frac{\beta L_{11} m(S_1,S_2)}{(\varphi + c_{12})((\varphi + c_{11})S_1 - \beta L_{11} m(S_1,S_1))} & -\frac{1}{c+\varphi} \end{pmatrix}. \tag{I.23}$$

From $\det(\mathbf{A}_{11}) = 0$ we get

$$0 = (c+\varphi)\left(c+\varphi - \frac{\beta L_{11} m(S_1,S_1)}{S_1}\right).$$

Solving this equation for φ yields two solutions

$$\begin{aligned}\varphi_1 &= -c,\\ \varphi_2 &= \frac{\beta m(S_1,S_1) L_{11}}{S_1} - c.\end{aligned}$$

The first solution is strictly negative and gives us an eigenvalue $\varphi_1 = -c$ of $\hat{\mathbf{J}}$. The second solution violates the existence of the inverse in Equation (I.23) and thus is not an eigenvalue of $\hat{\mathbf{J}}$. Further, from $0 = \det\left(\mathbf{A}_{22} - \mathbf{A}_{21}\mathbf{A}_{11}^{-1}\mathbf{A}_{12}\right)$ we get

$$\begin{aligned}0 = \frac{c+\varphi}{S_2(S_1(c+\varphi) - \beta L_{11} m(S_1,S_1))}\big[&c^2 S_1 S_2 - c(\beta L_{11} m(S_1,S_1) S_2 + \beta L_{22} m(S_2,S_2) S_1 - 2\varphi S_1 S_2)\\ &+(\beta L_{11} m(S_1,S_1) - \varphi S_1)(\beta L_{22} m(S_2,S_2) - \varphi S_2) - \beta^2 L_{12} L_{21} m(S_1,S_2)^2\big].\end{aligned}$$

Solving for φ gives the eigenvalues

$$\begin{aligned}\varphi_3 &= \frac{\beta}{2}\left(\frac{L_{11} m(S_1,S_1)}{S_1} + \frac{L_{22} m(S_2,S_2)}{S_2} + \sqrt{C}\right) - c,\\ \varphi_4 &= \frac{\beta}{2}\left(\frac{L_{11} m(S_1,S_1)}{S_1} + \frac{L_{22} m(S_2,S_2)}{S_2} - \sqrt{C}\right) - c,\end{aligned} \tag{I.24}$$

where we have denoted by

$$\begin{aligned}C &= \left(\frac{L_{11} m(S_1,S_1)}{S_1} + \frac{L_{22} m(S_2,S_2)}{S_2}\right)^2 + 4\left(\frac{L_{12}^2 m(S_1,S_2)^2}{S_1 S_2} - \frac{L_{11} L_{22} m(S_1,S_1) m(S_2,S_2)}{S_1 S_2}\right)\\ &= \left(\frac{L_{11} m(S_1,S_1)}{S_1} - \frac{L_{22} m(S_2,S_2)}{S_2}\right)^2 + \frac{4 L_{12} L_{21} m(S_1,S_2)^2}{S_1 S_2}.\end{aligned} \tag{I.25}$$

Note that $\varphi_3 > \varphi_4$. Setting $\varphi_3 = 0$ in Eq. (I.24) and solving for β gives:

$$\beta^c = \frac{2c}{\frac{L_{11} m(S_1,S_1)}{S_1} + \frac{L_{22} m(S_2,S_2)}{S_2} + \sqrt{C}}, \tag{I.26}$$

Inserting $[S_k, I_k, m(S_k,S_j), m(I_k,S_j)] = [\lambda/\mu, 0, \frac{\kappa_{kj}}{\nu+2\mu}\frac{\lambda^2}{\mu^2}, 0]$ so that $m(S_k,S_j)/S_k = m(S_k,S_j)/S_j = \frac{\kappa_{kj}}{\nu+2\mu}\frac{\lambda}{\mu}$ gives

$$\beta^c = \frac{2c(\nu+2\mu)\mu}{\lambda}\frac{1}{L_{11}\kappa_{11} + L_{22}\kappa_{22} + \sqrt{(L_{11}\kappa_{11} - L_{22}\kappa_{22})^2 + 4 L_{12} L_{21} \kappa_{12}^2}}, \tag{I.27}$$

which is consistent with Equation (B.2) for the case of $K = 2$. Similarly, setting $\varphi_3 = 0$ in Eq. (I.24) and solving for w yields

$$w^c = \frac{\beta\lambda}{2(\nu + 2\mu)\mu}\left(L_{11}\kappa_{11} + L_{22}\kappa_{22} + \sqrt{(L_{11}\kappa_{11} - L_{22}\kappa_{22})^2 + 4L_{12}L_{21}\kappa_{12}^2}\right) - (\gamma + 2\mu + \nu + q), \tag{I.28}$$

which is consistent with Equation (B.3) for the case of $K = 2$. Next, consider the case of three groups at the disease free equilibrium (which has $I_k = 0$ and $m(I_k, S_j) = 0$). Then the matrix $\mathbf{A} = \hat{\mathbf{J}} - \varphi\mathbf{I}_9$ has the following block structure

$$\mathbf{A} = \begin{pmatrix} \mathbf{A}_{11} & \mathbf{A}_{12} & \mathbf{A}_{13} \\ \mathbf{A}_{21} & \mathbf{A}_{22} & \mathbf{A}_{23} \\ \mathbf{A}_{31} & \mathbf{A}_{32} & \mathbf{A}_{33} \end{pmatrix}, \tag{I.29}$$

where

$$\mathbf{A}_{11} = \begin{pmatrix} \frac{\beta m(S_1,S_1)L_{11}}{S_1} - c - \varphi & 0 & 0 \\ \frac{\beta m(S_1,S_2)L_{11}}{S_1} & -c-\varphi & 0 \\ \frac{\beta m(S_1,S_3)L_{11}}{S_1} & 0 & -c-\varphi \end{pmatrix}$$

$$\mathbf{A}_{12} = \begin{pmatrix} \frac{\beta m(S_1,S_1)L_{21}}{S_1} & 0 & 0 \\ \frac{\beta m(S_1,S_2)L_{21}}{S_1} & 0 & 0 \\ \frac{\beta m(S_1,S_3)L_{21}}{S_1} & 0 & 0 \end{pmatrix}$$

$$\mathbf{A}_{13} = \begin{pmatrix} \frac{\beta m(S_1,S_1)L_{31}}{S_1} & 0 & 0 \\ \frac{\beta m(S_1,S_2)L_{31}}{S_1} & 0 & 0 \\ \frac{\beta m(S_1,S_3)L_{31}}{S_1} & 0 & 0 \end{pmatrix}$$

$$\mathbf{A}_{21} = \begin{pmatrix} 0 & \frac{\beta m(S_2,S_1)L_{12}}{S_2} & 0 \\ 0 & \frac{\beta m(S_2,S_2)L_{12}}{S_2} & 0 \\ 0 & \frac{\beta m(S_2,S_3)L_{12}}{S_2} & 0 \end{pmatrix}$$

$$\mathbf{A}_{22} = \begin{pmatrix} -c-\varphi & \frac{\beta m(S_2,S_1)L_{22}}{S_2} & 0 \\ 0 & \frac{\beta m(S_2,S_2)L_{22}}{S_2} - c - \varphi & 0 \\ 0 & \frac{\beta m(S_2,S_3)L_{22}}{S_2} & -c-\varphi \end{pmatrix}$$

$$\mathbf{A}_{23} = \begin{pmatrix} 0 & \frac{\beta m(S_2,S_1)L_{32}}{S_2} & 0 \\ 0 & \frac{\beta m(S_2,S_2)L_{32}}{S_2} & 0 \\ 0 & \frac{\beta m(S_2,S_3)L_{32}}{S_2} & 0 \end{pmatrix}$$

$$\mathbf{A}_{31} = \begin{pmatrix} 0 & 0 & \frac{\beta m(S_3,S_1)L_{13}}{S_3} \\ 0 & 0 & \frac{\beta m(S_3,S_2)L_{13}}{S_3} \\ 0 & 0 & \frac{\beta m(S_3,S_3)L_{13}}{S_3} \end{pmatrix}$$

$$\mathbf{A}_{32} = \begin{pmatrix} 0 & 0 & \frac{\beta m(S_3,S_1)L_{23}}{S_3} \\ 0 & 0 & \frac{\beta m(S_3,S_2)L_{23}}{S_3} \\ 0 & 0 & \frac{\beta m(S_3,S_3)L_{23}}{S_3} \end{pmatrix}$$

$$\mathbf{A}_{33} = \begin{pmatrix} -c-\varphi & 0 & \frac{\beta m(S_3,S_1)L_{33}}{S_3} \\ 0 & -c-\varphi & \frac{\beta m(S_3,S_2)L_{33}}{S_3} \\ 0 & 0 & \frac{\beta m(S_3,S_3)L_{33}}{S_3} - c - \varphi \end{pmatrix}$$

The block structure of $\mathbf{A}$ in Eq. (I.29) allows us to apply Lemma 3 and write the characteristic equation as follows:

$$\begin{aligned}
0 &= \det(\mathbf{A}) \\
&= \det(\mathbf{A}_{33}) \\
&\times \det(\mathbf{A}_{22} - \mathbf{A}_{23}\mathbf{A}_{33}^{-1}\mathbf{A}_{32}) \\
&\times \det\left(\mathbf{A}_{11} - \mathbf{A}_{13}\mathbf{A}_{33}^{-1}\mathbf{A}_{31} - (\mathbf{A}_{12} - \mathbf{A}_{13}\mathbf{A}_{33}^{-1}\mathbf{A}_{32})(\mathbf{A}_{22} - \mathbf{A}_{23}\mathbf{A}_{33}^{-1}\mathbf{A}_{32})^{-1}(\mathbf{A}_{21} - \mathbf{A}_{23}\mathbf{A}_{33}^{-1}\mathbf{A}_{31})\right)
\end{aligned} \tag{I.30}$$

if the inverse $\mathbf{A}_{33}^{-1}$ exists. The latter is given by

$$\mathbf{A}_{33}^{-1} = \begin{pmatrix} -\frac{S_3}{S_3(c+\varphi)-\beta L_{33}m(S_3,S_3)} & 0 & 0 \\ -\frac{\beta L_{33}m(S_3,S_2)}{(c+\varphi)(S_3(c+\varphi)-\beta L_{33}m(S_3,S_3))} & -\frac{1}{c+\varphi} & 0 \\ -\frac{\beta L_{33}m(S_1,S_3)}{(c+\varphi)(S_3(c+\varphi)-\beta L_{33}m(S_3,S_3))} & 0 & -\frac{1}{c+\varphi} \end{pmatrix} \tag{I.31}$$

We find that

$$\det(\mathbf{A}_{33}) = \frac{(c+\varphi)^2(\beta L_{33}m(S_3,S_3) - S_3(c+\varphi))}{S_3}.$$

Solving $\det(\mathbf{A}_{11}) = 0$ for φ gives two different solutions

$$\begin{aligned}
\varphi_1 &= -c, \\
\varphi_2 &= \frac{\beta L_{33}m(S_3,S_3)}{S_3} - c.
\end{aligned}$$

The first solution is strictly negative and an eigenvalue $\varphi_1 = -c$ of $\hat{\mathbf{J}}$ with multiplicity two. The second solution violates the existence of the inverse in Equation (I.31) and thus cannot be an eigenvalue. Moreover, we find that

$$\begin{aligned}
\det\left(\mathbf{A}_{22} - \mathbf{A}_{21}\mathbf{A}_{11}^{-1}\mathbf{A}_{12}\right) = -\frac{(c+\varphi)^2}{S_2(S_3(c+\varphi) - \beta L_{33}m(S_3,S_3))}\big(&c^2S_2S_3 - c(\beta L_{22}m(S_2,S_2)S_3 + \beta L_{33}m(S_3,S_3)S_2 \\
&-2\varphi S_2S_3) + (\beta L_{22}m(S_2,S_2) - \varphi S_2)(\beta L_{33}m(S_3,S_3) - \varphi S_3) - \beta^2 L_{23}^2 m(S_2,S_3)^2\big)
\end{aligned}$$

Solving $\det\left(\mathbf{A}_{22} - \mathbf{A}_{21}\mathbf{A}_{11}^{-1}\mathbf{A}_{12}\right) = 0$ for φ gives the eigenvalues

$$\varphi_3 = \frac{\beta\left(L_{22}m(S_2,S_2)S_3 + L_{33}m(S_3,S_3)S_2 \pm \sqrt{C}\right)}{2S_2S_3} - c, \tag{I.32}$$

where C is given by Equation (I.25). However, this violates the existence of the inverse $\left(\mathbf{A}_{22} - \mathbf{A}_{21}\mathbf{A}_{11}^{-1}\mathbf{A}_{12}\right)^{-1}$ in Equation (I.30). Further, evaluating $\det(\mathbf{A}_{33} - \mathbf{A}_{31}\mathbf{A}_{11}^{-1}\mathbf{A}_{31} - (\mathbf{A}_{32} - \mathbf{A}_{31}\mathbf{A}_{11}^{-1}\mathbf{A}_{12})(\mathbf{A}_{22} - \mathbf{A}_{21}\mathbf{A}_{11}^{-1}\mathbf{A}_{12})^{-1}(\mathbf{A}_{23} - \mathbf{A}_{21}\mathbf{A}_{11}^{-1}\mathbf{A}_{31}))$, dropping terms of the

order $O\left(\beta^3\right)$, and solving for φ such that the determinant becomes zero gives

$$\varphi_{4,5} = \frac{\beta}{2}\left(\frac{L_{11}m(S_1,S_1)}{S_1} + \frac{L_{22}m(S_2,S_2)}{S_2} + \frac{L_{33}m(S_3,S_3)}{S_3} \pm \sqrt{C}\right), \tag{I.33}$$

where

$$C = \left(\frac{L_{11}m(S_1,S_1)}{S_1} + \frac{L_{22}m(S_2,S_2)}{S_2} + \frac{L_{33}m(S_3,S_3)}{S_3}\right)^2 + 4\left(\frac{L_{12}^2 m(S_1,S_2)^2}{S_1S_2} - \frac{L_{11}L_{22}m(S_1,S_1)m(S_2,S_2)}{S_1S_2}\right.$$
$$\left. + \frac{L_{13}^2 m(S_1,S_3)^2}{S_1S_3} - \frac{L_{11}L_{33}m(S_1,S_1)m(S_3,S_3)}{S_1S_3} + \frac{L_{23}^2 m(S_2,S_3)^2}{S_2S_3} - \frac{L_{22}L_{33}m(S_2,S_2)m(S_3,S_3)}{S_2S_3}\right),$$

with $\varphi_4 > \varphi_5$. Summarizing the above we find that the largest eigenvalue for $K = 2$ and $K = 3$ can be written as

$$\varphi = \frac{\beta}{2}\left(\sum_{k=1}^{K}\frac{L_{kk}m(S_k,S_k)}{S_k} + \sqrt{C}\right) - c,$$

where

$$C = \left(\sum_{k=1}^{K}\frac{L_{kk}m(S_k,S_k)}{S_k}\right)^2 + 4\sum_{k=1}^{K}\sum_{j=k+1}^{K}\left(\frac{L_{kj}^2 m(S_k,S_j)^2}{S_kS_j} - \frac{L_{kk}L_{jj}m(S_k,S_k)m(S_j,S_j)}{S_kS_j}\right).$$

Next, using the fact that

$$\frac{m(S_k,S_j)}{S_k} = \frac{m(S_k,S_j)}{S_j} = \frac{\kappa_{kj}}{\nu+2\mu}\frac{\lambda}{\mu},$$

we can write the largest eigenvalue as

$$\varphi = \frac{\beta\lambda}{2\mu(\nu+2\mu)}\left(\sum_{k=1}^{K}\kappa_{kk}L_{kk} + \sqrt{C}\right) - c, \tag{I.34}$$

where

$$C = \left(\sum_{k=1}^{K}\kappa_{kk}L_{kk}\right)^2 + 4\sum_{k=1}^{K}\sum_{j=k+1}^{K}\left(\kappa_{kj}^2L_{kj}^2 - \kappa_{kk}L_{kk}\kappa_{jj}L_{jj}\right).$$

Setting $\varphi = 0$ in Eq. (I.34) and solving for β or w yields Equations (B.2) and (B.3), respectively. □

Proof of Lemma 1. To show this, we need to show that the dynamics of the aggregated system are the same as the dynamics of the single group process.

First, consider our multi-group equations for the disease dynamics

$$\begin{aligned}
\frac{dS_k}{dt} &= -\sum_{j\in\mathcal{K}} \beta m(S_k, I_j)(t), \\
\frac{dI_k}{dt} &= \sum_{j\in\mathcal{K}} \beta m(S_k, I_j)(t) - \gamma I_k(t), \\
\frac{dR_k}{dt} &= \delta_{rk} H_k(t) + \gamma(I_k(t) - H_k(t)), \\
H_k(t) &= \iota_k I_k(t), \\
\frac{dD_k}{dt} &= \delta_{dk} H_k(t).
\end{aligned} \tag{I.35}$$

Consider the equation for S_k without loss of generality. Define $S^A = \sum_{k\in\mathcal{K}} S_k$, so that

$$\begin{aligned}
\frac{dS^A}{dt} &= \sum_{k\in\mathcal{K}} \frac{dS_k}{dt} \\
&= -\sum_{k\in\mathcal{K}} \sum_{j\in\mathcal{K}} \beta m(S_k, I_j)(t) \\
&= -\beta m^A(I, S)(t).
\end{aligned}$$

Applying the same steps to each of the equations for the multi-group disease dynamics gives

$$\begin{aligned}
\frac{dS^A}{dt} &= -\beta m^A(S, I)(t) \\
\frac{dI^A}{dt} &= \beta m^A(S, I)(t) - \gamma I^A(t), \\
\frac{dR^A}{dt} &= \delta_r H^A(t) + \gamma(I^A(t) - H^A(t)), \\
H^A(t) &= \iota I^A(t), \\
\frac{dD^A}{dt} &= \delta_d H^A(t)
\end{aligned}$$

which is equivalent to the single group disease dynamics.

Next, consider the multi-group network dynamics:

$$\begin{aligned}
\frac{dm(S_k,S_j)}{dt} &= w\frac{S_k(t)}{\sum_{k'\in\mathcal{K}} S_{k'}(t)}\sum_{k'\in\mathcal{K}} m(I_{k'},S_j)(t) + w\frac{S_j(t)}{\sum_{k'\in\mathcal{K}} S_{k'}(t)}\sum_{k'\in\mathcal{K}} m(I_{k'},S_k)(t) \\
&\quad - \frac{\sum_{k'\in\mathcal{K}}\beta m(I_{k'},S_k)(t)m(S_k,S_j)(t)}{S_k(t)} - \frac{\sum_{k'\in\mathcal{K}}\beta m(I_{k'},S_j)(t)m(S_j,S_k)(t)}{S_j(t)}, \\
\frac{dm(I_k,S_j)}{dt} &= \frac{1}{S_k(t)}\sum_{k'\in\mathcal{K}}\beta' m(I_{k'},S_k)(t)m(S_k,S_j)(t) - \frac{1}{S_j(t)}\sum_{k'\in\mathcal{K}}\beta m(I_{k'},S_j)(t)m(I_k,S_j)(t) \\
&\quad - (\gamma+w)m(I_k,S_j)(t),
\end{aligned}$$

Consider the equation for $m(S_k,S_j)$ without loss of generality. Define $m^A(S_k,S_j) = \frac{1}{2}\sum_{k,j\in\mathcal{K}} m(S_k,S_j)$ to avoid double counting. Then

$$\begin{aligned}
\frac{dm^A(S,S)}{dt} &= \sum_{k,j\in\mathcal{K}}\frac{dm(S_k,S_j)}{dt} \\
&= \sum_{k,j\in\mathcal{K}}\Big(w\frac{S_k(t)}{\sum_{k'\in\mathcal{K}} S_{k'}(t)}\sum_{k'\in\mathcal{K}} m(I_{k'},S_j)(t) + w\frac{S_j(t)}{\sum_{k'\in\mathcal{K}} S_{k'}(t)}\sum_{k'\in\mathcal{K}} m(I_{k'},S_k)(t) \\
&\quad - \frac{\sum_{k'\in\mathcal{K}}\beta m(I_{k'},S_k)(t)m(S_k,S_j)(t)}{S_k(t)} - \frac{\sum_{k'\in\mathcal{K}}\beta m(I_{k'},S_j)(t)m(S_j,S_k)(t)}{S_j(t)}\Big) \\
&= wm(I^A,S^A)(t) - 2\beta\frac{m(I^A,S^A)(t)m(S^A,S^A)(t)}{S^A(t)}.
\end{aligned}$$

Applying the same steps for the other network state variables gives our result. □

Proof of Proposition 3. We have the following conditions for consistency from Newey and McFadden (1994, Theorem 2.7)]. If there is a function $Q_0(\theta)$ such that

1. $Q_0(\theta)$ is uniquely maximised at θ_0;
2. θ_0 is an element of the interior of the convex set Θ and $\hat{Q}_N(\theta)$ is concave; and
3. $\hat{Q}_N(\theta) \xrightarrow{p} Q_0(\theta)$ for all $\theta\in\Theta$

then $\hat{\theta}_N$ exists with probability approaching one and $\hat{\theta}_N \xrightarrow{p} \theta_0$.

We prove the proposition by proving that our estimator satisfies the conditions from above. We first want to show 3. We can write

$$\frac{dX(\theta)}{dt} = F(X,\theta), \tag{I.36}$$

with the function $F(X, \theta)$ corresponding to the RHS of Eqs. (1), (2), (3), (4), (5), (6) and (7). From Theorem 3 we then know that starting from $X(0)$, we have

$$\lim_{N\to\infty} \mathbb{P}\left(\sup_{t\in[0,T]} \left| X^N(\theta, t) - X(\theta, t) \right| \geq \varepsilon \right) = 0,$$

for any $0 \leq t \leq T < \infty$ and $\varepsilon > 0$. In other words, $X^N(\theta, t) \xrightarrow{p} X(\theta, t)$. Since convergence in probability of a vector implies convergence component wise, this implies that $Y^N(\theta, t) \xrightarrow{p} Y(\theta, t)$.

Next, note that the $L_{2,1}$ matrix norm $||.||_{2,1}$ is continuous in its argument, we can apply the continuous mapping theorem (Billingsley 2017) to show that:

$$\hat{Q}_N(\theta) = -||Y(\theta) - Y^N(\theta_0)||_{2,1} \xrightarrow{p} ||Y(\theta) - Y(\theta_0)||_{2,1} = Q_0(\theta).$$

This verifies 3.

Next, we want to establish 1. By the Picard-Lindelöf Theorem, Eq. (I.36) has a unique solution $X(\theta)$ if the function $F(X, \theta)$ is Lipschitz continuous with respect to X, and it is continuous in both X and t (Braun 1993). In Lemma 2 we have shown that $F(X, \theta)$ is Lipschitz continuous and thus the uniqueness of $X(\theta)$ follows.

Next, we need to show that uniqueness of X implies uniqueness of Y, which is the first, second, and fifth series in X. For a contradiction, assume that $X(\theta_1) \neq X(\theta_2)$ for $\theta_1 \neq \theta_2$, but $Y(\theta_1) = Y(\theta_2)$. This can only happen if $S(\theta_1) = S(\theta_2)$, $I(\theta_1) = I(\theta_2)$, $m(I, S)(\theta_1) = m(I, S)(\theta_2)$ but $m(S, S)(\theta_1) \neq m(S, S)(\theta_2)$. We have that

$$m(S, S)(t) = m(S, S)(0) + \int_0^t \left(w\, m(I, S)(s) - 2\beta \frac{m(I, S)(s)\, m(S, S)(s)}{S(s)} \right) ds.$$

From this equation we see that if θ_1 and θ_2 differ in w or β then $m(S, S)(\theta_1) \neq m(S, S)(\theta_2)$, which is a contradiction. Next, if θ_1 and θ_2 differ in γ, then from Eq. (2) it follows that $I(\theta_1) \neq I(\theta_2)$, which is a contradiction. Hence, $Y(\theta_1) = Y(\theta_2)$ if and only if $\theta_1 = \theta_2$.

We then know that $Y(\theta)$ and $Y(\theta_0)$ are distinct functions when $\theta \neq \theta_0$. At $\theta = \theta_0$, we clearly have:

$$Y(\theta_0) - Y(\theta_0) = 0,$$

so

$$\|Y(\theta_0) - Y(\theta_0)\|_{2,1} = 0,$$

and thus:

$$Q_0(\theta_0) = 0.$$

For $\theta \neq \theta_0$, the uniqueness of solutions implies that $Y(\theta) \neq Y(\theta_0)$, and therefore

$$\|Y(\theta) - Y(\theta_0)\|_{2,1} > 0,$$

which leads to:

$$Q_0(\theta) = -\|Y(\theta) - Y(\theta_0)\|_{2,1} < 0.$$

The norm $\|Y(\theta) - Y(\theta_0)\|_{2,1}$ is strictly positive for $\theta \neq \theta_0$ due to the uniqueness of the ODE solutions. This ensures that the value of $Q_0(\theta)$ is strictly less than zero for any $\theta \neq \theta_0$. Since $Q_0(\theta_0) = 0$ and $Q_0(\theta) < 0$ for all $\theta \neq \theta_0$, it follows that $Q_0(\theta)$ reaches its maximum value (which is zero) at $\theta = \theta_0$. Therefore, $Q_0(\theta)$ has a unique maximum at $\theta = \theta_0$. This shows 1.

Next, we want to show 2. Since the parameter space Θ is the non-negative orthant $\mathbb{R}_{\geq 0}$, it follows that Θ is convex. Further, we want to show that $\hat{Q}_N(\theta) = -||Y(\theta) - Y^N(\theta_0)||_{2,1}$ is concave in $\theta \in \Theta$. This is equivalent to showing that the following function

$$||Y(\theta) - Y^N(\theta_0)||_{2,1} = ||S(\theta) - S^N(\theta_0)||_2 + ||I(\theta) - I^N(\theta)||_2 + ||m(I,S)(\theta) - m^N(I,S)(\theta_0)||_2,$$

is convex in $\theta \in \Theta$. In order to show convexity, we first note the following: For every t, we have that

$$X(\nu\theta_1 + (1-\nu)\theta_2) = X_0 + \int_0^t F(X, \nu\theta_1 + (1-\nu)\theta_2)ds.$$

where $\frac{dX(\theta)}{dt} = F(X,\theta)$ from Eq. (I.10). This system of differential equations is linear in parameters, so that

$$
\begin{aligned}
&F(X, \nu\theta_1 + (1-\nu)\theta_2) \\
&= \begin{pmatrix} -(\nu\beta_1 + (1-\nu)\beta_2)X_3(t) \\ -(\nu\gamma_1 + (1-\nu)\gamma_2)X_2(t) + (\nu\beta_1 + (1-\nu)\beta_2)X_3(t) \\ -(\nu\gamma_1 + (1-\nu)\gamma_2)X_3(t) - (\nu w_1 + (1-\nu)w_2)X_3(t) + (\nu\beta_1 + (1-\nu)\beta_2)\frac{X_3(t)(2X_4(t)-X_3(t))}{X_1(t)} \\ (\nu w_1 + (1-\nu)w_2)X_3(t) - 2(\nu\beta_1 + (1-\nu)\beta_2)\frac{X_3(t)X_4(t)}{X_1(t)} \end{pmatrix} \\
&= \begin{pmatrix} -\nu\beta_1 X_3(t) \\ -\nu\gamma_1 X_2(t) + \nu\beta_1 X_3(t) \\ -\nu\gamma_1 X_3(t) - \nu w_1 X_3(t) + \nu\beta_1\frac{X_3(t)(2X_4(t)-X_3(t))}{X_1(t)} \\ \nu w_1 X_3(t) - 2\nu\beta_1 + \frac{X_3(t)X_4(t)}{X_1(t)} \end{pmatrix} \\
&+ \begin{pmatrix} -(1-\nu)\beta_2 X_3(t) \\ -(1-\nu)\gamma_2 X_2(t) + (1-\nu)\beta_2 X_3(t) \\ -(1-\nu)\gamma_2 X_3(t) - (1-\nu)w_2 X_3(t) + (1-\nu)\beta_2\frac{X_3(t)(2X_4(t)-X_3(t))}{X_1(t)} \\ (1-\nu)w_2 X_3(t) - 2(1-\nu)\beta_2\frac{X_3(t)X_4(t)}{X_1(t)} \end{pmatrix} \\
&= F(X, \nu\theta_1) + F(X, (1-\nu)\theta_2) \\
&= \nu F(X,\theta_1) + (1-\nu)F(X,\theta_2)
\end{aligned}
$$

For $\nu \in [0,1]$, we therefore have

$$
\begin{aligned}
X_0 + \int_0^t F(X, \nu\theta_1 + (1-\nu)\theta_2)ds &= \nu(X_0 + \int_0^t F(X,\theta_1)ds) + (1-\nu)(X_0 + \int_0^t F(X,\theta_2)ds) \\
&= \nu X(\theta_1) + (1-\nu)X(\theta_2),
\end{aligned}
$$

which leads to

$$
X(\nu\theta_1 + (1-\nu)\theta_2) = \nu X(\theta_1) + (1-\nu)X(\theta_2). \tag{I.37}
$$

This holds for every component of X in Eq. (G.1), and thus for S, I and $m(I,S)$. We next want to show that

$$
\|Y(\theta) - Y^N(\theta_0)\|_{2,1} = \|S(\theta) - S^N(\theta_0)\|_2 + \|I(\theta) - I^N(\theta)\|_2 + \|m(I,S)(\theta) - m^N(I,S)(\theta_0)\|_2
$$

is convex in θ.[30] We apply the triangle inequality to each component:

$$\begin{aligned}\|S(\nu\theta_1 + (1-\nu)\theta_2) - S^N(\theta_0)\|_2 &= \|\nu S(\theta_1) + (1-\nu)S(\theta_2) - S^N(\theta_0)\|_2 \\ &= \|\nu(S(\theta_1) - S^N(\theta_0)) + (1-\nu)(S(\theta_2) - S^N(\theta_0))\|_2 \\ &\leq \nu\|S(\theta_1) - S^N(\theta_0)\|_2 + (1-\nu)\|S(\theta_2) - S^N(\theta_0)\|_2,\end{aligned}$$

where we have used Eq. (I.37) in the first equality. Similarly, one can show that

$$\|I(\theta) - I^N(\theta)\|_2 \leq \nu\|I(\theta_1) - I^N(\theta_0)\|_2 + (1-\nu)\|I(\theta_2) - I^N(\theta_0)\|_2,$$

and

$$\|m(I,S)(\theta) - m^N(I,S)(\theta_0)\|_2 \leq \nu\|m(I,S)(\theta_1) - m^N(I,S)(\theta_0)\|_2 + (1-\nu)\|m(I,S)(\theta_2) - m^N(I,S)(\theta_0)\|_2.$$

Combining these inequalities, we have

$$\|Y(\nu\theta_1 + (1-\nu)\theta_2) - Y^N(\theta_0)\|_{2,1} \leq \nu\|Y(\theta_1) - Y^N(\theta_0)\|_{2,1} + (1-\nu)\|Y(\theta_2) - Y^N(\theta_0)\|_{2,1}.$$

Thus, $\|Y(\theta) - Y^N(\theta_0)\|_{2,1}$ is convex in θ. This shows 2 and the result follows. □

30. A function $f(\theta)$ is convex over the support Θ if and only if, for all $\theta_1, \theta_2 \in \Theta$ and $\nu \in [0,1]$ we have that $f(\nu\theta_1 + (1-\nu)\theta_2) \leq \nu f(\theta_1) + (1-\nu)f(\theta_2)$.